NASA CR-159703

LOW SIDELOBE LEVEL LOW-COST EARTH STATION ANTENNAS FOR THE 12 Ghz. BROADCASTING SATELLITE SERVICE

by

R.E. COLLIN and L.R. GABEL

ELECTRICAL ENGINEERING AND APPLIED PHYSICS DEPARTMENT

Case Institute of Technology

Case Western Reserve University

Cleveland, Ohio

Prepared for

NATIONAL AERONAUTICS AND SPACE ADMINISTRATION

NASA Lewis Research Center

Contract NAS3-21365

NASA CR-159703

ERRATA FOR

LOW SIDELOBE LEVEL LOW-COST EARTH STATION ANTENNAS FOR THE 12 GHZ. BROADCASTING SATELLITE SERVICE

by

R. E. Collin and L. Gabel

Report Date: Sept. 1979

Page 38, Eq. 3.3 should read

$$\Delta\phi = - \frac{2 k_o p \rho^2}{\rho^2 + 4f^2}$$

Eq. 3.4 should read

$$p = \frac{2ft}{a^2} (a^2 + 4f^2)^{1/2}$$

Pg. 39, Line 5 after Eq. 3.6

$$\beta = k_o p x^2/(x^2 + 16f^2/D^2)$$

Pg. 40, Eq. 3.9, The real parts of the expression for E(u) for the $\phi = 0$ and $\phi = \pi/2$ planes should be transposed - thus

$$E(u) = I_o - 0.75 \gamma^2 I_2 - \gamma^2 I_4 - 0.25 \gamma^2 I_6 - j\gamma(I_1+I_3), \ \phi = 0 \text{ plane}$$

$$= I_o - 0.75 \gamma^2 I_2 + \gamma^2 I_4 - 0.25 \gamma^2 I_6 - j\gamma(I_1-I_3), \ \phi = \frac{\pi}{2} \text{ plane}$$

Pg. 40, 1st line after Eq. 3.10 should read

where $\gamma = k_o p$ and

Pg's. 40-41, Eq's. 3.11b, 3.11c, 3.11d, 3.11e and 3.11f

The denominator in the integrands should read

$$x^2 + 16(f/D)^2$$

With the exception of the error in Eq. 3.9 these errors are typographical and do not effect the numerical calculation. However, because of the error in Eq. 3.9, Fig's. 3.8 and 3.10 on pages 43 and 44 are in error. Corrected Figures are supplied to replace them.

The author's appreciate these errors being brought to their attention by Dr. Levent Ersoy of the Ford Aerospace and Communications Corporation.

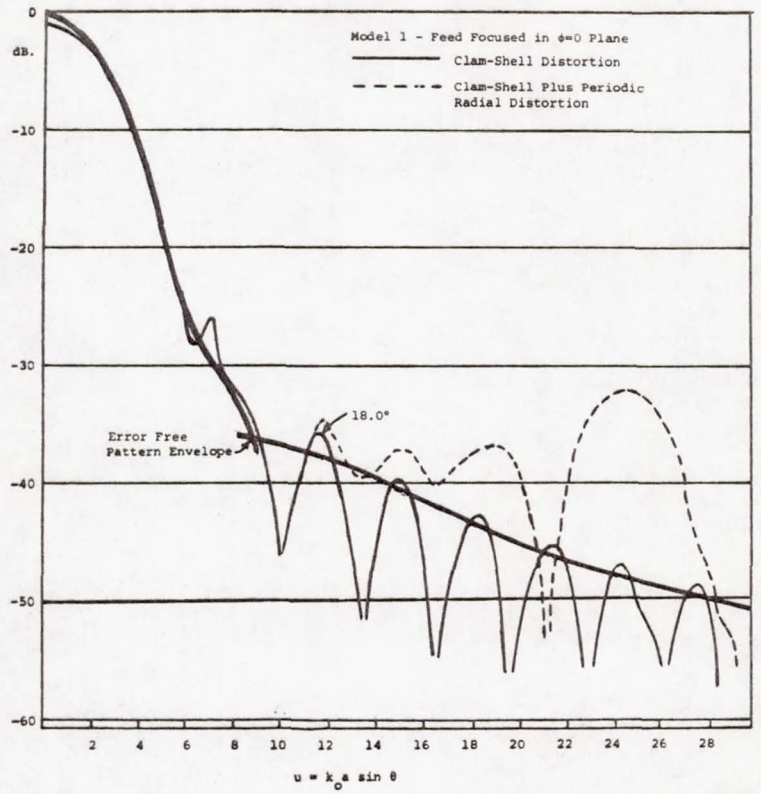

Figure 3.8

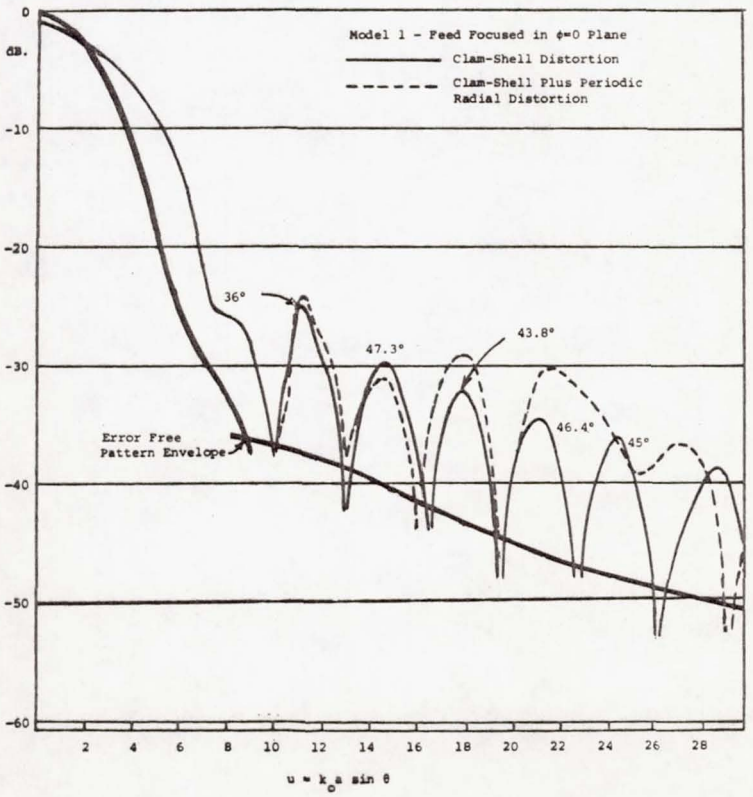

Figure 3.10

1. Report No. NASA CR 159703	2. Government Accession No.	3 Recipient's Catalog No
4. Title and Subtitle LOW SIDELOBE LEVEL LOW-COST EARTH STATION ANTENNAS FOR THE 12 Ghz. BROADCASTING SATELLITE SERVICE		5. Report Date September 1979 6. Performing Organization Code
7. Author(s) R. E. Collin and L. R. Gabel		8. Performing Organization Report No. 10. Work Unit No.
9. Performing Organization Name and Address Case Western Reserve University 10900 Euclid Avenue Cleveland, Ohio 44106		11. Contract or Grant No NAS 3-21365
12. Sponsoring Agency Name and Address		13. Type of Report and Period Covered Contractor Report 14 Sponsoring Agency Code

15. Supplementary Notes

Technical Monitor, Jerry Smetana, Communications Applications Division
NASA Lewis Research Center

16. Abstract

An experimental investigation of the performance of 1.22m and 1.83m diameter paraboloid antennas with an f/D ratio of 0.38 and using a feed developed by Kumar is reported. It is found that sidelobes below 30 dB. can be obtained only if the paraboloids are relatively free of surface errors. A theoretical analysis of "clam shell" distortion shows that this is a limiting factor in achieving low sidelobe levels with many commercially available low-cost paraboloids. The use of absorbing pads and small reflecting plates for sidelobe reduction is also considered.

17. Key Words (Suggested by Author(s))	18. Distribution Statement
Antenna, Paraboloid, Antenna Feed, Low Sidelobe, Paraboloid Errors, Satellite Communications	Uncalssified - Unlimited

19. Security Classif. (of this report)	20 Security Classif. (of this page)	21. No. of Pages	22. Price*
Unclassified	Unclassified	114	

* For sale by the National Technical Information Service, Springfield, Virginia 22161

Table of Contents

CHAPTER I

GROUND STATION ANTENNA SIDELOBE REQUIREMENTS FOR THE 12 GHZ. SATELLITE BROADCASTING SERVICE

The eventual direct transmission of television signals from synchronous orbit satellites to the home consumer depends on the development of low cost ground stations suitable for installation on the consumer's premises. Microwave technology has advanced to the point where, with mass production, such low cost receiving stations are feasible. A major factor that has helped to bring this about is the development of highly efficient high power traveling wave tubes suitable for use in a satellite. A clear example of this technology is the Communication Technology Satellite (CTS) launched by NASA which uses a 200 watt traveling wave tube. The CTS system produced at 58.9 dB signal to noise ration (CCIR weighted) when used with a 27 mhz. bandwidth FM television signal, a receiver with noise temperature T = 800 degrees, and a 16 foot ground station antenna (1). With a 4 foot ground station antenna a signal to noise ratio of 46.9 dB. would be obtained and this is sufficient for a high quality television picture in the absence of interference from signals transmitted by other nearby satellites.

There is only one synchronous orbit so one can readily appreicate that eventually all satellite space in this orbit will be utilized. For efficient use of the space in the synchronous orbit it is important to space the satellites as close together as possible. However, because

the available frequency band is limited a serious problem of interference from adjacent satellites transmitting on essentially the same frequency arises. In general this leads to the requirement of very low sidelobe levels for the ground station antenna in order to discriminate against unwanted signals that could be received from a direction coinciding with a sidelobe peak. If all sidelobes can be kept below a certain minimum value such that interference signals from adjacent satellites are sufficiently discriminated against the satellite spacing will then be limited only by the main lobe angular width of the ground station antenna and maximum space utilization of the synchronous orbit will be achieved (2). In practice some margin must also be allowed for antenna pointing error.

A number of studies have been carried out to determine the tolerable level of interference for FM television signals (3-7). The degree of interference perceptibility depends on the amount of thermal noise present and permits a higher level of interference when the picture is degraded by the presence of thermal noise. The guidelines suggested by CCIR is expressed in terms of a protection ratio PR which in turn is related to a protection constant PC as follows (2,8,9):

$$\begin{aligned} PR &= PC - (49 - S/N) \qquad S/N < 49 \text{ dB.} \\ &= PC \qquad\qquad\qquad\quad S/N > 49 \text{ dB.} \end{aligned} \tag{1.1}$$

where all quantities are expressed in decibels and S/N is the peak-peak luminance signal to RMS thermal noise ratio. Figure 1.1 shows the required protection ratio as a function of S/N for various FM bandwidths.

These protection ratios will result in just perceptible interference during less than 5% of the time. Since it can generally be expected that S/N will equal 49 dB. or more the required protection ratio will equal the protection constant. Thus, for example, a 8 mhz. bandwidth FM television signal will require the level of interference to be 36 dB. below the desired signal. It is apparent that the sidelobe level of the ground station antenna should be at least 36 dB. below the main lobe in order to provide adequate discrimination against unwanted signals for FM television broadcasting with bandwidth as low as 8 mhz.

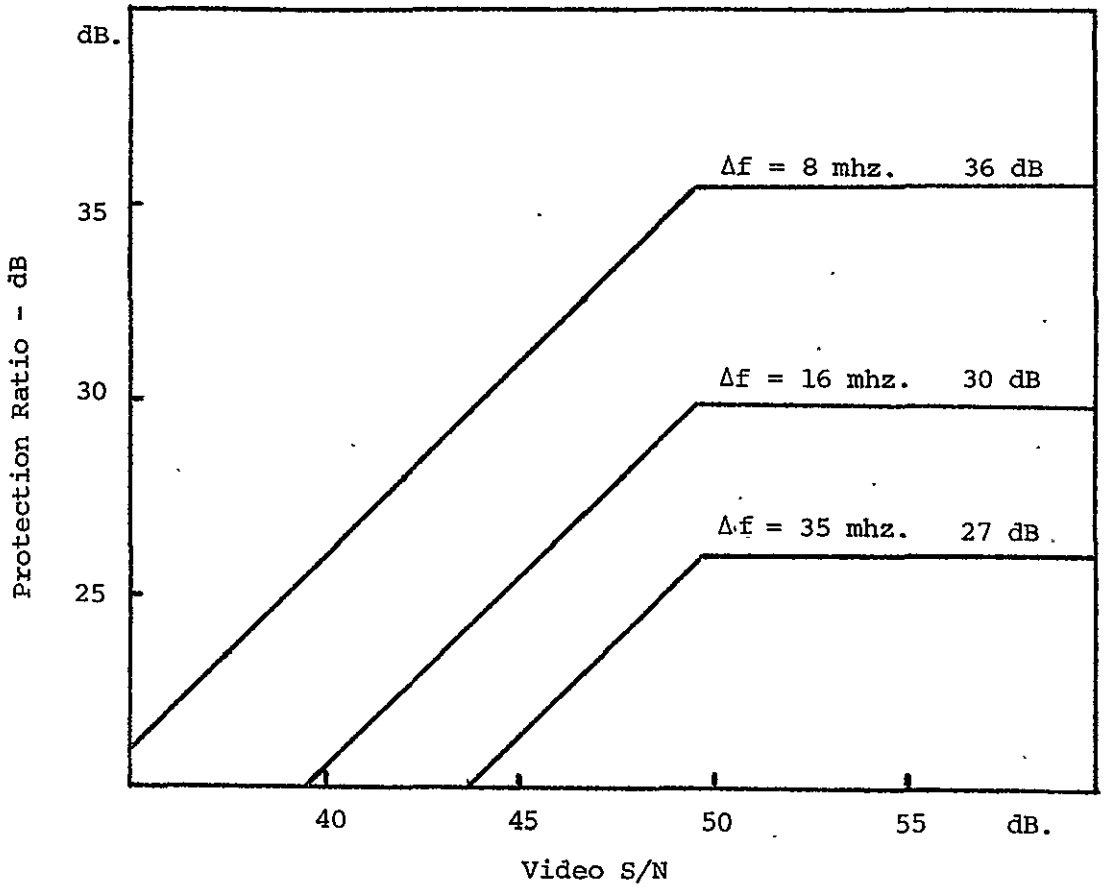

Figure 1.1 Protection ratio as a function of video signal to noise ratio.

The currently available low cost ground station paraboloidal antennas for the 12 ghz. band and in the 4 foot and 6 foot diameter size have near-in sidelobes in the range of -20 dB. to -25 dB. and therefore do not provide sufficient attenuation of unwanted signals in the sidelobe region. For communication system planning CCIR has given a model antenna pattern specified in dB. by

$$
\begin{aligned}
G &= 0, && 0 \leq \theta \leq \theta_o/4 \\
&= -12\ (\theta/\theta_o)^2\ \text{dB.}, && \theta_o/4 \leq \theta \leq \theta_o/\sqrt{2} \\
&= -[9+20\log\ \theta/\theta_o]\text{dB.}, && \theta_o/\sqrt{2} \leq \theta \leq 12.26\ \theta_o \\
&= -[8.5+25\ \log\ \theta/\theta_o]\ \text{dB.}, && 1.26\ \theta_o \leq \theta \leq 15.14\ \theta_o \\
&= -\ 38\ \text{dB.}, && \theta > 15.14\ \theta_o
\end{aligned}
\qquad (2.2)
$$

where θ_o is the half-power antenna beamwidth. The currently available low cost antennas usually come close to meeting the requirements of this model pattern.

As noted there is a need to reduce the sidelobe level below that of currently available low cost antennas in order to permit closer spacing of the satellites in the synchronous orbit. The objective of the work described in this report was to examine various known sidelobe reduction techniques and specifically to shoose a technique that would reduce the sidelobe level by a modest 5 dB. below that of the CCIR model pattern for detailed study. The method selected was to use a new type of prime focus feed as described by Kumar (10). This feed produced in excess of 20 dB. of taper over the paraboloidal

aperture and resulted in sidelobe levels of 5 dB. or more below that of the CCIR model pattern when used with a commercially available 4 foot diameter paraboloidal. An important experimental finding of this study was that in order to achieve sidelobe levels below -30 dB. the paraboloidal surface contour had to be accurate to within about one thirty second of a wavelength.

A factor that simplifies the antenna design is that all satellites in the synchronous orbit lie very close to a single scan plane of the receiving antenna. Hence it is only necessary to achieve low sidelobe levels in a single scan plane. Figure 1.2 illustrates a number of satellites in the equatorial or synchronous orbit with satellite s located at a longitude ϕ_s relative to a ground station.

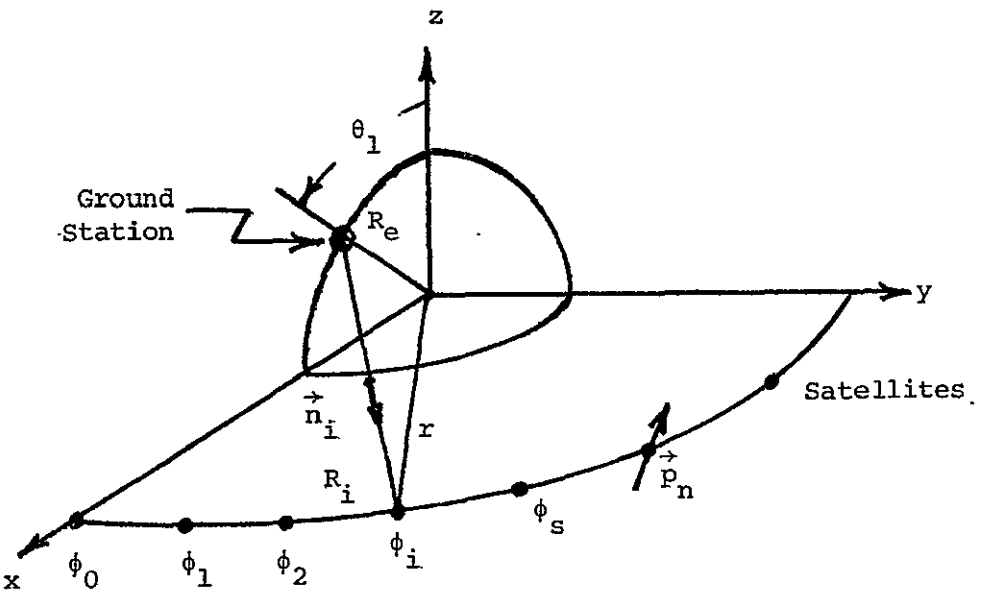

Figure 1.2 Satellites in an equatorial orbit.

Figure 1.3 shows the azimuth and polar positions ϕ and θ of a satellite located at ϕ_s as seen by a ground station antenna located at a latitude of 41.5° (Cleveland, Ohio location) and having its antenna pointed at a satellite with relative longitude ϕ_i of 0° or 30°. As may be seen from Figure 1.3 all viewable satellites are within 10° of a fixed scan plane of the receiving antenna, in particular for satellites within $\pm$ 20° of the desired satellite being viewed, the satellites are less than 2° away from a fixed scan plane of the receiving antenna. There is a small polarization mismatch introduced between satellites not in the line of sight direction from the ground station and the receiving antenna, but this effect is small as shown in Figure 1.4. The derivation of the formulas leading to the results shown in Figures 1.3 and 1.4 is given in Appendix I.

Chapter II of this report reviews past work on sidelobe reduction techniques as applied to paraboloidal antennas with the emphasis placed on prime focus feed design. Chapter III describes the Kumar feed which was chosen for a detailed evaluation. Also discussed in this chapter is the effect of certain types of systematic paraboloidal contour errors on the sidelobe level of paraboloidal antennas. Chapter IV presents experimental results obtained using a Kumar feed and commercially available 4 and 6 foot diameter paraboloidal reflectors.

The final chapter, Chapter V, summarizes the findings and makes a number of recommendations for future consideration and investigation.

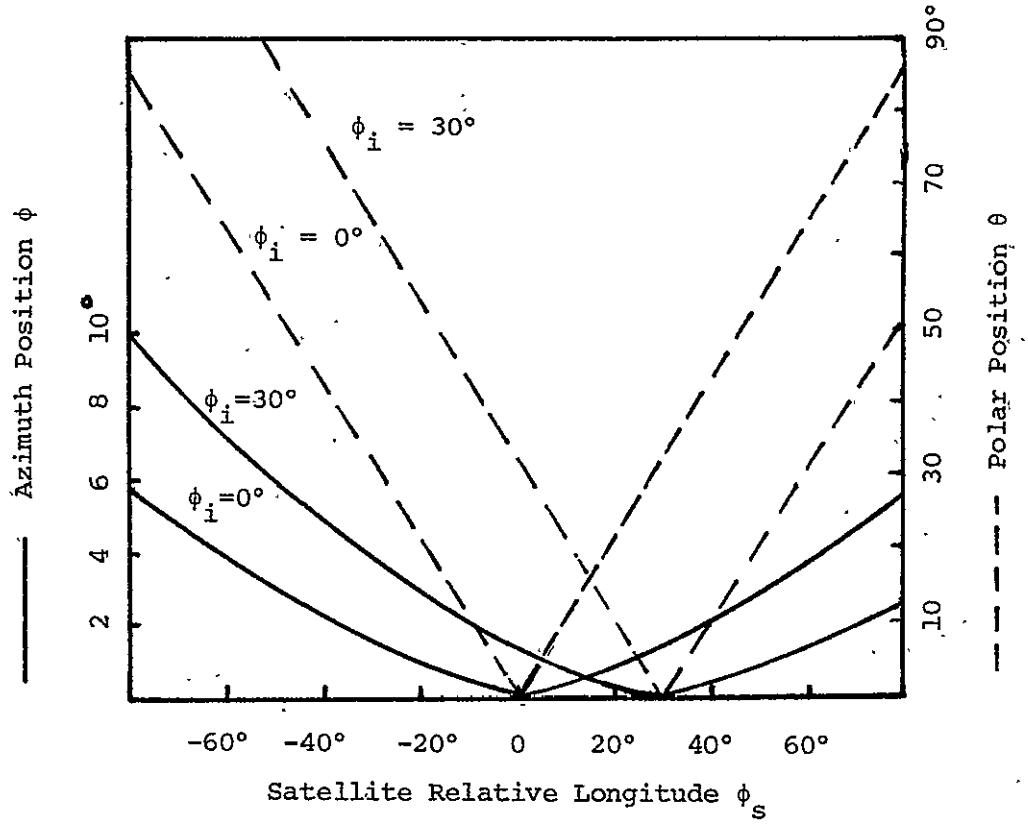

Figure 1.3 Satellite position as seen by receiving antenna, ϕ=0 corresponds to H-plane of antenna. $\phi_s = \phi_i$, θ = 0 is receiving antenna axis. ϕ_i is relative longitude receiving antenna is pointed in. $|\phi_s| > 78.35°$ is below the horizon.

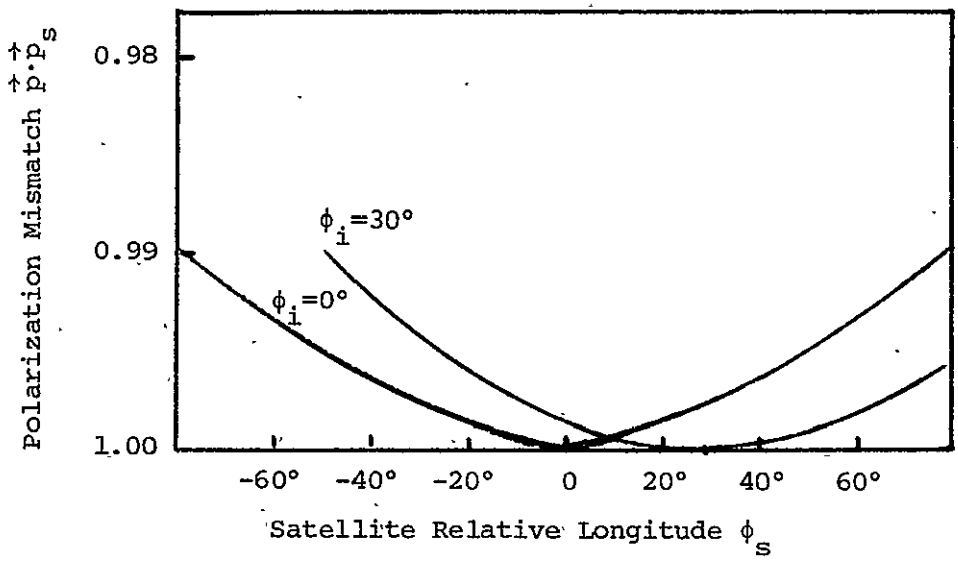

Figure 1.4 Polarization mismatch.

CHAPTER 2

REVIEW OF PAST WORK ON SIDELOBE REDUCTION TECHNIQUES

2.1 Introduction

The evaluation of the far zone radiated field from a paraboloidal reflector antenna may be done in terms of the induced currents on the paraboloidal surface or in terms of the tangential electric field distribution over a plane aperture surface in front of the reflector. In either case, the induced currents or aperture field is determined using ray optics concepts. For paraboloids that are many wavelengths in diameter both methods yield essentially the same results and are generally considered to give accurate results for the main diffraction lobe and the near-in sidelobes. For a linearly polarized aperture field described by a function $f(\rho,\phi)$ it may be shown that the radiated electric field is given by (11,12)

$$\vec{E}(\vec{r}) = \frac{jk_o}{2\pi r} \cos\theta \, e^{-jk_o r} \int_0^{2\pi} \int_0^{a} f(\rho,\phi') e^{jk_o \rho \sin\theta \cos(\phi-\phi')} \rho \, d\rho \, d\phi' \qquad (2.1)$$

where $k_o = 2\pi/\lambda_o$, λ_o the wavelength, a is the radius of the aperture, and θ is the polar angle and ϕ is the azimuth angle shown in Figure 2.1. The integral is a two dimensional Fourier transform of the aperture field and consequently the radiation pattern, including the sidelobes, is determined by the aperture field distribution function $f(\rho,\phi)$. If the aperture field has circular symmetry (2.1) becomes

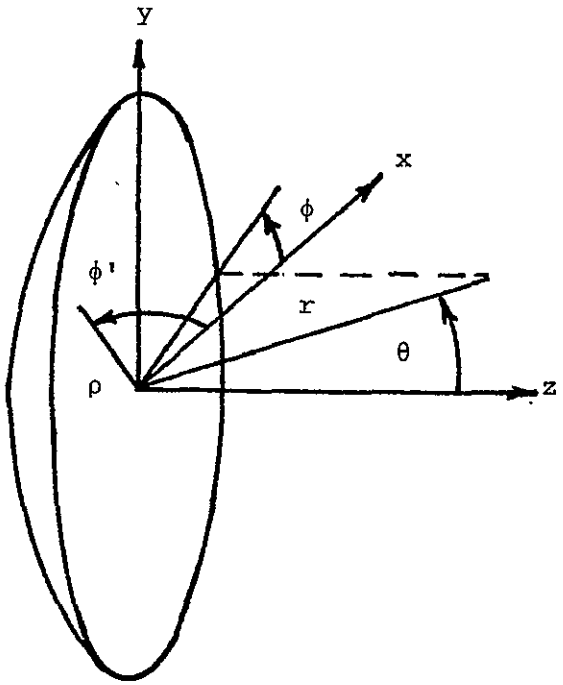

Figure 2.1 Paraboloidal Antenna

$$\vec{E}(\vec{r}) = \frac{jk_o}{2\pi r} \cos\theta \, e^{-jk_o r} \, 2\pi \int_0^a f(\rho) \, J_o(k_o \rho \sin\theta) \, \rho d\rho \qquad (2.2)$$

where J_o is the Bessel function of the first kind and order zero.

The maximum power flux per unit solid angle occurs at $\theta = 0$ when $f(\rho)$ is a real function and is given by

$$P = \frac{k_o^2}{2Z_o} \left[\int_0^a f(\rho) \, \rho d\rho \right]^2 \qquad (2.3)$$

where $Z_o = 377$ ohms is the intrinsic impedance of free space. In order to estimate the gain or directivity of the antenna, it is commonly assumed that the aperture field is well approximated by a plane wave and the total power through the aperture surface is evaluated by the following expression:

$$P_r = \frac{I}{2Z_o} \int_0^a \int_0^{2\pi} |f(\rho,\phi)|^2 \rho d\rho \qquad (2.4)$$

The directivity D of the antenna is then given by

$$D = 4\pi \frac{P}{P_r} = \frac{8\pi^2}{\lambda_0^2} \frac{\left(\int_0^a f(\rho)\rho d\rho\right)^2}{\int_0^a f^2(\rho)\ \rho d\rho} \qquad (2.5)$$

for a circular symmetric aperture field. In the case of a uniform aperture field $D_m = (4\pi/\lambda_0^2)\pi a^2$ and this represents the maximum directivity obtainable from all constant phase aperture fields. The ratio D/D_m gives the aperture illumination efficiency.

The sidelobe level is primarily determined by the aperture field distribution. By tapering the aperture field towards the edge lower sidelobes are obtained but at the expense of reduced directivity. Other factors that play a significant role in determining the sidelobe level below -30 dB. are feed blockage, scattering from the feed support structure, and error in the countour of the reflector surface. The overall antenna gain is influenced by the aperture illumination efficiency, feed spill over loss, cross-polarization loss, and feed ohmic losses. The design of an antenna with low sidelobes must take all of these factors into account as well as those pertaining to mechanical simplicity and low cost.

There are essentially two approaches that may be followed to reduce the sidelobe level. One is to design a feed that will produce an aperture field distribution that results directly in a radiation field pattern with low sidelobes and the other is to modify the reflector surface in such a way that a cancellation of undesired high level sidelobes is achieved.

Both of these approaches have been investigated by many authors and this work is reviewed in the following sections.

2.2 Sidelobe Reduction By Amplitude Tapering

It is well known that the sidelobe level can be reduced by tapering the aperture field distribution towards the edge of the aperture (11). Paraboloidal antenna feed systems are commonly designed to produce from 10 to 12 dB. of tapering at the edge of the reflector since this leads to maximum gain. By increasing the taper beyond this value the illumination efficiency decreases faster than the reduction in spill over loss so the overall gain decreases. The amount of taper alone does not determine the sidelobe level that can be achieved or the resultant gain since this depends on the amplitude variation across the whole aperture. Some feed designs producing the same amount of edge taper will yield higher illumination efficiencies, and thus a larger gain, as well as lower sidelobe levels and cross polarization. Various models for the amplitude distribution over a circular aperture have been studied and these serve the useful purpose of indicating typical results that could be expected in practice. Two models are described below in order to illustrate the need for a relatively large amount of tapering in order to achieve sidelobes below -30 dB. These models also show that the loss in gain incurred by increasing the taper to 20 dB is not serious.

The properties of a circular aperture with a truncated Gaussian amplitude distribution of the form

$$f(\rho) = e^{-\alpha\rho^2}, \quad \rho \leq a \tag{2.6}$$

was first studied by Ramsay (13). Further calculations of gain, sidelobe

level, illumination efficiency, etc. using this model have been carried out by Goebels, et. al. (14). The results of this investigation are shown in Fig's. 2.2 and 2.3 as a function of edge taper in dB. The edge taper is given by

$$- 20 \log [f(a)/f(0)] = \alpha a^2 \log e \qquad (2.7)$$

Figure 2.2 shows that maximum efficiency, and hence gain, occurs for 10 to 12 dB. of taper. With 20 dB. of taper the loss in gain is about 0.6 dB. Figure 2.3 shows that 20 dB. of tapering will yield a first sidelobe below - 40 dB. and a second sidelobe below - 35 dB. By contrast with 10 dB. of tapering both the first and second sidelobe levels are above -30 dB. Thus increasing the amount of tapering from 10 dB. to 20 dB. reduces the sidelobes to below - 35 dB. at a penalty of a modest 0.6 dB. loss in gain.

A second model that yields similar results are aperture fields described by the following family of functions:

$$f(\rho) = A + (1-A)\ (1 - \rho^2/a^2)^n \qquad (2.8)$$

The constant A determines the amount of edge taper and n controls the rate of tapering. Figure 2.4 shows some results obtained using this model (2). With 20 dB. of taper i.e. A = 0.1, and $n \geq 2$ sidelobes below -35 dB. are obtained. Again the loss in gain in increasing the taper from 10 dB. to 20 dB. is less than 1 dB.

From a theoretical point of view it appears that the use of a feed producing around 20 dB. of taper in the aperture field distribution can reduce the sidelobe level to below -35 dB. In practice, other factors

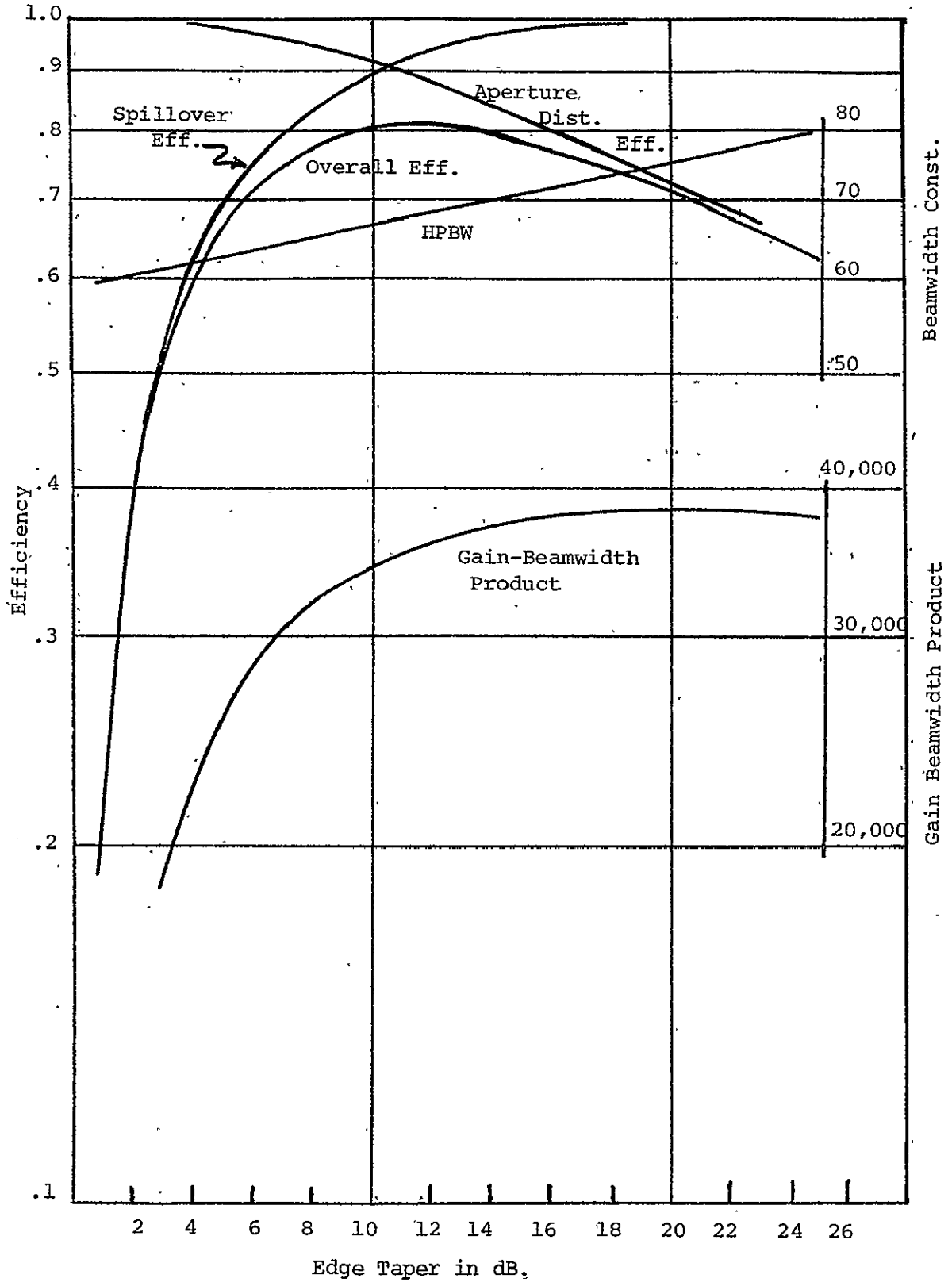

Figure 2.2 Properties of a circular aperture with a truncated gaussian amplitude distribution. (From Goebels 14).

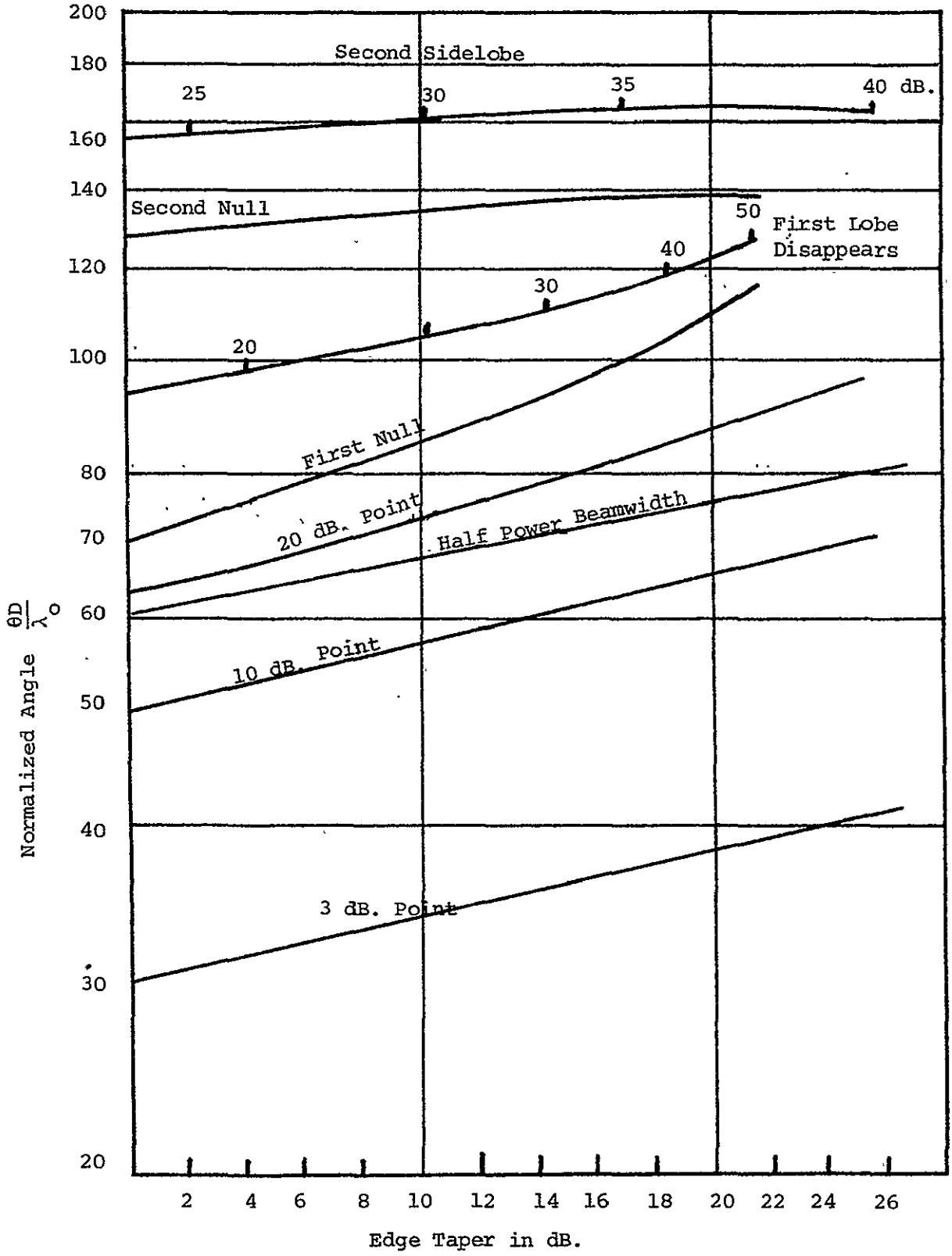

Figure 2.3 Properties of a circular aperture with a truncated gaussian amplitude distribution (From Goebels 14).

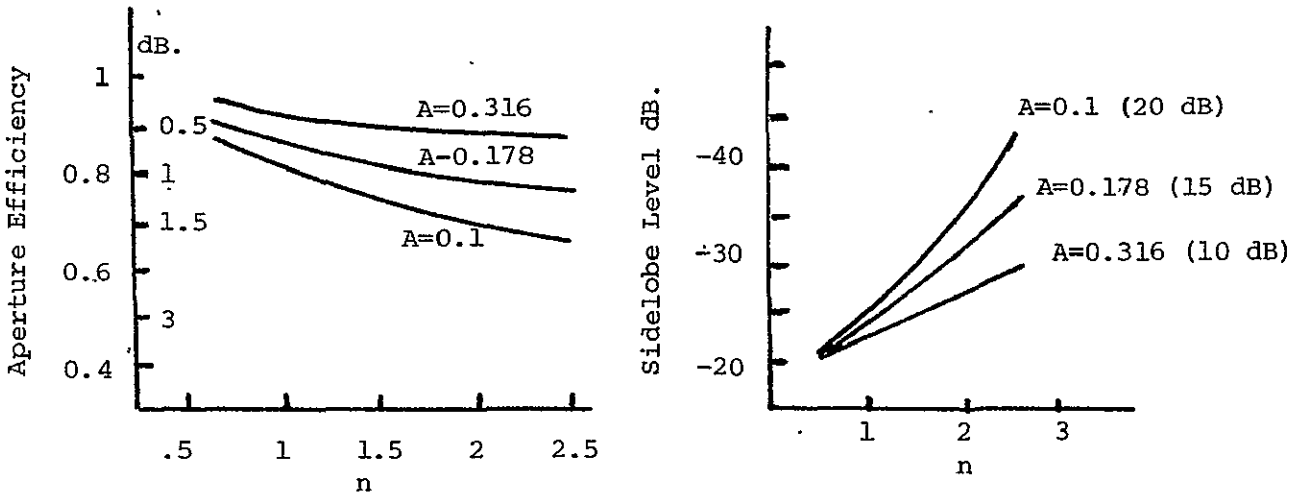

Figure 2.4 Properties of a circular aperture with aperture field distribution $A + (1-A)(1-r^2)^n$

enter in that result in higher sidelobe levels and lower gains than those predicted by these ideal models. Aperture field phase errors introduced by errors in the reflector surface contour and feed positioning errors will increase the sidelobe level and reduce the gain. The presence of cross-polarized radiation will also reduce the gain.

2.3 Prime Focus Feeds

A common type of prime focus feed of World War II vintage is the "button-hook" waveguide feed (11). With this type of feed the waveguide may be flared at the end into a small pyramidal horn in order to increase the aperture field taper. This type of feed is often used in currently produced low cost antennas. Generally this type of feed produces a fairly high level of cross-polarized radiation in planes

45° to the principal E and H-planes of the antenna. When it is designed to give about 10 to 12 dB. of taper the sidelobe level is around -22 dB. The design of this type of feed is treated in detail in a paper by Rudge and Withers (15).

A considerable amount of work has been carried out in recent years on improved designs for prime focus feeds. A comprehensive and detailed review of much of this work has been given by Clarricoats and Poulton (16) and hence the review given here will be quite brief. The theoretical basis for much of the new developments on prime focus feeds was carried out many years ago. Rumsey investigated the requirements for a circular horn to yield equal E and H-plane beamwidths and pure circular or linear polarization (17). It was found that the field in the horn was a combination of the TE and TM modes, i.e., a hybrid mode, with boundary conditions that cannot be satisfied by a perfectly conducting surface. By using a corrugated surface the required surface impedance boundary condition could be established. Minnett and Thomas further substantiated the need for hybrid modes in a conical horn in order to achieve equal E and H-plane patterns with no cross polarization (18,19). Their approach was to examine the structure of the field in the focal plane when a linearly polarized plane wave is incident on the paraboloid along the axial direction. Prior to the above work Kay described a corrugated conical horn with the desired radiation properties and referred to this as a scalar feed (20). Potter also showed that hybrid modes in a conical horn would produce a rotationally symmetric pattern with low sidelobes (21).

A number of investigators have further developed the theory and design of hybrid mode horns and corrugated conical horns and circular

waveguides for use as prime focus feeds. A dual mode horn for use in sattllite systems was described by Ajioka and Harry (22). The use of several modes in a circular waveguide to control the radiation pattern was described by Ludwig (23). It was shown that a feed using four modes and illuminating a paraboloid with angular aperture of 120° gave an experimental efficiency of 82% (including spill over losses and aperture blockage). The optimization of corrugated feed horns was treated by Vu (24). Narashiman and Rao presented solutions for hybrid modes in conical corrugated horns (25). Knop and Weissenforth showed that a corrugated circular waveguide excited with a hybrid HE_{11} mode resulted in a feed with higher efficiency and lower cross polarization than a conventional circular waveguide feed (26). An experimental model of a low noise dual hybrid-mode corrugated horn was described by Vu and an overall antenna efficiency of 80% was achieved including a spill over loss of 3.5% (27). A detailed study of the properties of corrugated feeds was carried out by Clarricoats and Saha (28). The diffraction patterns of wide flare angle horns of this type was also studied by Narasimhan and Rao (29). The theoretical performance of paraboloids using hybrid-mode prime focus feeds was studied by Thomas (30) as was the bandwidth properties of corrugated conical horns (31). Narasimhan and Malla have described a method to calculate the horn flare angle in order to achieve a specified sidelobe level for a paraboloid with a given f/D ratio (32). A high efficiency corrugated coaxial conical horn for use as a feed has been described by Vokurka (33). The use of a high efficiency scalar feed for a communication antenna is described by Kosky and Calla (34).

The above review of work on corrugated horns and waveguides is not exhaustive but is representative of what has been achieved. It has clearly established the principle that for low cross-polarization the radiation pattern must have rotational symmetry. This implies equal E and H-plane patterns. The feeds that will produce these characteristics must generate hybrid-modes in the feed aperture plane. By an appropriate combination of hybrid modes high aperture illumination efficiencies and low spill over can be achieved. Low sidelobes can be achieved in a paraboloidal antenna system by using an adequate amount of tapering, i.e., a highly directive feed. The use of corrugated circular waveguides or conical horns is one general approach to feed design that allows the desired results to be obtained. Useful design data for conical corrugated horns has been compiled by Chan (35). The cross section of a typical corrugated conical horn is shown in Figure 2.5.

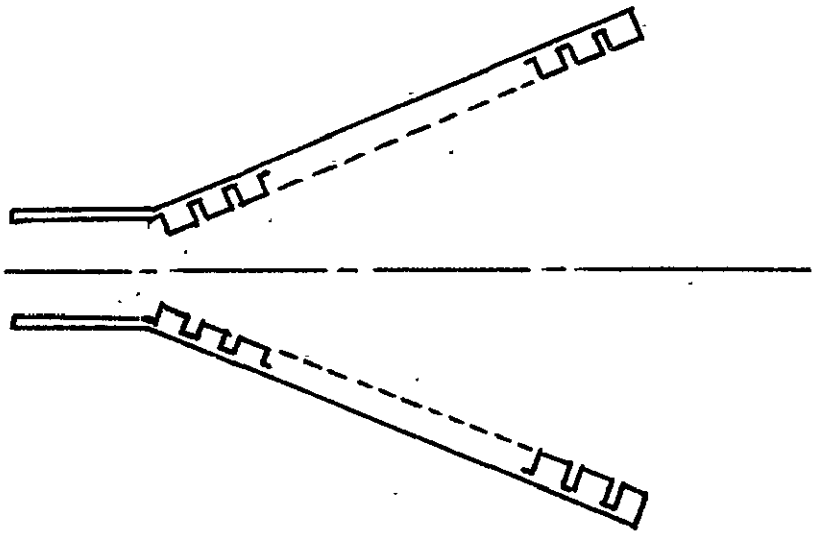

Figure 2.5 Cross-section of a corrugated conical horn.

In more recent years the research effort on feeds has shifted in the direction of developing simpler coaxial circular waveguide structures that will generate the appropriate mixture of hybrid modes in the aperture of the feed to yield the desired radiation pattern for illuminating paraboloidal reflectors. A number of relatively simple coaxial type structures have been developed that, when experimentally optimized, have lead to useful prime focus feeds.

Koch designed a coaxial type feed that could produce an aperture efficiency as high as 80% (36). The feed resulted in cross polarization not exceeding -40 dB. in the E and H-planes and below -35 dB. in the 45° planes. Scheffer designed a simpler coaxial feed that theoretically would also give an aperture efficiency of 80% with a paraboloid having an angular aperture of 140° (37). The actual measured efficiency was 70% which is higher than the theoretical value of 63% for a simple circular waveguide excited with the TE_{11} mode and used as a feed.

Figure 2.6 illustrates one of the coaxial type feeds considered by Scheffer and the resultant feed radiation pattern. The pattern is characterized by a dip in the axial direction and this results in a more uniform overall aperture field distribution over the aperture of a paraboloid reflector for a given amount of edge taper. In Figure 2.7 the theoretical aperture efficiency for coaxial type feeds is shown as a function of the angular aperture (calculations by Koch and for H_{11} mode excitation). It is noted that the largest increase in efficiency occurs in adding one coaxial ring to a circular waveguide. Additional rings improve the efficiency further but the increase for each additional ring added is less. By using multi-mode excitation even higher aperture efficiencies are obtained.

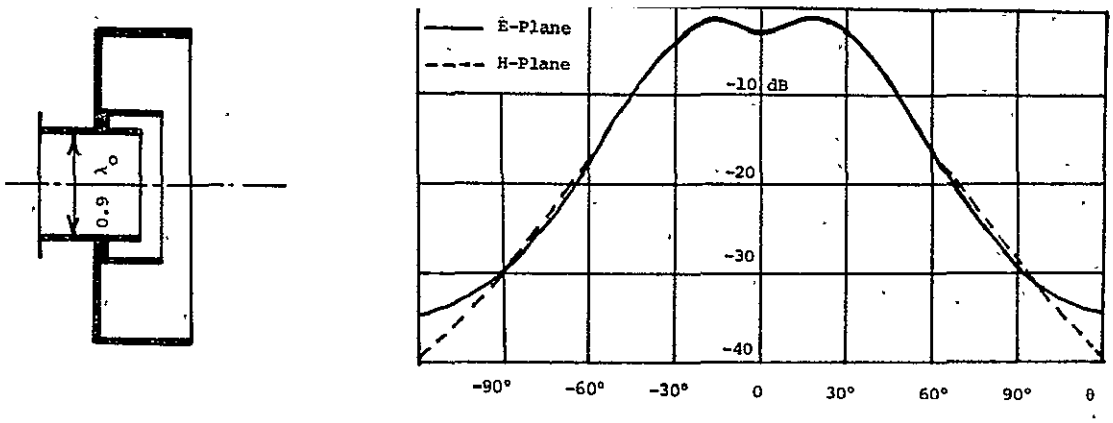

Figure 2.6 A coaxial feed and its radiation pattern as described by Scheffer (37).

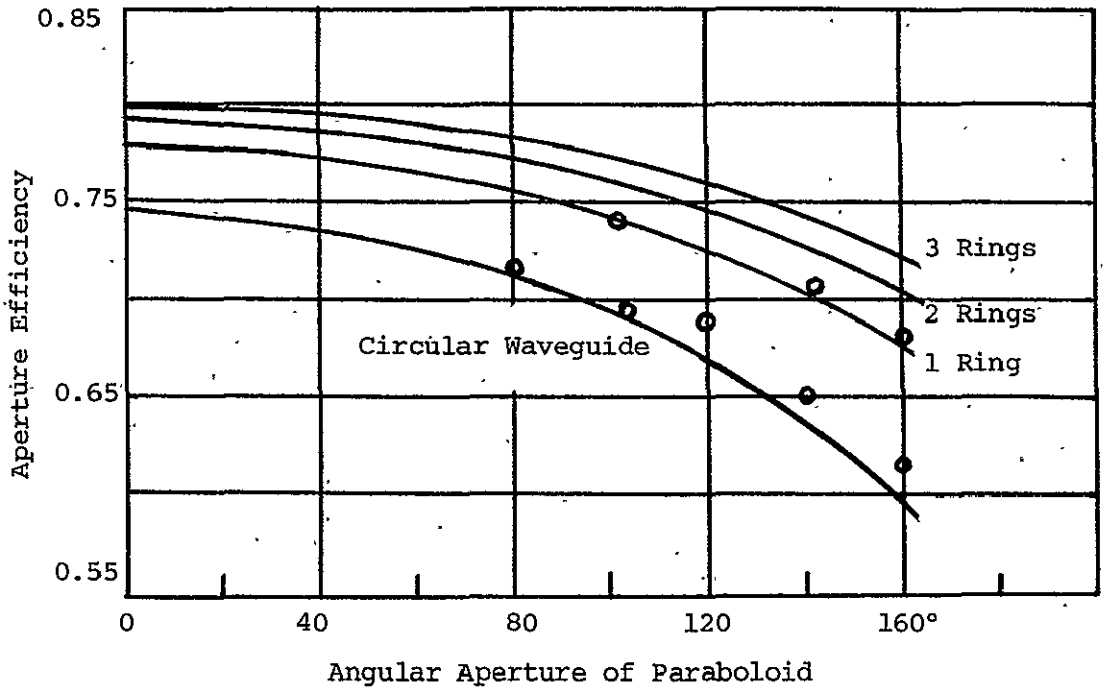

Figure 2.7 Aperture efficiency for coaxial feeds (after Koch 36) Small circles show measured values.

In order to evaluate the potential of a Scheffer type feed for producing low sidelobes when used with a 4 foot paraboloid with f/D equal to 0.375 the published radiation pattern was converted to an amplitude pattern and this was then converted to an aperture field distribution by multiplying by the inverse distance space attenuation factor. The resultant aperture field distribution is shown in Figure 2.8 and produces an edge taper of 20.9 db. The radiation pattern was computed numerically using (2.2) and the aperture efficiency was calculated by means of the method described in Sec. 2.1 of this report. It was found that the aperture efficiency was 64% when spill over losses were neglected. With more than 20 dB. of edge taper the spill over loss would be very small. The computed radiation pattern is shown in Figure 2.9 and shows a maximum sidelobe level of -31 dB. These results show that low sidelobes can, in principal, be obtained without a large sacrifice in overall antenna gain. In addition low cross polarization would be obtained because of the inherent circular symmetry in the feed radiation pattern.

Kumar has developed several coaxial type feeds that are useful for prime focus feeds. One feed developed by Kumar is similar to the feed described by Scheffer (38). In another design a series of corrugated rings are placed around the outside of a circular waveguide (39). A third design incorporated a dielectric rod extending beyond the front of a circular waveguide along with a coaxial cup around the outside (10). This latter type feed was the one chosen for use in the experimental work reported here and is described more fully in the next chapter.

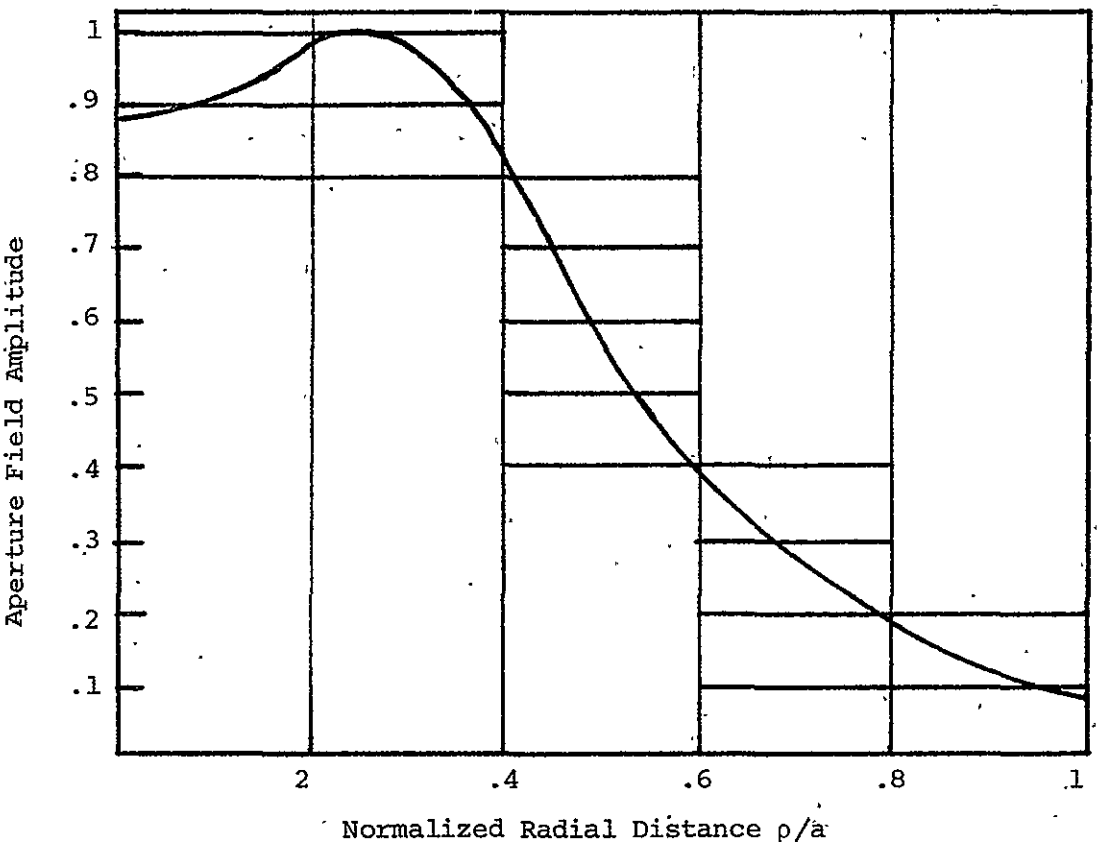

Figure 2.8 Computed aperture field distribution for the Scheffer Feed. Angular aperture of paraboloid is 135°.

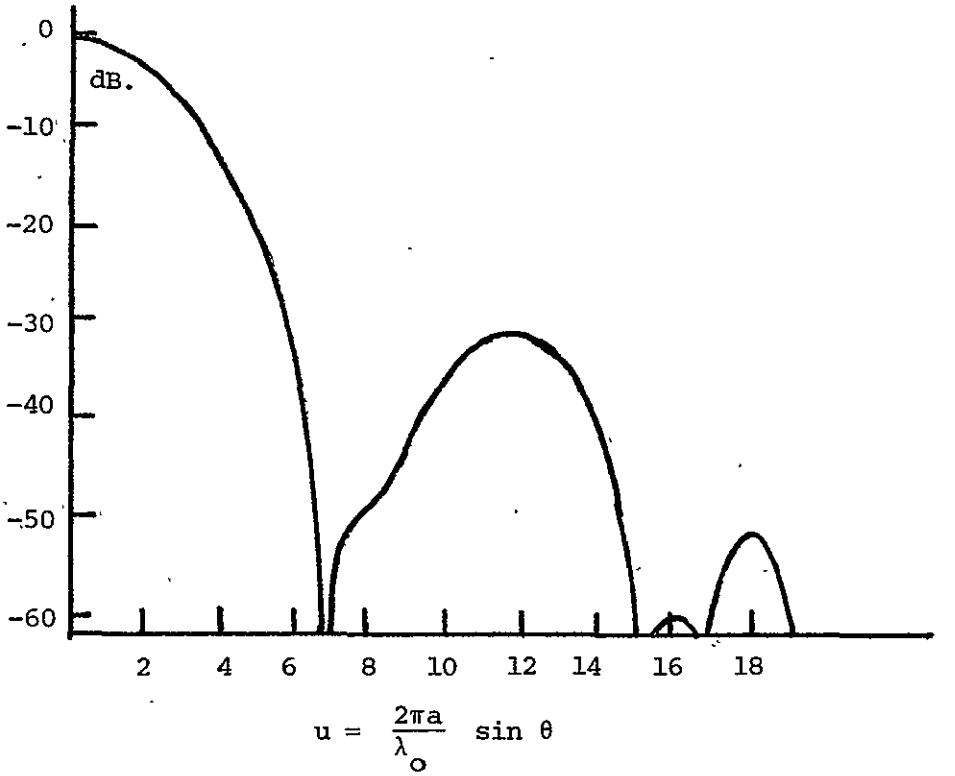

Figure 2.9 Computed radiation pattern for a circular aperture with amplitude distribution shown in Fig. 2.8 (Scheffer feed).

A circular waveguide feed with four choke type outer rings has been studied by Wohleben, Mattes, and Lochner (40). This feed is similar to the one described by Kumar and is useful for paraboloids with f/D less than 0.35. Choke type flanges have also been used to improve the performance of pyramidal horns (41).

A type of feed that is of interest from the point of view of not requiring support rods is the splash-plate feed. Very little work on feeds of this type has been carried out although there has been some recent attention given to splash-plate feed design(41,42). A major problem with splash-plate feeds is the difficulty of obtaining a low VSWR because of strong reflections back into the feed waveguide.

2.4 Absorber Arrays and Phase Reversal Plates

When the objective is to reduce the sidelobes in a single scan plane of the antenna an alternative method to reduce the sidelobes is to introduce some modification in the reflector surface such that a cancelling field is radiated. The viability of such a method depends on the amount of sidelobe cancellation required and if one design is to work for a series of antennas of a particular type the manufacturing tolerances must be such that the sidelobe patterns are reproducible from one antenna to the next. In general this tends to place a requirement on the antenna tolerances that are just as stringent as those required for low sidelobes using a feed producing a large edge taper. Also the loss in gain is about the same as that which occurs by increasing the edge taper to 20 dB. In principle, reflector modifications can be introduced that cancel or reduce the sidelobes in more than one plane but the design of such systems can become quite

complex if the sidelobe pattern departs appreciably from one with circular symmetry. The two simplest modifications that can be made consists of the use of absorber pads placed on the reflector surface or the use of small reflector plates located an effective quarter-wavelength in front of the paraboloidal surface so as to introduce the required 180° phase change.

The use of absorber rings on a paraboloid to reduce the sidelobe amplitude was considered by Goebels et al (14) but the most extensive study of the use of absorber pads in a two-element array configuration was carried out by Albernaz (2,44). The configuration considered by albernaz is illustrated in Figure 2.10. It consists of two pads of absorbing material whose

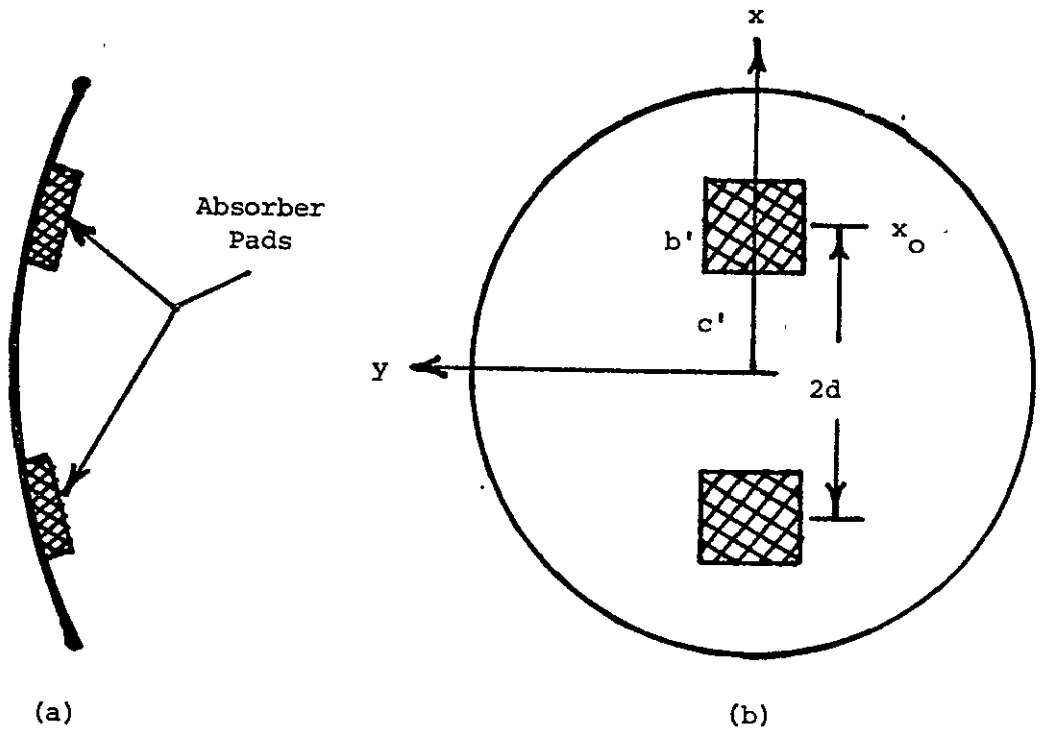

Figure 2.10-(a) Edge view of absorber pads on a paraboloid reflector, (b) Projection of absorber pad area onto aperture surface.

projected dimensions on the aperture surface are b', c' and with a center-to-center spacing of 2d. The effect that these absorber pads have is to reduce the amplitude of the aperture field to zero over the projected area S_a of the absorber pads. This change in the aperture field distribution results in a modification of the original radiation field that may be determined by computing the field radiated by two pads with an amplitude distribution which is the negative of that existing over the area S_a in the absence of the pads and adding this to the original unperturbed radiation field.

The field radiated by the absorber pad array may be computed using (2.1) and is given by

$$\vec{E}(\vec{r}) = -\frac{jk_o}{2\pi r}\cos\theta\, e^{-jk_o r}\int\int_{S_a} f(x,y)e^{jk_x x+jk_y y}\,dxdy \qquad (2.9)$$

where $k_x = k_o \sin\theta\cos\phi$ and $k_y = k_o \sin\theta\sin\phi$. If the original sidelobes are at least 25 dB. below the main lobe the size of absorber pads needed are small enough that f(x,y) may be approximated by its value at the center of each pad. Thus (2.9) reduces to

$$\vec{E}(\vec{r}) = -\frac{jk_o}{2\pi r}\cos\theta\, e^{-jk_o r}\, 2b'c'\, f(x_o,0)\,\frac{\sin k_x\frac{b'}{2}}{k_x\frac{b'}{2}}\,\frac{\sin k_y\frac{c'}{2}}{k_y\frac{c'}{2}}$$

$$\times\cos k_x d \qquad (2.10a)$$

In the xz or $\phi = 0$ plane this expression simplifies to

$$\vec{E}(\vec{r}) = -\frac{jk_o}{2\pi r}\cos\theta\, e^{-jk_o r}\, 2b'c'\, f(x_o,0)\,\frac{\sin(k_o\frac{b'}{2}\sin\theta)}{k_o\frac{b'}{2}\sin\theta}\cos(k_o d\sin\theta) \qquad (2.10b)$$

The significant factor in this field pattern is the two element array factor $\cos(k_o d \sin\theta)$ which produces an essentially cosinusoidal oscillation in the pattern. The spacing d must be chosen such that the period of this oscillation will result in the absorber array field to always add out of phase with the original sidelobe pattern. It is generally not possible to achieve complete alignment of the peaks of the absorber array pattern with those of the original sidelobe pattern. The envelope function $\sin(k_o \frac{b'}{2} \sin\theta)/(k_o \frac{b'}{2} \sin\theta)$ represents a rather broad lobe when b' is small and will reudce the absorber array pattern to zero at $\sin\theta = \lambda_o/b'$. Beyond this angle the absorber array field remains small. The field from the absorber array along the boresight direction $\theta = 0$ always subtracts from the original field and thus reduces the gain of the antenna. Since the power radiated by the feed has not changed by using an absorber array the loss in gain can be computed directly in terms of the reduction in the field along the boresight direction. As an example, consider an antenna with a normalized maximum radiated field amplitude of unity. A close-in sidelobe of -23 dB. would have an amplitude of 0.0707. In order to reduce this sidelobe to a level of - 36 dB. (normalized amplitude of 0.0158) a cancelling field of amplitude 0.055 is required. This results in a gain reduction by a factor $0.945^2 = 0.89$ or 0.49 dB.

In order to illustrate the design procedure for an absorber array consider a circular aperture with an aperture field distribution $0.316 + 0.684\ (1 - \rho^2/a^2)^2$ corresponding to 10 dB. of edge taper. The normalized radiated field is

$$E_o = \frac{2\pi}{0.427} \int_o^a [0.316 + 0.684 \ (1 - \frac{\rho^2}{a^2})^2] \ \rho \ J_o(k_o \ \rho \ \sin \theta) d\rho$$

$$= \frac{2\pi a^2}{0.427} \ [\ 0.316 \ \frac{J_1(u)}{u} \ + 5.472 \ \frac{J_2(u)}{u^3} \ ] \qquad (2.11)$$

where $u = k_o a \sin \theta$ and 0.427 is a normalization constant. The corresponding absorber array pattern is given by

$$E_A = - \ [0.316 + 0.684 \ (1 - \frac{d^2}{a^2})^2 \ ] \ \frac{2b'c'}{0.427} \ \frac{\sin u \frac{b'}{2a}}{u \frac{b'}{2a}} \cos u \frac{d}{a} \qquad (2.12)$$

The sidelobe pattern from (2.11) is shown in Fig. 2.11 along with the absorber array pattern and the resultant compensated pattern. The radius a was chosen as 0.5m and the spacing 2d was chosen equal to $\pi a/2.5$ in order to align the absorber array pattern with the sidelobe pattern for the two nearest sidelobes. A maximum normalized absorber array field amplitude of 0.04 was chosen so, from (2.12),

$$b'c' = \frac{0.427 \times 0.04}{2[0.316 + 0.684 \ (1 - \frac{\pi^2}{25})^2 \ ]} = 0.0151$$

For b' = c' it is then required that each pad be 12.27 cm. on a side. For this example, the first sidelobe is reduced from - 27 dB. to -35 dB. and the second sidelobe is reduced from - 30.5 dB. to - 40 dB. However since the lobe alignment is not perfect the 3rd and 4th sidelobes are increased to about - 28 dB. The loss in gain is 0.35 dB. If the amplitude of the compensating field is reduced by a factor of two then the first sidelobe is reduced to - 31 dB. and all other sidelobes remain

below this level. This example shows that for a simple two-element array it is usually difficult to reduce the first few sidelobes by more than a few dB. without increasing the further out sidelobes to undesirable levels because of not being able to align all of the absorber array lobes with the sidelobe peaks to achieve cancellation for all lobes. In principle a multi-element absorber array could be designed to achieve better overall cancellation but at the expense of greater complexity.

It should be clear that absorber arrays produce fields that are either in phase or out of phase with the field in the boresight direction. Thus, if some of the sidelobes have a significantly different phase because of phase errors introduced from contour errors in the reflector or feed displacement from the focus the degree of cancellation will be less.

The use of microwave absorber pads in practice would require a radome covering since the absorbing material is not very resistant to weathering. An alternative to the use of microwave absorber pads is the use of small reflector plates of thickness t as shown in Figure 2.12. In order to achieve a phase reversal in the radiated field the required thickness t must be chosen according to the relationship

$$t = \frac{\lambda_o}{4} \sec \frac{\theta}{2} \qquad (2.13)$$

as reference to Figure 2.12 shows. Since the reflectors do not absorb the incident radiation but re-radiates it with a phase reversal the compensating field is twice as large as that produced by absorber pads

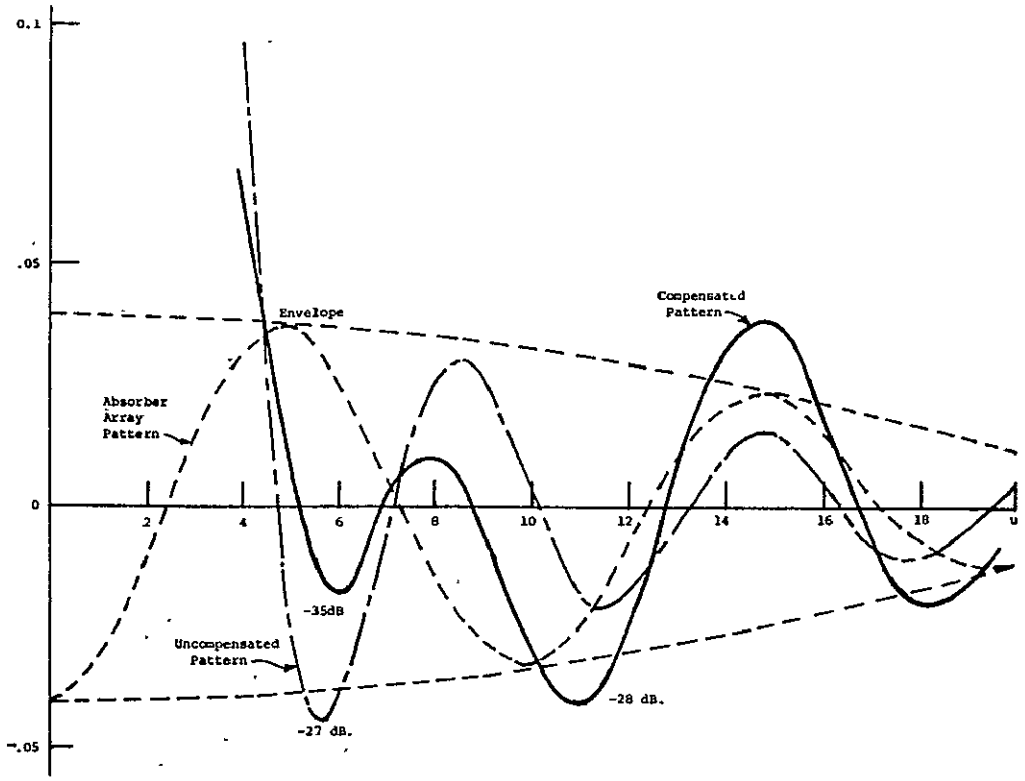

Figure 2.11 Illustration of sidelobe reduction using absorber pads.

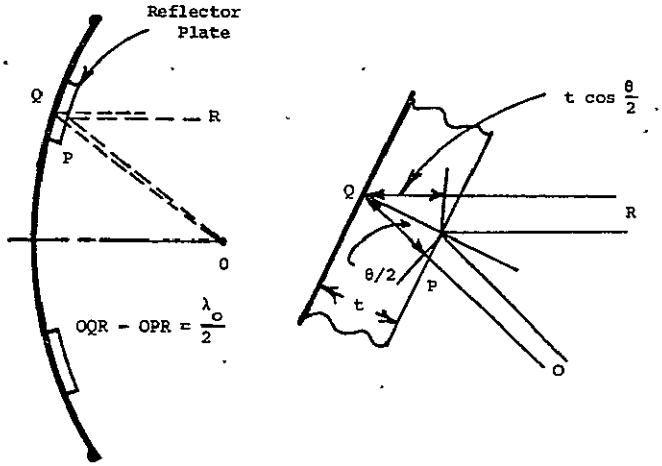

Figure 2.12 Edge view of phase reversal plates on a paraboloid.

with the same area. Consequently the field radiated by two phase reversal plates in an array like that shown in Fig. 2.10 is given by (2.10) multiplied by a factor of two. Reflector plates can also be used to produce a compensating field with arbitrary phase by choosing the thickness t appropriately. The plates can, of course, be made from sheet metal and mounted to the paraboloid surface using spacers. Because of diffraction effects, (2.10) should be regarded only as a first approximation to the field radiated by the reflector-plate array, particularly for small plates.

Williams considered the use of phase reversal aperture rings to reduce the close-in sidelobes for paraboloids with circularly symmetric illumination (45). He noted that it was difficult to cancel several lobes using a single ring (equivalent to using a two-element reflector-plate array for sidelobe cancellation in a single plane). By using a combination of four rings the first three sidelobes could be reduced to below -37 dB. but a far out sidelobe of - 28 dB. was then produced and the loss in gain was 2.2 dB. Williams suggested the use of a waveguide lens with 180° phase shifters in the appropriate waveguide sections as a means of implementing the concept. A simpler way would be to place phase-reversal rings of the correct thickness t on the paraboloid. Figure 2.12 can be viewed as a cross-section of a paraboloid with one phase-reversal ring.

CHAPTER 3

KUMAR FEED AND THE EFFECT OF PARABOLOIDAL CONTOUR ERRORS

3.1 Kumar Feed

The objective of the work undertaken was to choose the most promising method to achieve sidelobes at least 5 dB. below the CCIR model patterns. After evaluating the existing methods for sidelobe reduction it was concluded that the most promising approach was to use a high efficiency hybrid-mode feed producing around 20 dB. of edge taper. The two paraboloidal reflectors that were to be used had a f/D ratio equal to 0.38 and hence an angular aperture of 133°. The Kumar feed as described in the literature (10) appeared to have the desired radiation pattern and met the requirement of also being simple and economical to fabricate.

A simplified drawing of the Kumar feed is shown in Figure 3.1. The dimensions were obtained by scaling the feed dimensions given by Kumar for operation at 8.86 Ghz. to a new frequency of 12.1 Ghz. Thus all dimensions were reduced by the factor 8.86/12.1 = 0.7322. The feed consists of a circular waveguide with a protruding dielectric rod and a coaxial cup placed around the protruding dielectric rod.

The radiation pattern, as measured by Kumar, at a frequency of 8.5 Ghz. is shown in Figure 3.2. The cross polarization was measured and found to be below -33 dB. It was also found that the feed had a constant and equal E and H-plane phase center for polar angles up to 70° off axis. The phase center was 0.005m behind the front surface of the coaxial cup.

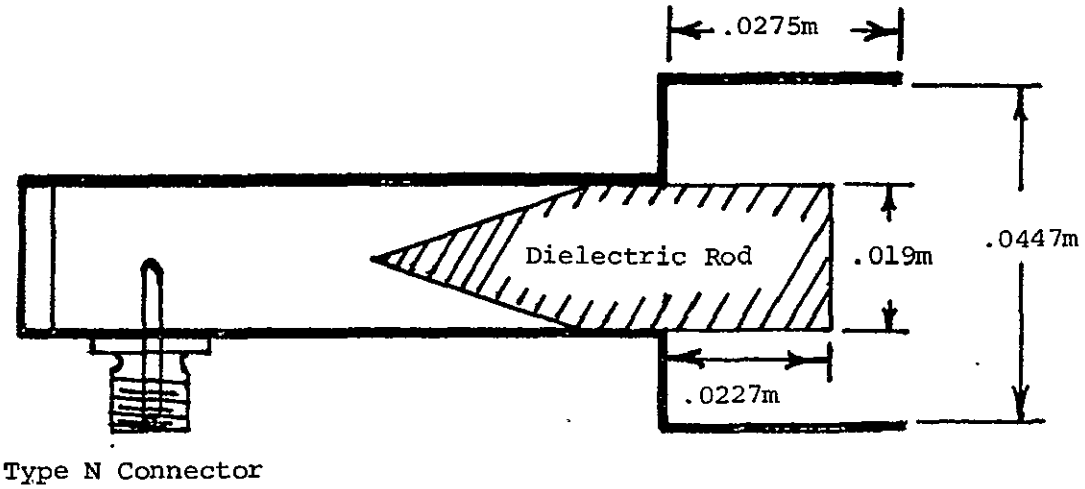

Figure 3.1 Simplified drawing of Kumar feed.

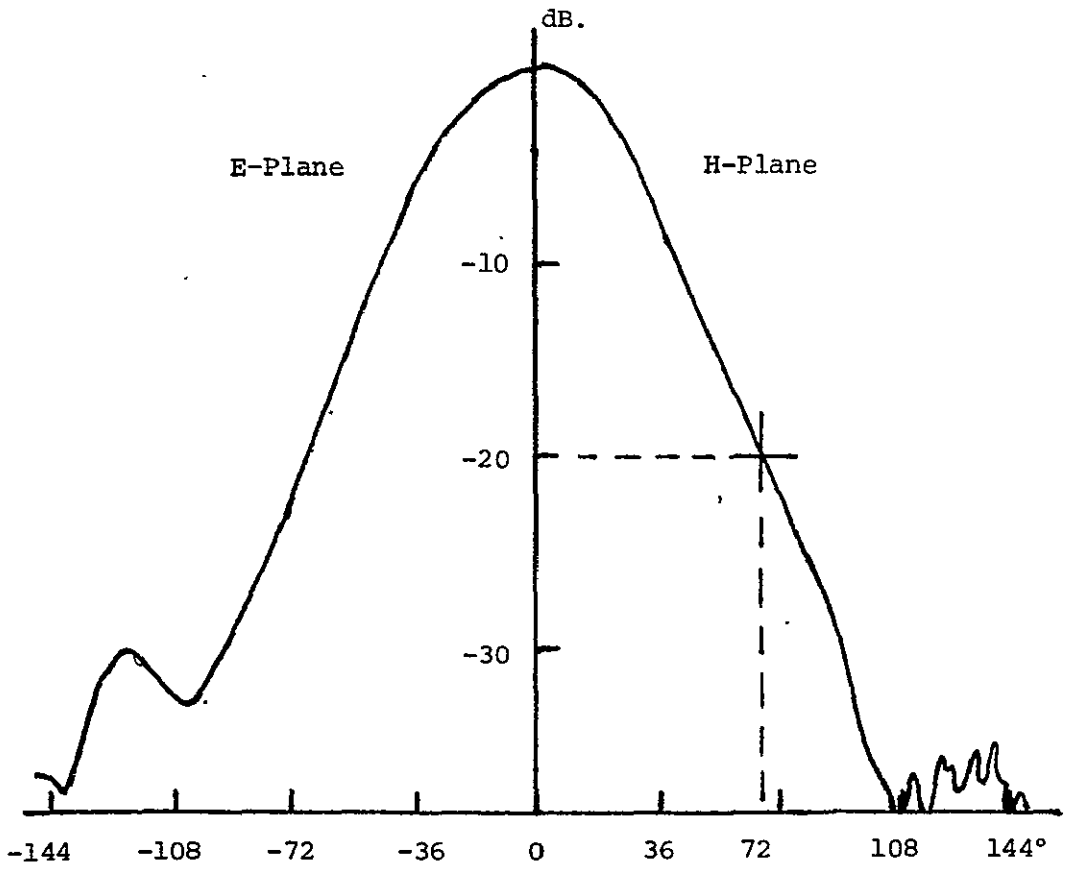

Figure 3.2 Radiation pattern of Kumar feed (10).

In order to evaluate the potential use of the Kumar feed the published radiation pattern was converted to an amplitude pattern and after multiplying by the inverse distance attenuation factor the aperture field distribution was found to be described with good accuracy by the following polynomial

$$f(x) = 1 - 3.15x^2 + 3.88x^4 - 1.655x^6 \qquad (3.1)$$

where $x = \rho/a$ is the normalized radial coordinate. The radiation pattern from this aperture field was evaluated numerically using a TI-59 programmable calculator (see Appendix II) and is shown in Figure 3.3. The pattern function can also be found in analytical form and is given by

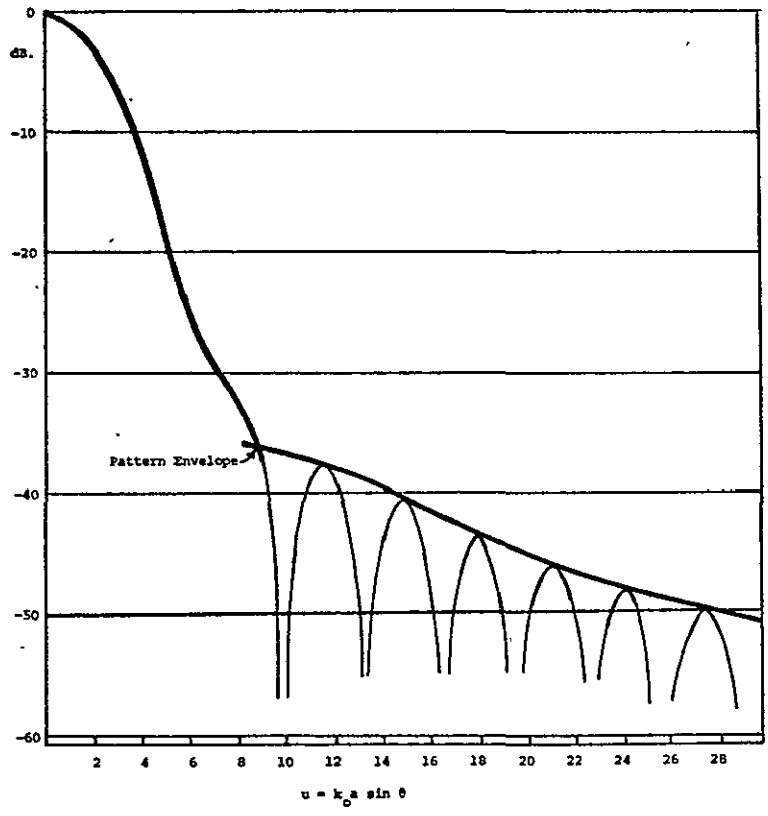

Figure 3.3 Computed radiation pattern for Kumar feed.

$$\int_0^1 f(x)\ x\ J_o(ux)\,dx = 0.075\ \frac{J_1(u)}{u} + 0.71\ \frac{J_2(u)}{u^2}$$

$$- 8.68\ \frac{J_3(u)}{u^3} + 79.44\ \frac{J_4(u)}{u^4} \qquad (3.2)$$

This expression was evaluated at selected points and verified that the numerical evaluation was accurate to within a small fraction of a dB. The computed radiation pattern shows that the largest sidelobe is -36.7 dB. below the main lobe. The 3 dB. beamwidth is 1.7° and the computed aperture efficiency was 60.75%.

A series of patterns were measured for the Kumar feed shown in Figure 3.1 at a frequency of 12 Ghz. and for various positions of the dielectric rod. The measured H-plane patterns are shown in Figure 3.4 and show that the patterns broaden as the dielectric rod is moved further out from the circular waveguide. The E-plane patterns are shown in Fig. 3.5 and were found to be essentially independent of the position of the dielectric rod. Equal E and H-plane patterns are obtained when the dielectric rod is positioned according to the design value shown in Figure 3.1 (approximately 4.8 mm (3/16")) as may be seen by reference to Figure 3.5.

3.2 The Effect of Paraboloidal Contour Errors on Sidelobe Level

When the radiation patterns of a 1.22m (4 foot) and a 1.83m (6 foot) paraboloid reflector illuminated with a Kumar feed were measured the sidelobe level was much higher than expected and the main lobe was considerably broader at the base than the theory predicted. The paraboloids

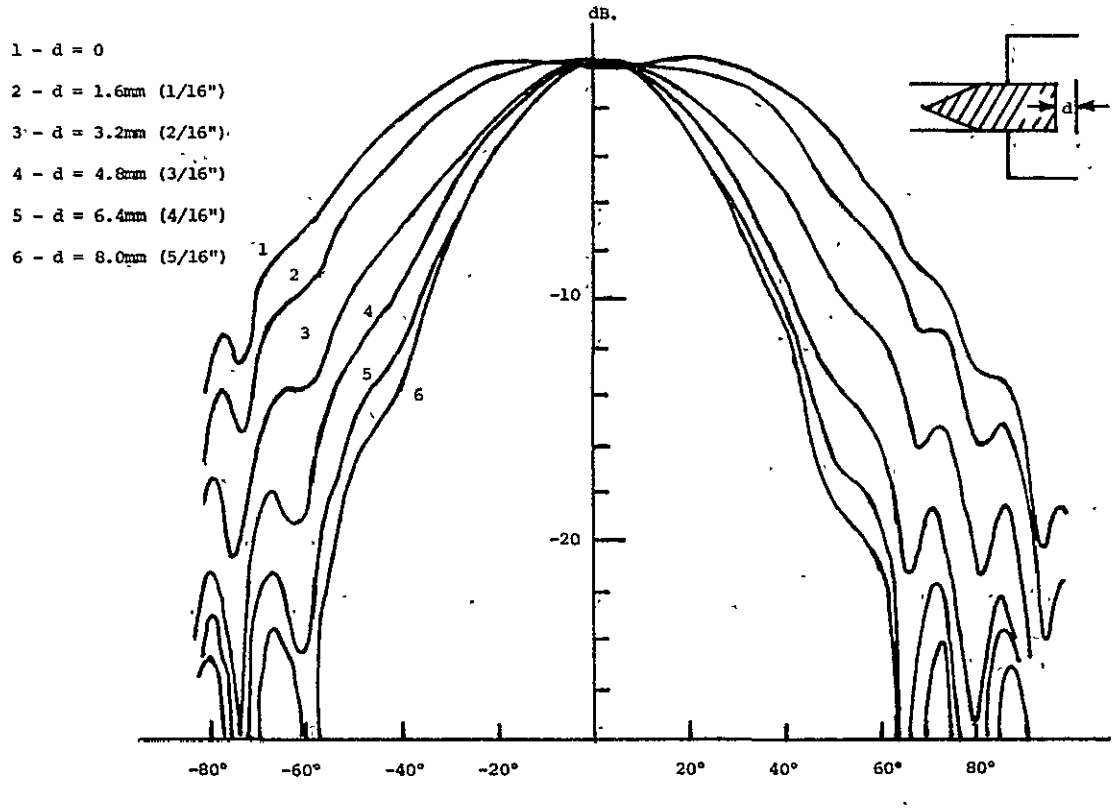

Figure 3.4 Measured H-plane pattern of Kumar feed at 12 Ghz.

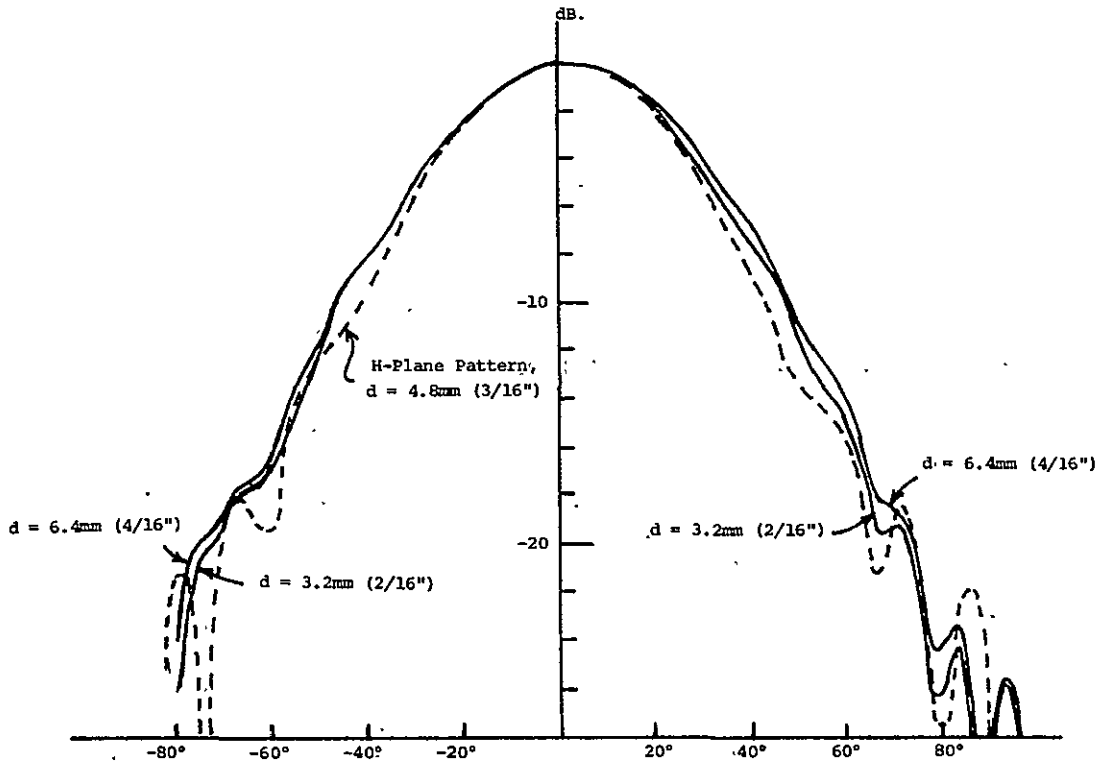

Figure 3.5 Measured E-plane pattern of Kumar feed at 12 Ghz.

were subsequently checked for accuracy using a template and it was discovered that there were significant errors in the overall contour in different cross sections. In particular it was found that both paraboloids, as received, had rather large "clam-shell" distortion. Clam-shell distortion manifests itself as an opening up of the paraboloid in one plane and a closing up of the paraboloid in the orthogonal cross section. The effect is to increase the focal length in one plane and to decrease it in the orthogonal plane as shown in Figure 3.6. This type of distortion may occur during shipping if the paraboloid is dropped on one edge. It may also occur when the supporting structure is welded to the paraboloid because of the application of heat in concentrated areas that either relieves some of the stress in the paraboloid due to the spinning operation or introduces new stresses because of uneven heating and expansion. In fiber glass paraboloids this type of distortion may arise from uneven curing during the manufacturing process. For the 1.83m antenna it was found that the surface contour deviated from the template contour by approximately 6.4mm (1/4 inch) in the plane with maximum deviation.

The model that was used to analyze the effect of clam-shell distortion on the radiation pattern was to assume that all cross-sections were parabolic but that the focal length varied from a maximum to a minimum with angle according to the cos 2ϕ function. With reference to Figure 3.7 let f be the focal length for the error free paraboloid and let f' be the focal length for the distorted paraboloid. If the feed is positioned at a distance f from the vertex then the phase error introduced in the aperture field at a radial position ρ from the axis is given by

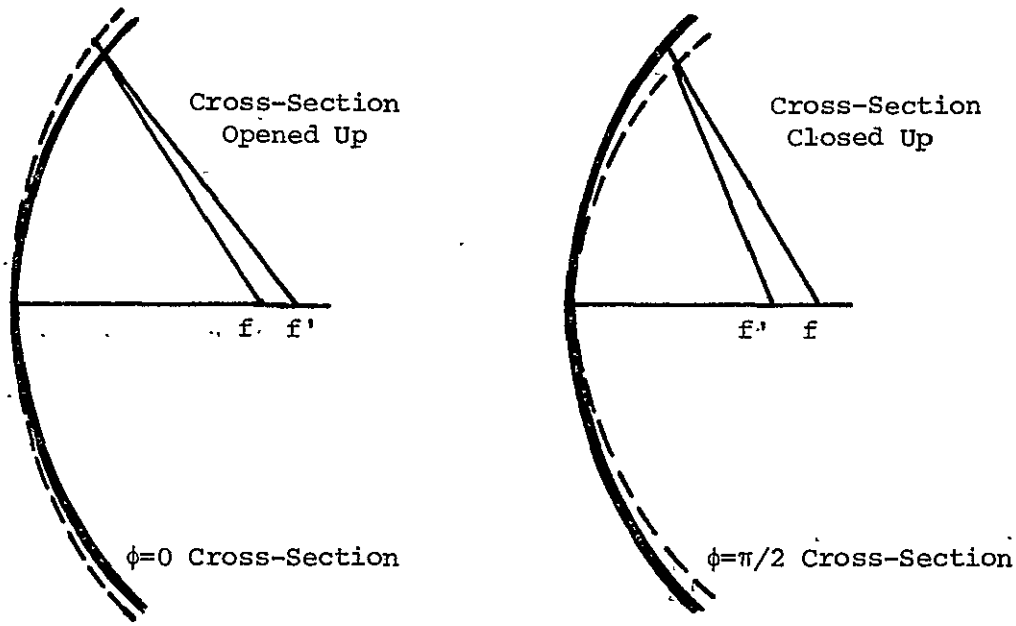

Figure 3.6 Illustration of clam-shell distortion in a paraboloid reflector.

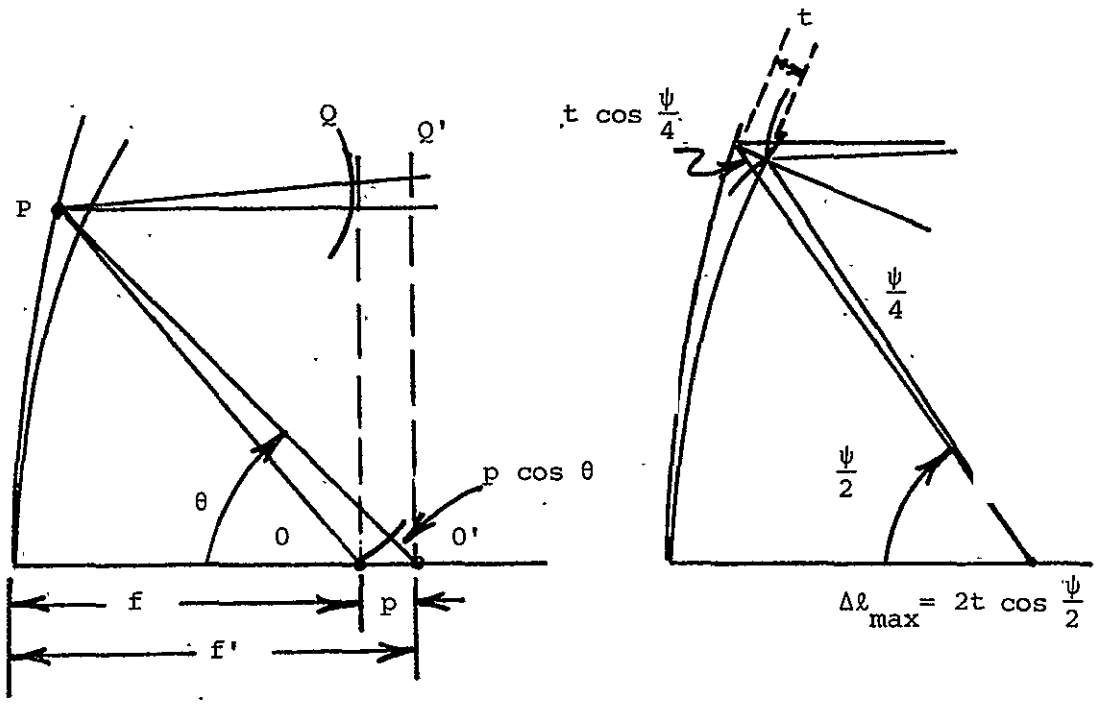

Figure 3.7 Illustration for finding phase error.

$$\Delta\phi = - \frac{k_o p \rho^2}{\rho^2 + 4f^2} \qquad (3.3)$$

where $p = f' - f$ is the effective change in focal length. The derivation of (3.3) is as follows: From the properties of a parabola $O'P\,Q' = 2f'$ in Fig. 3.7 and hence $O'PQ = 2f' - p$. Also $OPQ = 2f' - p - p\cos\theta$ and hence relative to the path length $2f$ at $\rho = 0$ the change in path length at ρ is

$$\Delta\ell = 2f' - p - p\cos\theta - 2f = p(1-\cos\theta) = p\sin^2\frac{\theta}{2}$$

Now $\rho = r\sin\theta = 2f\tan\frac{\theta}{2}$ which can be solved to give $\sin^2\frac{\theta}{2} = \rho^2/(\rho^2 + 4f^2)$.

When this result is substituted in the expression for $\Delta\ell$ and then multiplied by $-k_o$ the result (3.3) is obtained. With reference to Figure 3.7 again it can be seen that if t is the maximum contour deviation normal to the surface at the edge of the paraboloid then the maximum phase error is $-2k_o t\cos\psi/4$ where ψ is the angular aperture. The change in focal length can be related to t by equating this latter expression to (3.3) with $\rho = a$ and gives

$$p = \frac{4ft}{a^2}\,(a^2 + 4f^2)^{1/2} \qquad (3.4)$$

Two models of clam-shell distortion were analyzed. In Model 1 the phase error was chosen as

$$\Delta\phi = -\frac{k_o p\, \rho^2}{\rho^2 + 4f^2} \quad (1 - \cos 2\phi) \qquad (3.5)$$

and for Model 2

$$\Delta\phi = -\frac{k_o p\, \rho^2}{\rho^2 + 4f^2} \quad \cos 2\phi \qquad (3.6)$$

The first one corresponds to a feed that is focused in the $\phi = 0$ plane and has a maximum phase error occuring in the $\phi = \pi/2$ plane. The second one corresponds to focusing the feed in the $\phi = \pi/4$ plane with maximum phase errors of opposite signs occuring in $\phi = 0$ and $\phi = \pi/2$ planes.

By introducing the notation $x = \rho/a$, $D = 2a$, $2\beta = k_o p x^2/(x^2 + f^2/D^2)$, the radiation pattern for the two models are readily shown to be proportional to the following two integrals:

$$E(u) = \frac{1}{2\pi} \int_0^{2\pi}\int_0^1 f(x)\, e^{-j\beta(1-\cos 2\phi')}\, e^{jk_o u x \cos(\phi-\phi')}\, x\,dx\,d\phi' \qquad (3.7)$$

and

$$E(u) = \frac{1}{2\pi} \int_0^{2\pi}\int_0^1 f(x)\, e^{-j\beta\cos 2\phi'}\, e^{jk_o u x \cos(\phi-\phi')}\, x\,dx\,d\phi' \qquad (3.8)$$

In order to carry out the ϕ' integration the following approximations were used

$$e^{-j\beta(1-\cos 2\phi')} \approx 1 - j\beta - 0.75\,\beta^2 + (j\beta + \beta^2)\cos 2\phi' - 0.25\,\beta^2 \cos 4\phi'$$

and

$$e^{-j\beta\cos 2\phi'} \approx 1 - 0.25\beta^2 - j\beta\cos 2\phi' - 0.25\beta^2 \cos 4\phi'$$

along with the expansions

$$e^{jv\cos\phi'} = J_o(v) - 2J_2(v)\cos 2\phi' + 2J_4(v)\cos 4\phi' + \text{----}$$

$$e^{jv \sin\phi'} = J_o(v) + 2J_2(v) \cos 2\phi' + 2J_4(v) \cos 4\phi' + \text{----}$$

The final results obtained are:

For Model 1 with the feed focused in the ϕ=0 plane

$$E(u) = I_o - 0.75\,\gamma^2 I_2 + \gamma^2 I_4 - 0.25\,\gamma^2 I_6$$

$$-j\gamma\,(I_1+I_3),\ \phi = 0 \text{ plane}$$

$$= I_o - 0.75\,\gamma^2 I_2 + 0.25\,\gamma^2 I_6 - j\gamma\, I_1,\ \phi = \frac{\pi}{4} \text{ plane}$$

$$= I_o - 0.75\,\gamma^2 I_2 - \gamma^2 I_4 - 0.25\,\gamma^2 I_6 - j\gamma\,(I_1-I_3),\ \phi = \frac{\pi}{2} \text{ plane} \qquad (3.9)$$

while for Model 2 with the feed focused in the $\phi = \pi/4$ plane

$$E(u) = I_o - 0.25\,\gamma^2(I_2+I_6) + j\gamma I_3,\ \phi = 0 \text{ plane}$$

$$= I_o - 0.25\,\gamma^2(I_2-I_6),\ \phi = \pi/4 \text{ plane}$$

$$= I_o - 0.25\gamma^2(I_2+I_6) - j\gamma I_3,\ \phi = \pi/2 \text{ plane} \qquad (3.10)$$

where $\gamma = k_o p/2$ and

$$I_o(u) = \int_0^1 f(x) J_o(ux)\, x\,dx \qquad (3.11a)$$

$$I_1(u) = \int_0^1 f(x) J_o(ux)\, \frac{x^3}{x^2+(f/D)^2}\, dx \qquad (3.11b)$$

$$I_2(u) = \int_0^1 f(x) J_o(ux)\, \frac{x^5}{[x^2+(f/D)^2]^2}\, dx \qquad (3.11c)$$

$$I_3(u) = \int_0^1 f(x) J_2(ux) \frac{x^3}{x^2+(f/D)^2} dx \qquad (3.11d)$$

$$I_4(u) = \int_0^1 f(x) J_2(ux) \frac{x^5}{[x^2+(f/D)^2]^2} dx \qquad (3.11e)$$

$$I_6(u) = \int_0^1 f(x) J_4(ux) \frac{x^5}{[x^2+(f/D)^2]^2} dx \qquad (3.11f)$$

These integrals were evaluated numerically for f/D = 0.38 (see Appendix II) and with f(x) being the aperture field produced by the Kumar feed and given by (3.1).

The patterns given by (3.9) and (3.10) are shown in Figs. 3.8 to 3.13 for the case when t = 0.00635m (1/4 inch) for which $\gamma = 4.41$. For the Model 1 case for which the feed is focused in the $\phi=0$ plane it is seen that the main lobe is broadened and a 1.15 dB. loss in gain occurs. In the $\phi=0$ plane (Fig. 3.8) the first sidelobe is increased from -36.7dB. to -24.5 dB. relative to the main lobe and a second sidelobe of the same amplitude is also produced. The remaining sidelobes are generally 8 to 10 dB. above those of the error free pattern. A similar affect occurs in the $\phi = \pi/2$ plane (Fig. 3.10) although the first sidelobe is increased only to about - 27.5 dB. In this plane a rather large shoulder is also formed on the main lobe. The best pattern is obtained in the $\phi = \pi/4$ plane (Fig. 3.9) and this is because the relative phase error in the $\phi = 0$ and $\phi = \pi/2$ planes are of opposite sign and tend to produce cancelling effects in the $\phi = \pi/4$ plane. There is still a first sidelobe at a level of - 29 dB. relative to the main lobe and about a 4 dB. increase in the level of the remaining sidelobes in the $\phi = \pi/4$ plane.

For the Model 2 with the feed focused in the $\phi = \pi/4$ plane the phase error is of opposite sign in the $\phi = 0$ and $\phi = \pi/2$ planes and hence the sidelobes are not increased as dramatically as for Model 1. There is also only a 0.79 dB. loss in gain. The highest sidelobe occurs in the $\phi = \pi/4$ plane (Fig. 3.12) and has a relative value of -25.7 dB. The remaining sidelobes in this plane are essentially the same as for the error free pattern. In the $\phi = 0$ and $\pi/2$ planes the first sidelobe has a relative level of about -30 dB. and the rest are increased by about 4 dB. over those of the error free pattern.

In addition to clam-shell distortion the 1.83m paraboloid was found to have a small circularly symmetric but periodic radial variation in its contour as shown in Fig. 3.14. This distortion probably occurred during the spinning operation. The deviation from a true parabola was estimated to be $\pm$ 0.8 mm ($\pm$ 1/32 inch). The model that was used to represent the phase error due to this periodic radial variation was the phase function

$$e^{-j\alpha\cos 7\pi x} \approx 1 - j\alpha \cos 7\pi x \qquad (3.12)$$

since α is small (equal to 0.2 for $\pm \lambda_o/32$ phase deviation). For small errors the overall effect on the pattern is the sum of the effects caused by each type of error. This assumption was made and the error pattern

$$-j\alpha \int_0^1 f(x) J_o(ux)\, x \cos 7\pi x \; dx \qquad (3.13)$$

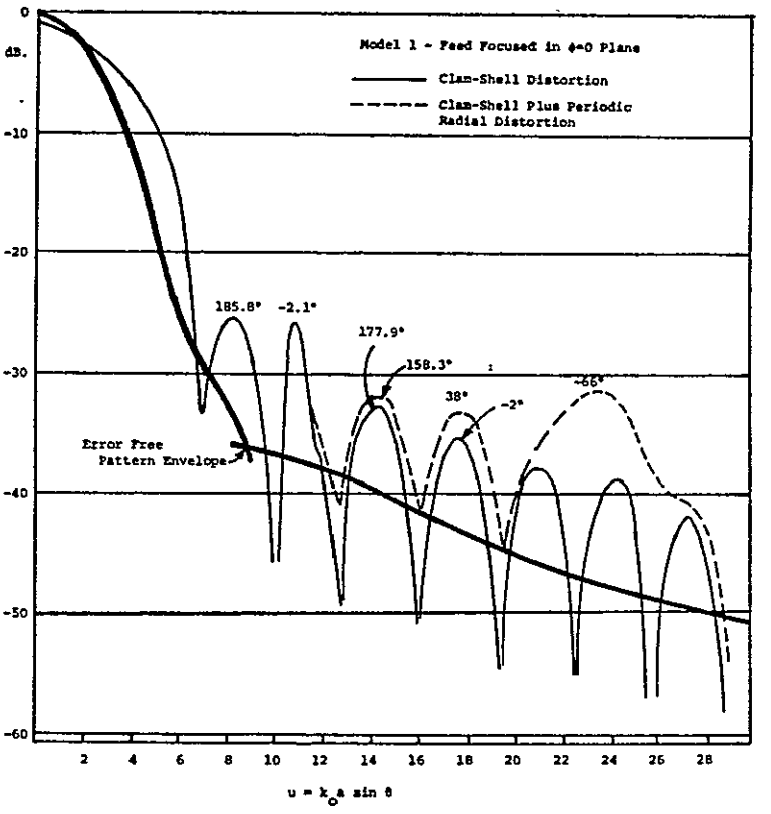

Figure 3.8 Radiation pattern in $\phi = 0$ plane for Model 1.

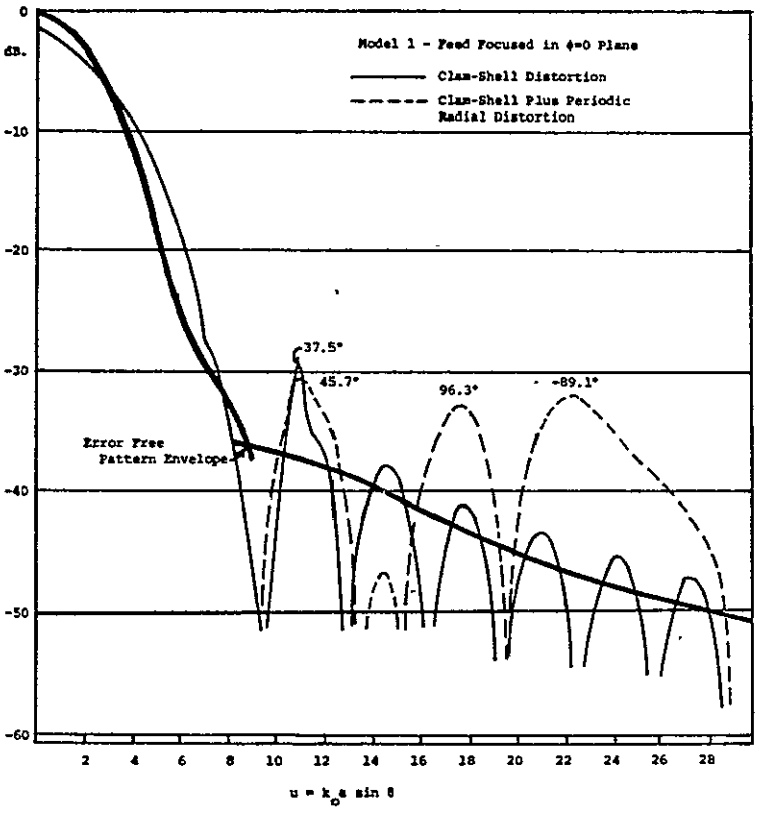

Figure 3.9 Radiation pattern in $\phi = \pi/4$ plane for Model 1.

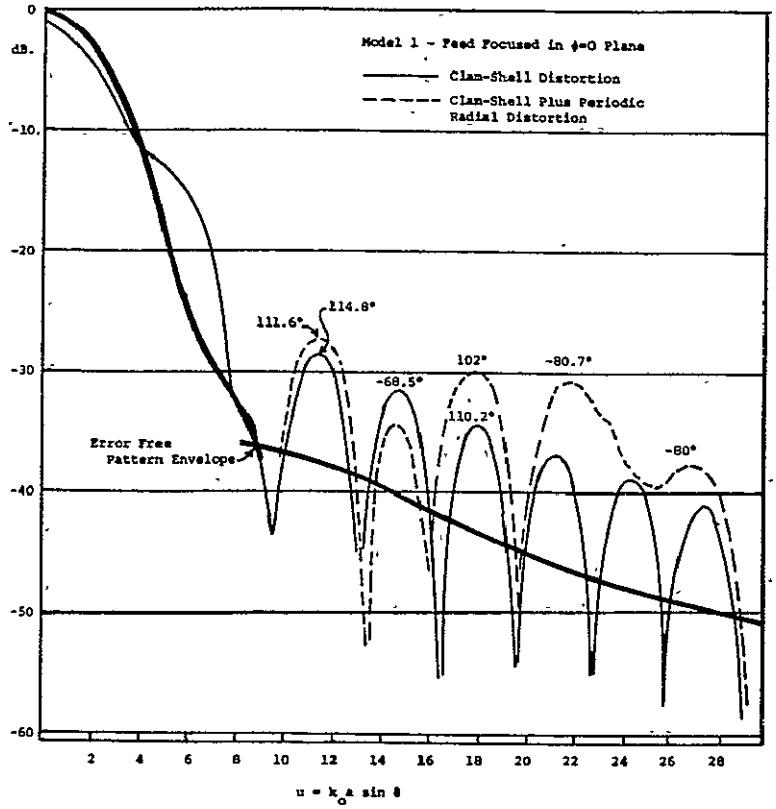

Figure 3.10 Radiation pattern in $\phi = \pi/2$ plane for Model 1.

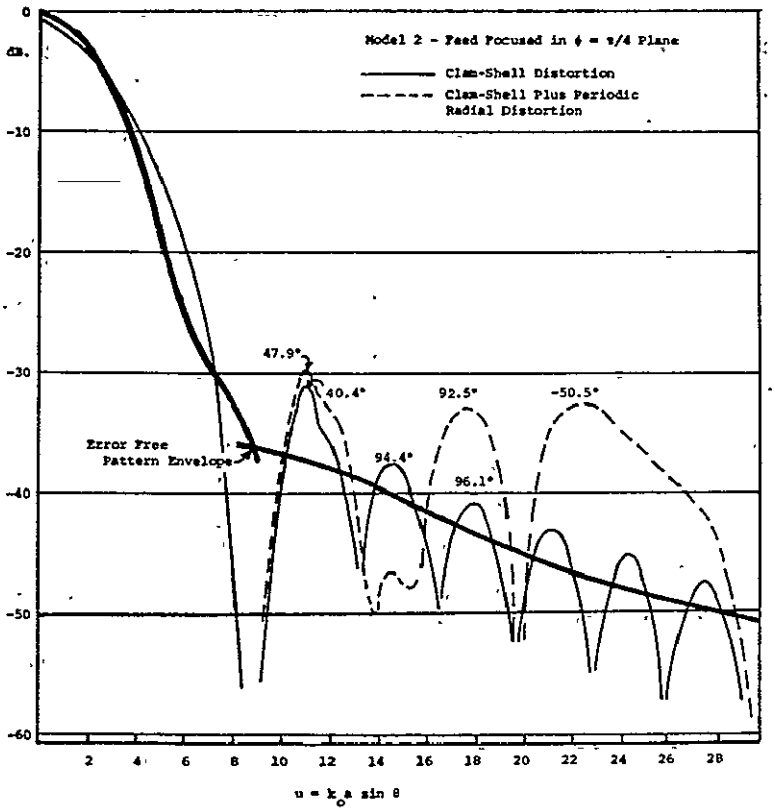

Figure 3.11 Radiation pattern in $\phi = 0$ plane for Model 2.

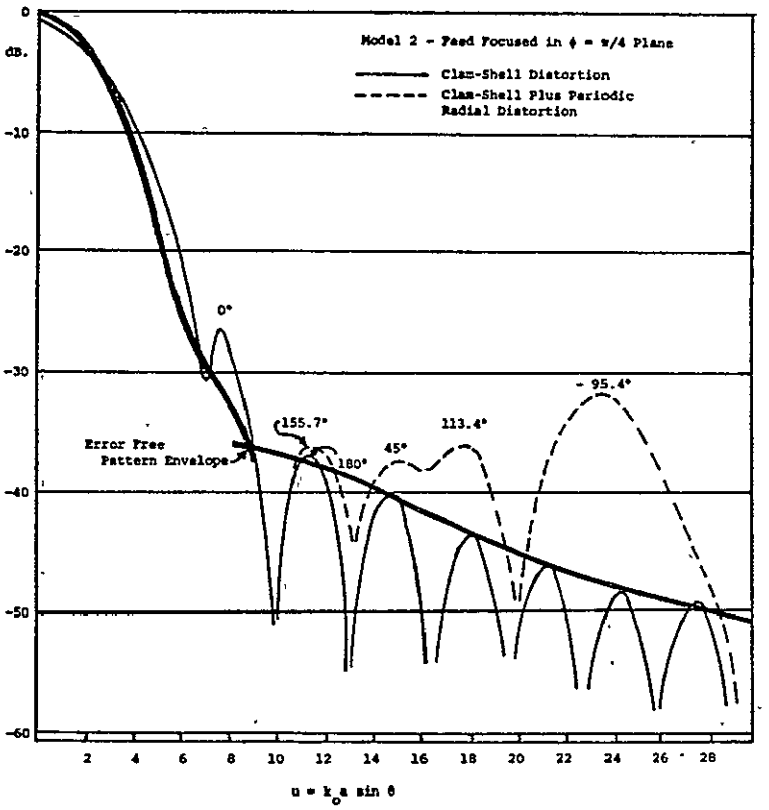

Figure 3.12 Radiation pattern in $\phi = \pi/4$ plane for Model 2.

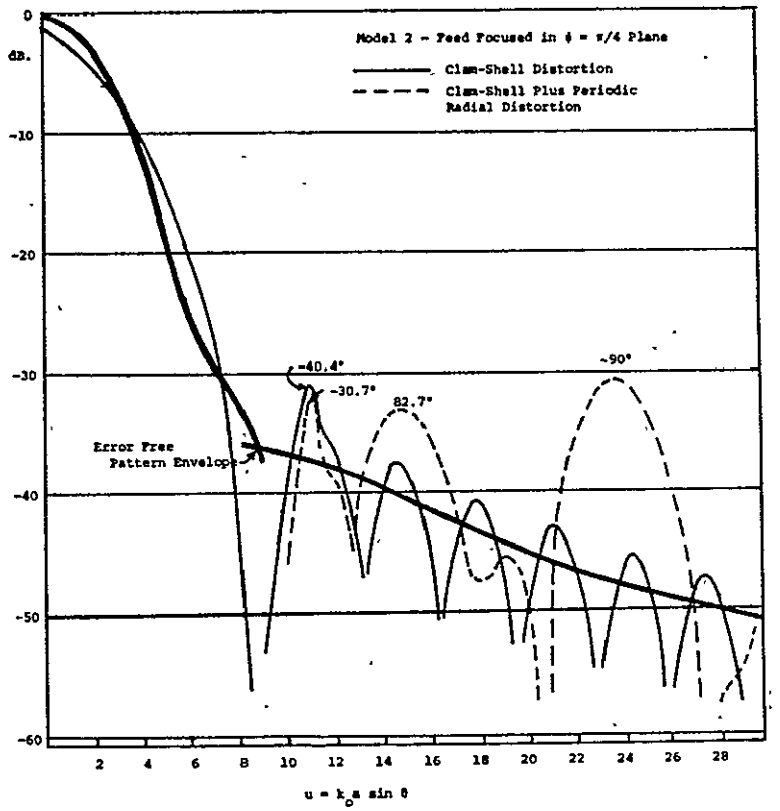

Figure 3.13 Radiation pattern in $\phi = \pi/2$ plane for Model 2.

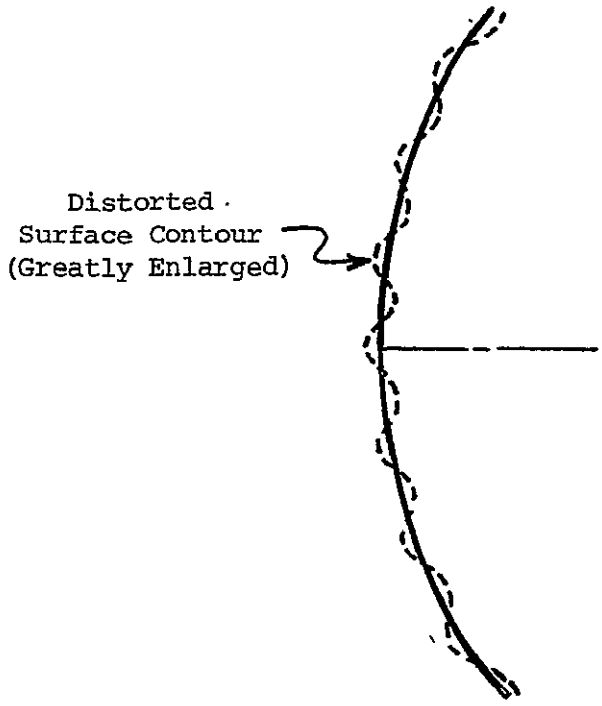

Figure 3.14 Illustration of periodic radial variation in paraboloid surface.

was computed for $\alpha = 0.2$ and added to the patterns computed for clam-shell distortion. The results are shown in Fig's. 3.8 to 3.13 by the broken line patterns. The periodic radial variation in the contour results in a large sidelobe in the region around u = 22 to 24 where the quasi-period of the Bessel function $J_o(ux)$ matches that of the cos $7\pi x$ function. At this angle the field from the periodic source adds up constructively. The sidelobes in the region u = 16 to u = 28 are increased quite substantially by this periodic radial variation. The generally accepted tolerance on paraboloids for the 12 Ghz. band is $\lambda_o/16$ but this is not adequate if the deviation is a periodic radial one since then the effect is a strong constructive interference resulting in a large sidelobe region away from the main lobe.

The phase of the field at the peaks of the sidelobes are shown in Fig's. 3.8 to 3.13. It should be noted that the effect of errors is to change the phase from 0° or 180° by varying amounts which sometimes are as large as 90° or more. For this reason it is difficult, if not impossible, to cancel some of the sidelobes using absorber pads. Reflector plates can produce cancelling fields with arbitrary phase but no simple design will be adequate if the phase of the field varies significantly from one sidelobe to the next. Thus the effect of paraboloidal contour errors makes it difficult to achieve low sidelobes using feeds giving a large amount of edge taper and also makes it equally difficult to use absorber or reflector plate arrays to cancel the high sidelobes.

3.3 The Effect of Random Errors on Sidelobe Levels

With the current manufacturing methods small scale random errors in the paraboloid surface do not appear to be as much of a problem as large scale deterministic errors are. The sidelobe amplitudes, phase, and positions caused by random errors cannot be predicted exactly. Only the average or expected values of these parameters can be computed by assuming some kind of statistical model to apply to the class of antennas under consideration. Ruze has carried out such an investigation and his results are useful for predicting the general effects of random errors and also provides some guidance as to the required tolerances on the surface contour in order to keep the effect of random errors to within some specified limit (46).

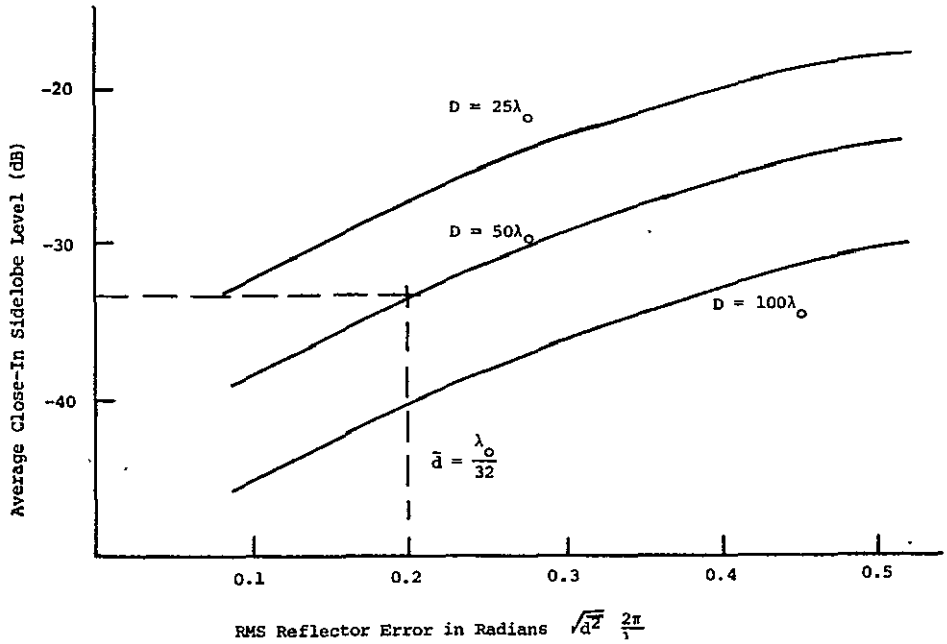

Figure 3.15 The effect of random errors on sidelobes in a paraboloid.

Figure 3.15 shows the average close-in sidelobe level for paraboloids of various diameters when the illumination is a cosine squared function and the correlation length equals one wavelength. For an RMS error equal to $\lambda_o/32$ the expected sidelobe level is - 33 dB. for a paraboloid $50\lambda_o$ in diameter. Some of the sidelobes would exceed this level. Thus in order to ensure that all sidelobes remain below - 35 dB. the RMS error would probably have to be kept below $\lambda_o/64$. The sidelobe level depends on the illumination function but no calculations have been made to show this dependency. Also the effect of longer correlation distances has not been examined in detail. Currently manufactured paraboloids do not have surface deviations of as much as $\lambda_o/32$ with a correlation length as short as one wavelength. Surface deviations of this size are more likely to have correlation distances of 5 or more wavelengths at 12 Ghz. More work needs to be done to evaluate the effects of random errors on paraboloidal antennas as regards sidelobe levels for various aperture field distributions.

CHAPTER 4

EXPERIMENTAL RESULTS USING THE KUMAR FEED

4.1 Introduction

The practical realization of low sidelobes by using a feed producing around 20 dB. of edge taper was tested by purchasing two low cost spun aluminum paraboloids and illuminating these with the fabricated Kumar feed described in Chapter 3. The diameter of the two paraboloids are 1.22m (4 ft.) and 1.83 m (6 ft.) and both have a nominal f/D ratio of 0.38. These paraboloids were supplied with a "button-hook" rectangular waveguide feed and both incorporated a flat circular 0.216m (8.5 in) vertex plate.

The radiation patterns of both paraboloids were measured using the feed supplied by the manufacturer. The vertex plates were then removed and new paraboloidal central sections were turned on a lathe and bolted in place of the vertex plates. The Kumar feed is supported by four 9.5 mm (3/8 in.) diameter rods. A photograph of the 1.22m antenna with the feed mounted is shown in Figure 4.1. The coaxial mixer for the microwave receiver is connected directly to the Kumar feed to avoid unnecessary attenuation. RG-214 coaxial cable is used to connect the mixer to the microwave receiver.

The antenna under test is mounted on a Scientific Atlanta Model 5303 positioner which in turn is mounted on a 1.5m high platform located on the roof of the Glennan Building. The transmitter consists of a Scientific Atlanta Model 2960 signal source and a 0.61m (2 ft.) paraboloid that is

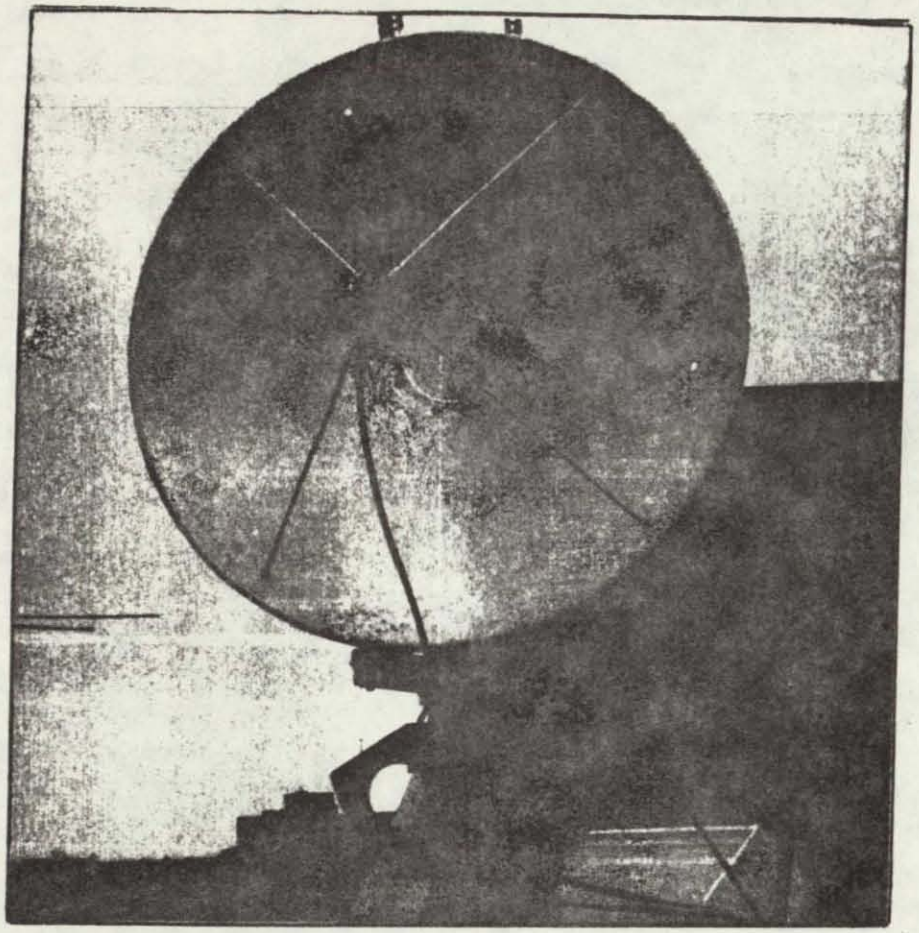

Fig. 4.1 View of 1.22m antenna with Kumar feed.

housed in a tower on the roof of University Circle Development Corporation Research Building No. 2. The line-of-sight separation between the transmitting and receiving stations is approximately 160m and is located approximately 35m above ground. This antenna range is free of ground reflections and other multipath effects for the highly directional antennas that were tested.

A Scientific Atlanta Model 1710 microwave receiver with an external coaxial mixer is used. The receiver output is fed to a digital display unit and also to the y-axis input of an x-y recorder. The angular position of the positioner is obtained on a digital synchro display. This unit also provides a binary coded decimal (BCD) output of the angle information which is converted to an analog signal and used for the x-axis input of the recorder. The digital to analog converter that was built had

a finite resolution so the recorded patterns show a step-like variation as a function of angle. Since the interest was primarily in the sidelobe levels and positions a more expensive higher resolution converter was not considered justifiable for this project.

The paraboloids that were received from the manufacturer had clam-shell distortion that resulted in poor performance. Fortunately, the supporting structure was not very rigid so much of this distortion could be removed by pounding on the rim of the paraboloid with a rubber mallet (a few blows was sufficient to cause a surface deviation of 3 to 4 mm.) By removing as much of the distortion as possible the overall performance of the antennas was improved very significantly although not to the point expected from the theoretical predictions. Additional rods were taped to the four support rods and no noticeable change occurred in the sidelobe patterns above the -36 dB. level so it was concluded that the scatter from the feed support rods was not a limiting factor on the sidelobe levels that were achieved.

In the following sections the experimentally measured patterns for the 1.22m and 1.83m paraboloids are presented. Some measured patterns when small absorber pads and reflector plates were incorporated are also presented. In addition the H-plane pattern for the 1.22m paraboloid illuminated by the Kumar feed and using the CTS satellite as a source is given. The signal to noise ratio for the latter measurement was not adequate to measure the sidelobe pattern below -26 dB. so no sidelobe detail was obtained. On the antenna range the signal strength was sufficient to measure sidelobes as low as -55 dB. to -60 dB. but because the dynamic range of the receiver is only 40 dB. this limited the range covered. The accuracy of the microwave

receiver and digital display unit was checked using a Hewlett-Packard rotary attenuator and it was concluded that the measured patterns were accurate to within a few tenths of a decibel.

4.2 Experimental Results for the 1.22m Paraboloid

The E-and H-plane patterns of the 1.22m paraboloid using the waveguide feed supplied by the manufacturer were measured at a number of different frequencies. Typical patterns that were measured are shown in Figures 4.2 to 4.7 for frequencies of 12.0, 12.1, and 12.2 Ghz. When these patterns are examined it is readily apparent that very poor focusing of the field is obtained. This shows up as a very broad beam between nulls and shoulders on the main lobe. It also showed up as a significant reduction in gain which was measured to be 37.2 dB. versus 41 dB. as quoted by the manufacturer. The gain was measured relative to an optimum gain horn whose gain is given by $6.4\ ab/\lambda_o^2$ where a is the aperture width, b is the aperture height, and λ_o is the wavelength. The calculated gain of the horn was 20.7 dB. and is known to be accurate to a small fraction of a dB. for horns of this type. The poor performance of the antenna as supplied was attributed in part to the use of a rather large flat circular central section which was part of the feed mounting structure and also served as a vertex plate. As was discovered later the paraboloid also had a warp in it (clam-shell distortion).

When the manufacturer's feed is removed a 0.216m circular hole is left. A paraboloid section with a focal length of 0.457m was machined in place of the original feed structure. The Kumar feed is mounted using four aluminum rods attached 0.05m from the outer rim of the paraboloid and at 45° to the chosen E and H-planes.

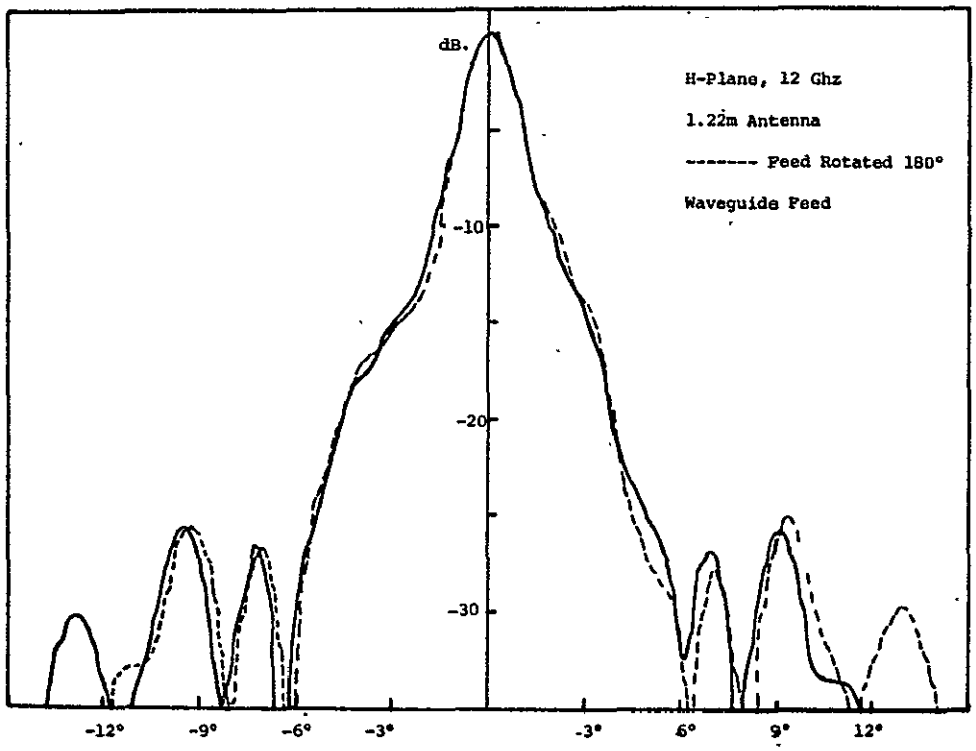

Figure 4.2 H-plane radiation pattern

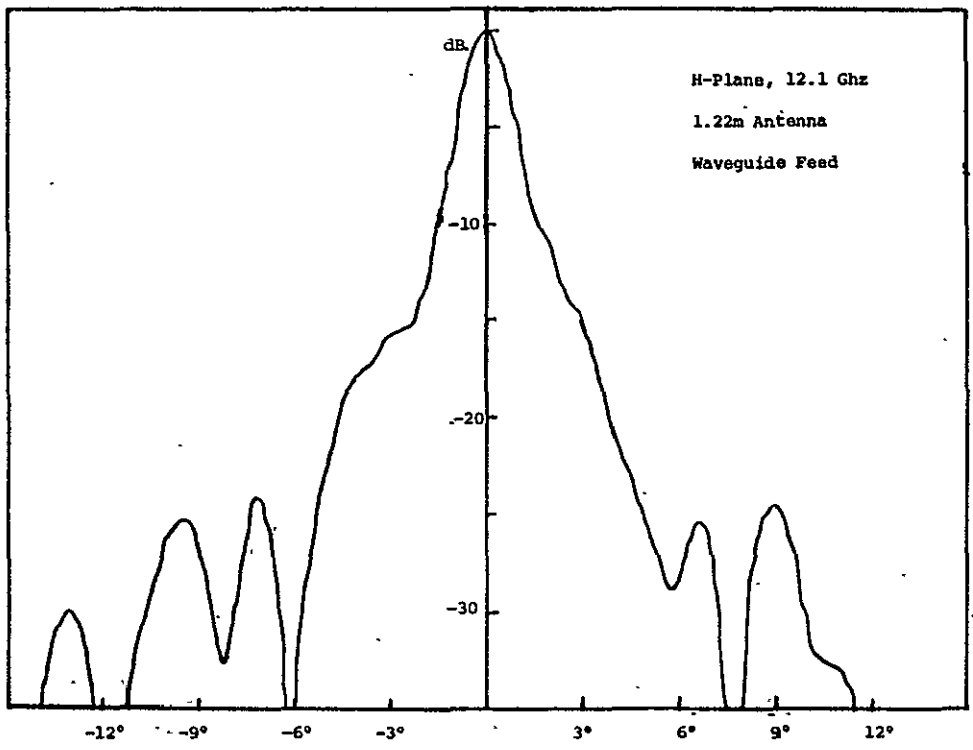

Figure 4.3 H-plane radiation pattern.

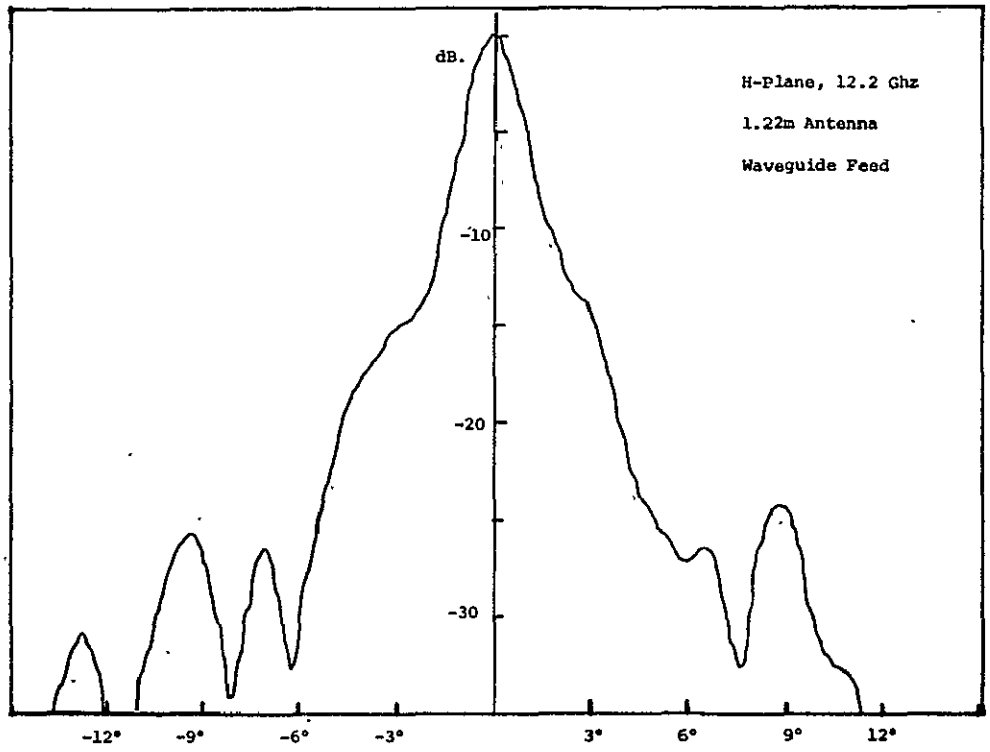

Figure 4.4 H-plane radiation pattern.

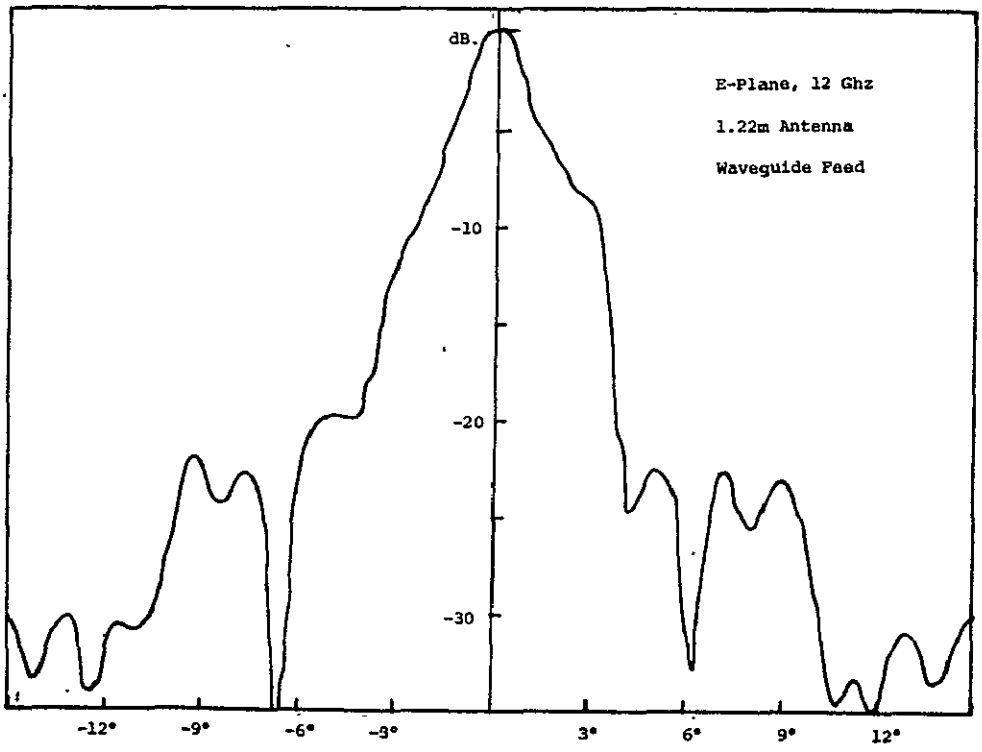

Figure 4.5 E-plane radiation pattern.

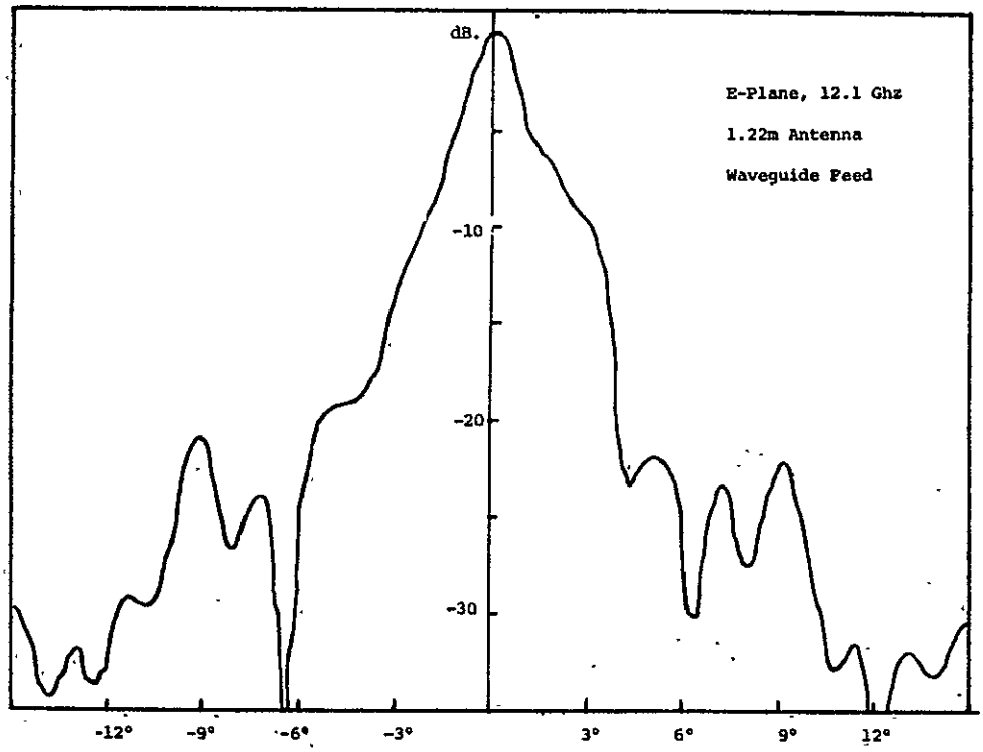

Figure 4.6 E-plane radiation pattern.

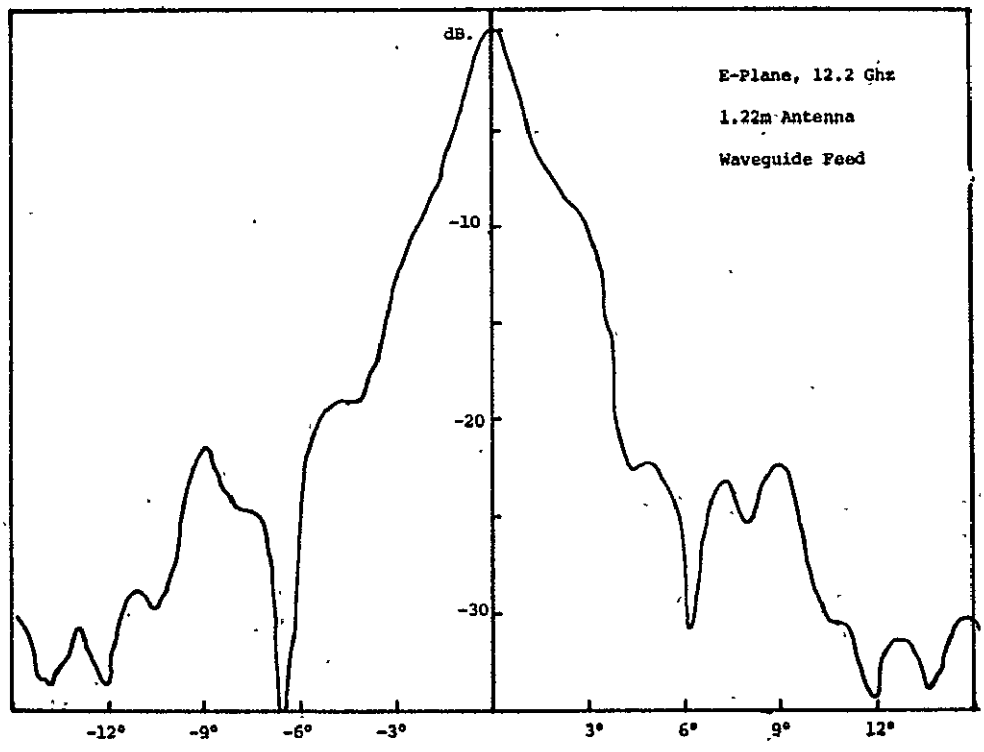

Figure 4.7 E-plane radiation pattern.

When patterns on the antenna thus modified were measured the poor focusing properties were still present. Figures 4.8 and 4.9 show typical patterns (a great many more were taken but are not included since later modifications of the paraboloid gave better results). These patterns, labelled series A, also exhibit a very broad beamwidth between poorly defined nulls and sidelobes as high as -26 dB. The calculated pattern for the Kumar feed with 1.22m paraboloid indicates a width of about 6° between nulls. The measured patterns were about 10° wide between nulls.

It was expected that the paraboloid was in error so a 0.61m (2 ft.) long template was made to check the accuracy of the central position of the paraboloid. It was found that the 0.216m diameter section that was added was about 3.2 mm (1/8 in.) too far back relative to the main section of the paraboloid. This may have been caused by spring-back occuring when the 0.216m diameter hole is cut in the spun paraboloid. It was found possible to deform the central section through judicious use of a rubber mallet to bring it into conformity with the rest of the paraboloid covered by the 0.61m long template.

A new series of patterns, series B, was then taken and some of these are shown in Fig.'s 4.10 to 4.14. Considerably better focusing was obtained as evidenced by a better defined main lobe and lower sidelobe levels. The focal position f_e was optimized at about 0.457m to 0.46m (18 to 18-1/8 in.) at 12.1 Ghz. and E and H-plane patterns at this frequency (Fig's. 4.11 and 4.14) look quite good and have the expected 6° width between nulls. However, the sidelobe level was fairly well filled in below -30 dB. and the patterns deteriorated with a change in frequency. Also the H-plane pattern at 12.1 Ghz. did not exhibit a null

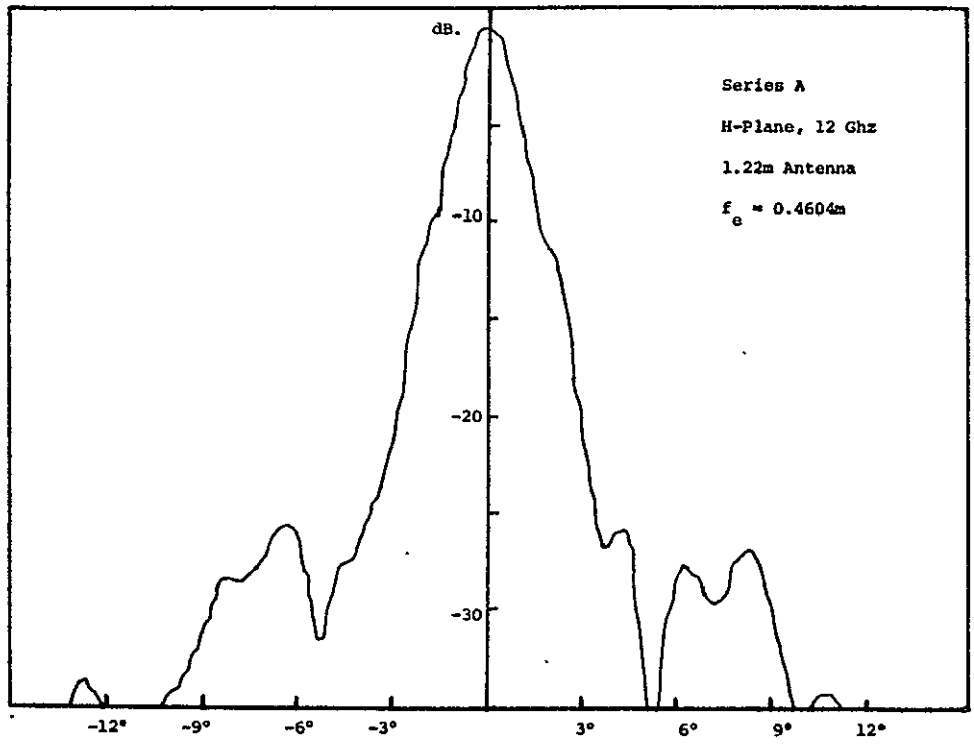

Figure 4.8 H-plane radiation pattern.

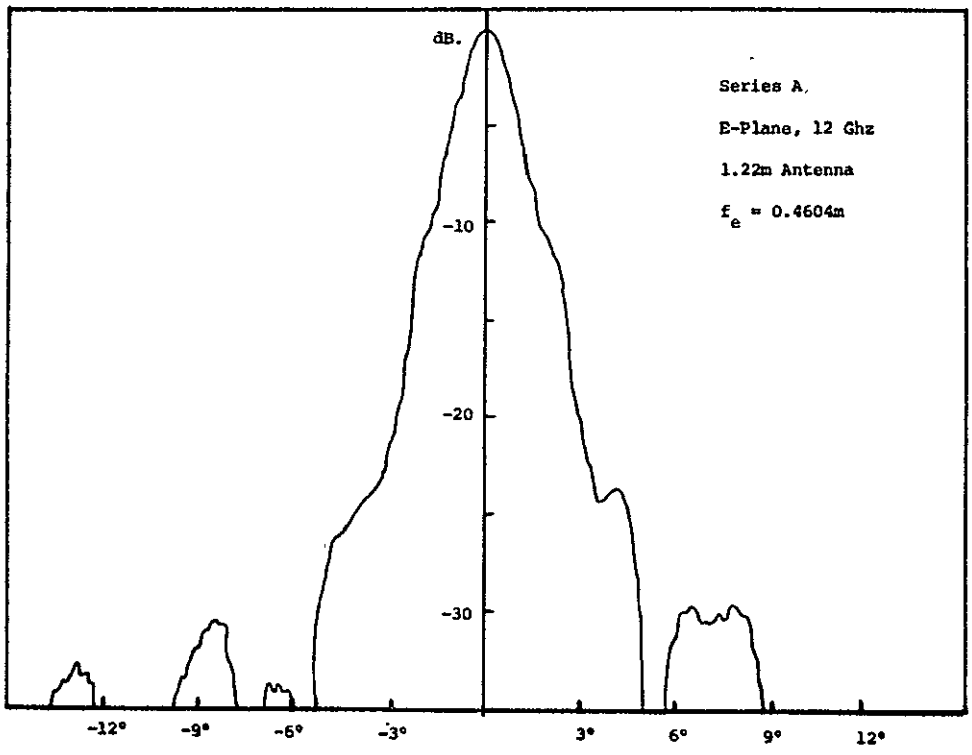

Figure 4.9 E-plane radiation pattern.

on one side of the main lobe. The overall evaluation of these patterns led to the conclusion that there were still significant phase errors associated with the paraboloid.

A 1.22m long template was then constructed in order to check the contour of the whole paraboloid. In checking the paraboloid with this template it was found that it was warped. In one cross-section the template touched at the center but had a clearance of 3.2 mm (1/8") (corresponding to a 90° phase error) at the edge. In the cross-section at right angles to this the template touched at the outer edge and had a clearance of 0.003m (1/8 in.) at the center. Fortunately, the structural rigidity of the antenna was such that by pounding on the rim with a rubber mallet in the vicinity of the tubular supporting rods it was possible to remove most of the warp. The paraboloid was recontoured as well as possible and in general a reasonably good overall contour was obtained but there definitely were small irregularities left in the surface that were estimated not to exceed $\pm$ 1.6 mm ($\pm$ 1/32 in.).

A new series of patterns were taken after this work on reshaping the paraboloid. These are shown as series C in Fig's.4.15 to 4.28 and are xerox copies of the recorded patterns. The small steps are due to the finite resolution of the digital to analog conversion of the angle information. Figures 4.15 to 4.19 and 4.22 show the H-plane pattern at 12.1 Ghz. for various focal positions f_e of the feed and positions d of the dielectric rod from the front face of the feed. Note that a well-defined main lobe could be obtained. The best gain and sidelobe definition was obtained with f_e = 0.4604m (18-1/8 in.) and d = 3.2 mm (1/8 in.) and is shown in Figure 4.22. Note that with f_e = 0.4636m (18-1/4 in.) as in

Fig. 4.15 defocusing effects are apparent. A similar defocussed pattern with $f_e = 0.451$ m (17-3/4 in.) was expected but as seen in Fig. 4.19 this did not occur. In fact, the main lobe is somewhat narrower with $f_e = 0.451$ m than with $f_e = 0.460$ m. This seems to indicate that there was still some overall error in the contour of the paraboloid.* An indication that this is the case may be seen by comparing the H-plane patterns in Fig.'s 4.20 and 4.21 where the only change is a 5° rotation of the paraboloid about its axis. There is a non-negligible change in the sidelobe pattern between the two cross-sections.

The sidelobe structure shown in Fig. 4.22 is quite well defined but the far out lobes are higher than expected for a high quality paraboloid. Nevertheless a margin generally greater than 5 dB. below the CCIR Model pattern was obtained. The CCIR model pattern was based on (2.2) given in Chap. 2 using 1.7° for the measured 3 dB. beamwidth. For example, in Fig. 4.28 the sidelobe at 15° is - 37.5 dB. which is 4.5 dB. below the CCIR model but bearing in mind that the model pattern does not call for sidelobes below - 38 dB., and indeed are not required, it can be stated that the pattern shown in Fig. 4.28 is better than the CCIR model by 6.5 dB. or more.

It was found that the sidelobe structure below - 35 dB. is very sensitive to small perturbations in the surface of the paraboloid. Thus the random perturbations in the surface resulting from the reshaping of the paraboloid was expected to have increased the sidelobe level above

---

*According to Kumar (10) the phase center is 0.005m behind the front face of the feed and since the focal length of the 1.22m paraboloid is supposed to be 0.457m (18 in.) the optimum value of f_e should have been 0.452m (17.8 in.).

that of what could have been obtained with a higher quality paraboloid. The effect of random phase errors has been analyzed by Ruze (45). The prediction is that for a dish 50 wavelengths in diameter (50 inches at 12 Ghz.), with cosine squared illumination and, an RMS reflector error of $\lambda_o/32$ (1/32 in.) with a correlation length of λ_o (1 in.) will result in near-in sidelobes at a -33 dB. level. An RMS reflector error of twice this amount will result in a general sidelobe level of -26 dB. Since sidelobes due to random errors show very little regularity it is clear that a surface tolerance of better than $\lambda_o/32$ must be maintained in order to achieve sidelobes below - 35 dB. Of course, systematic overall errors in the basic paraboloid contour must also be avoided since these produce defocussing, loss in gain, and large sidelobes.

Figures 4.20 to 4.23 show the H-plane pattern at various frequencies. The sidelobes remain below 30 dB. and the main lobe is well defined but the sidelobe detail changes quite a bit, also an indication of random phase errors. Of particular interest, is the H-plane pattern at 12 Ghz. and shown in Fig. 4.20 which has quite low near-in sidelobes. This pattern was taken twice to verify that it was correct. Also of note is the 12.1 Ghz. H-plane pattern shown in Fig. 4.28. This pattern shows somewhat higher sidelobes than the H-plane pattern at 12.1 Ghz. as shown in Fig. 4.22. The two patterns were taken on different days and the difference is probably due to error in setting the frequency at exactly 12.1 Ghz. and the angular position of the paraboloid. This seems to be a reasonable explanation in view of the marked change in the pattern with a change in the frequency from 12.1 Ghz. to 12.0 Ghz. and with rotation

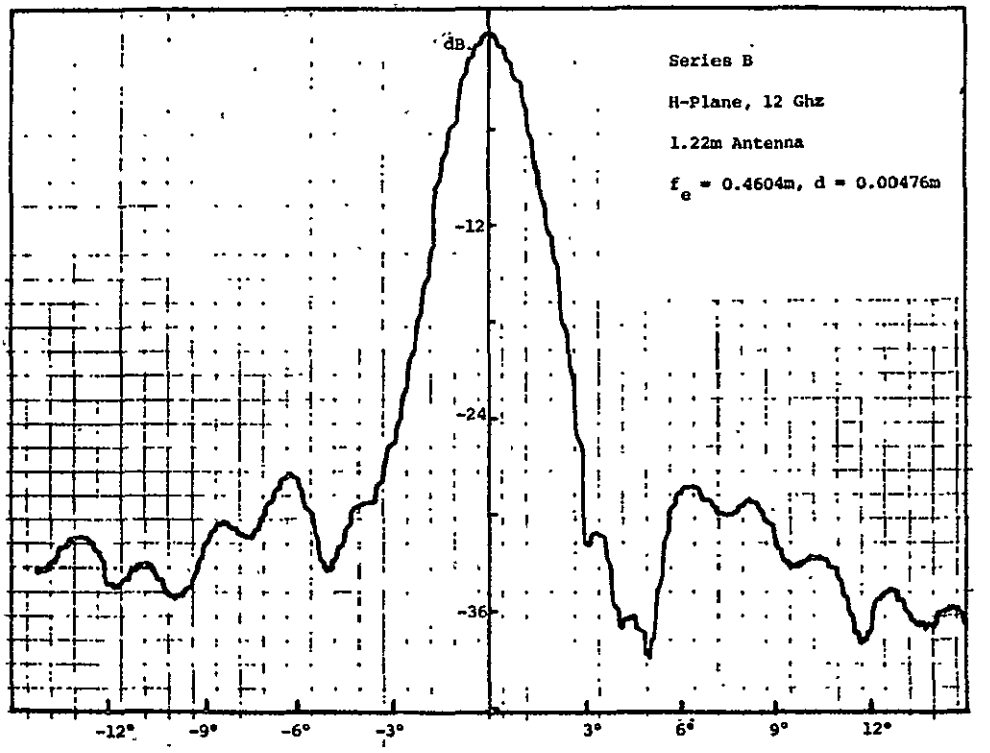

Figure 4.10 H-plane radiation pattern.

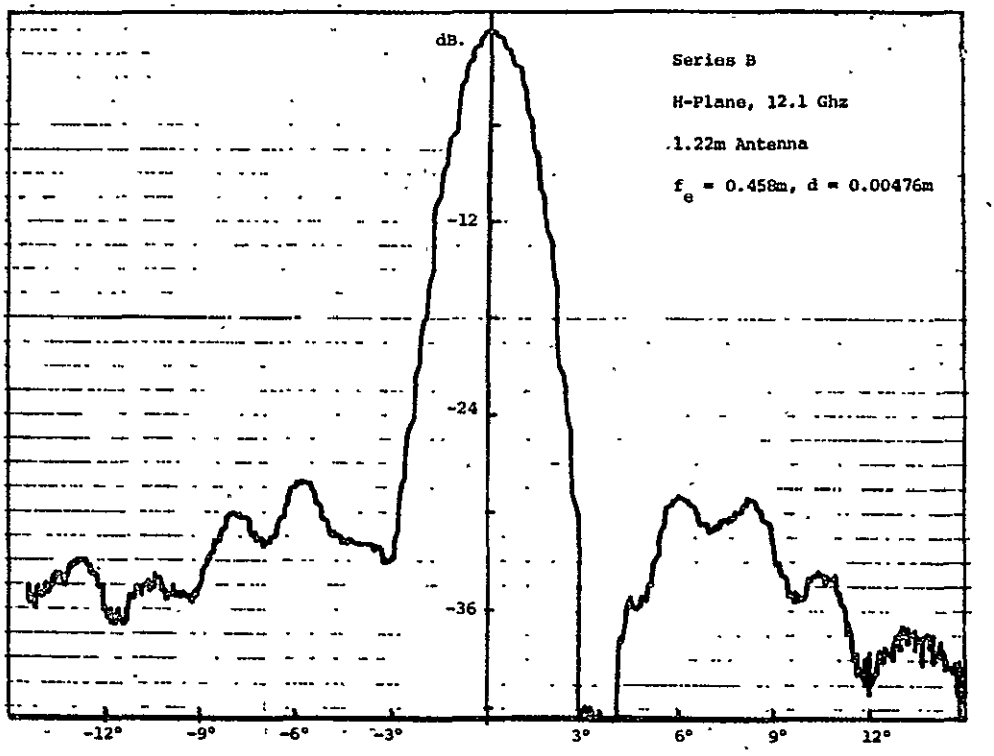

Figure 4.11 H-plane radiation pattern.

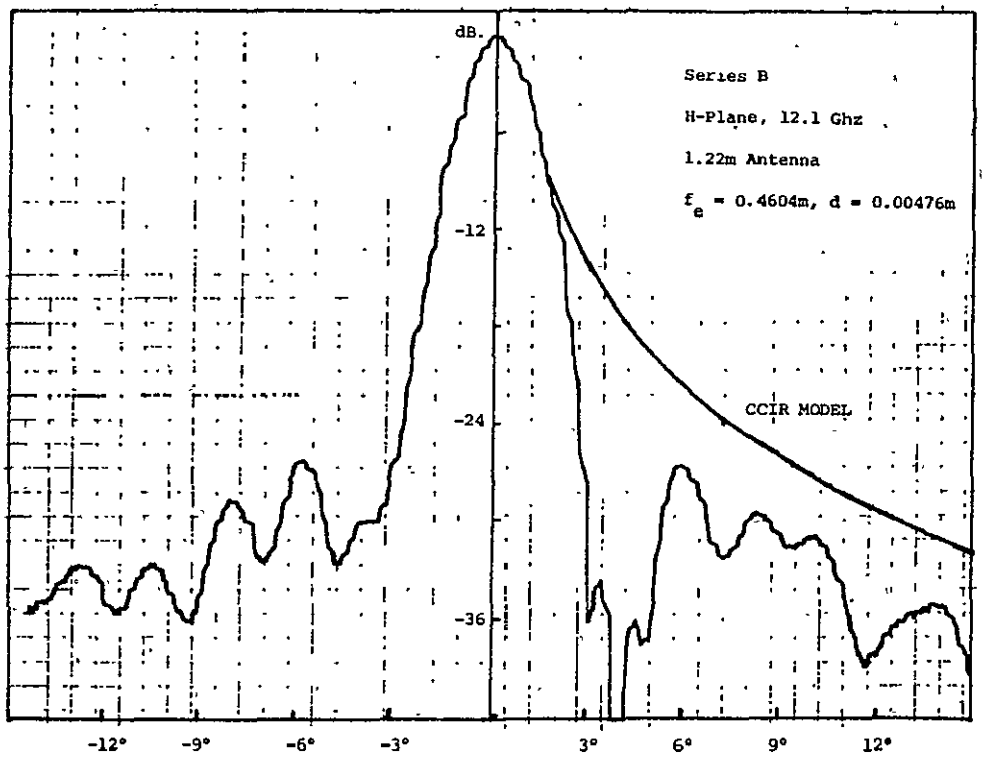

Figure 4.12 H-plane radiation pattern.

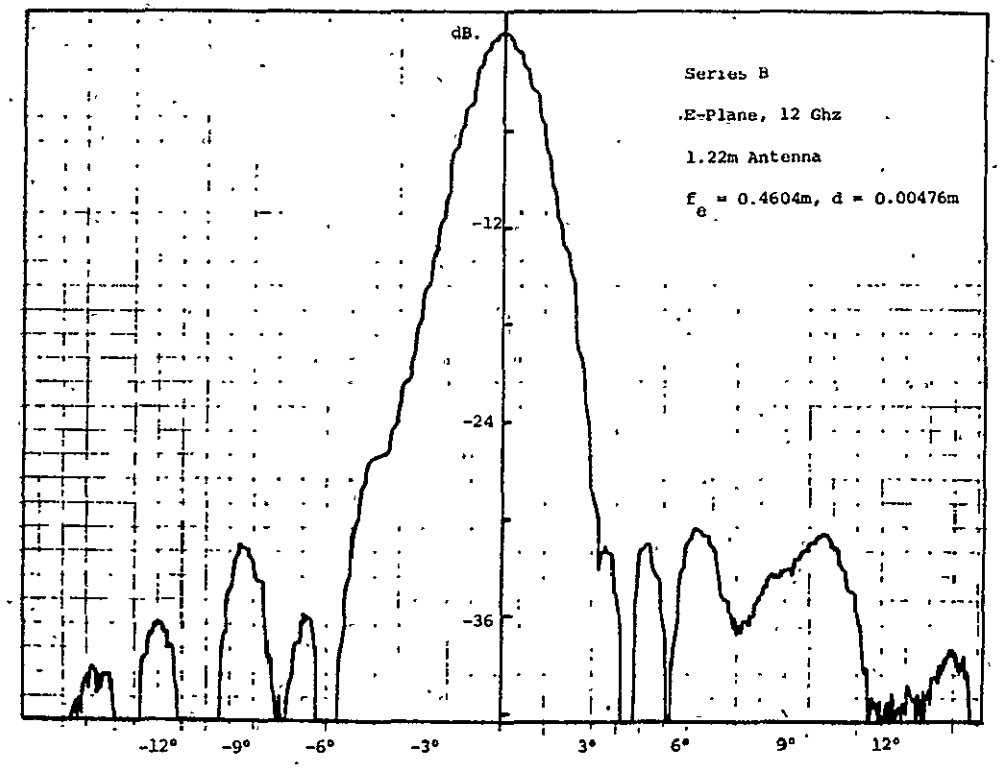

Figure 4.13 E-plane radiation pattern.

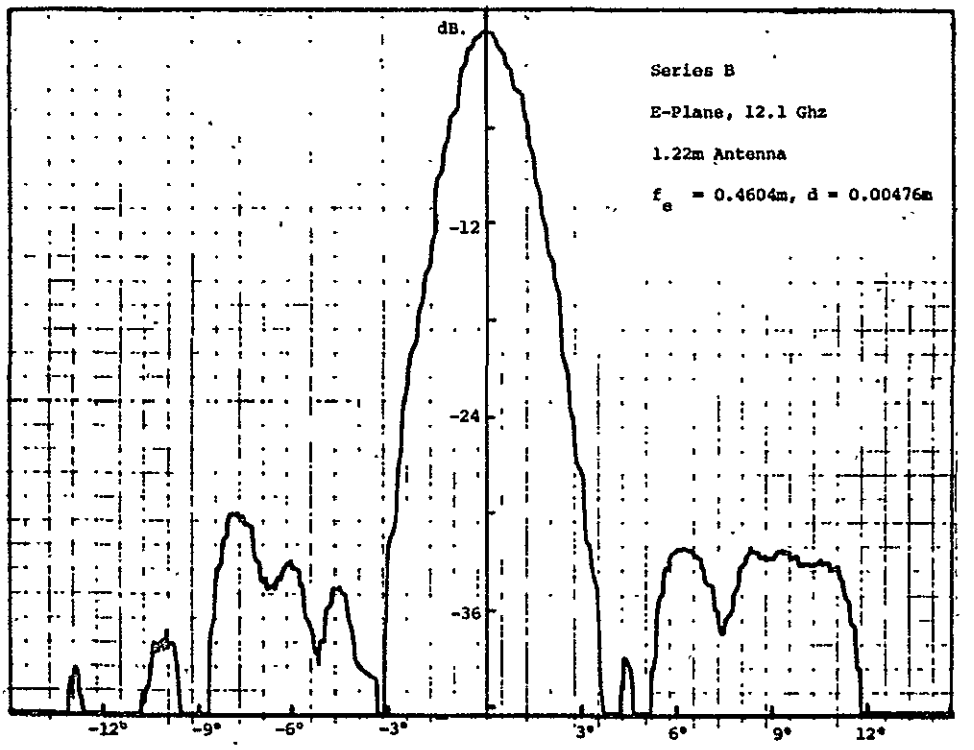

Figure 4.14 E-plane radiation pattern.

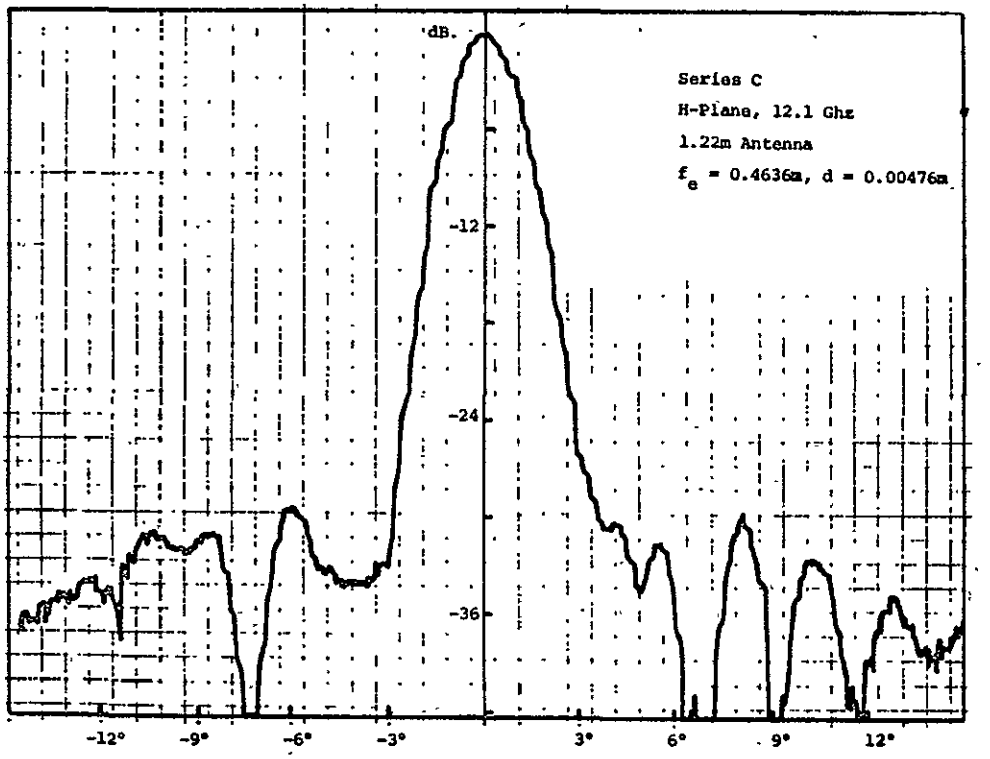

Figure 4.15 H-plane radiation pattern.

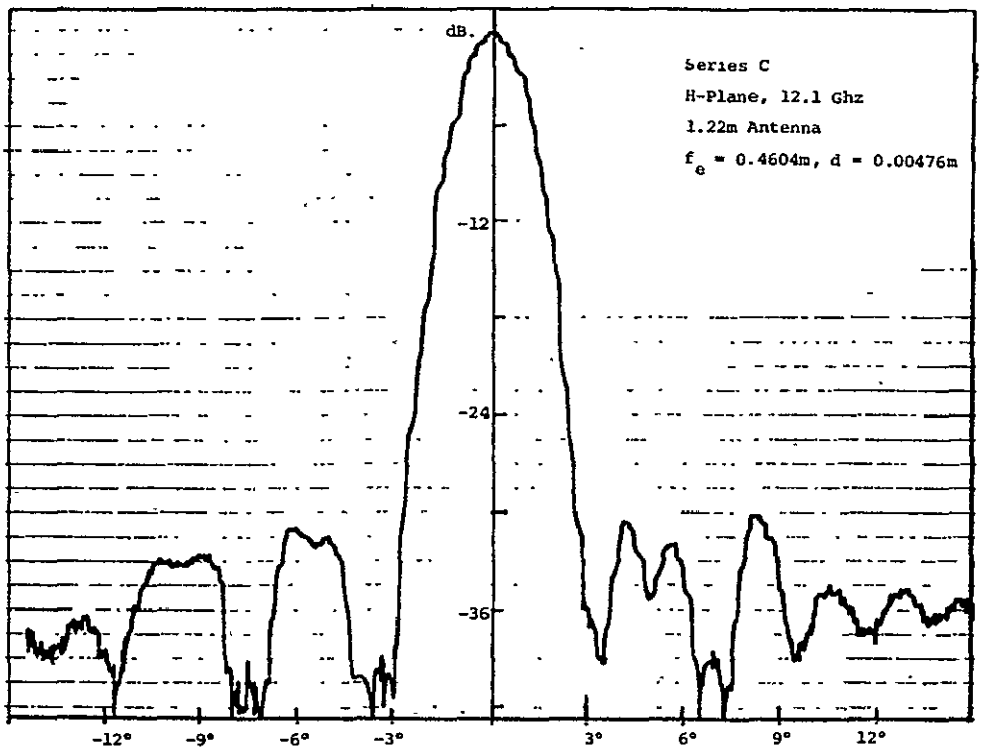

Figure 4.16 H-plane radiation pattern.

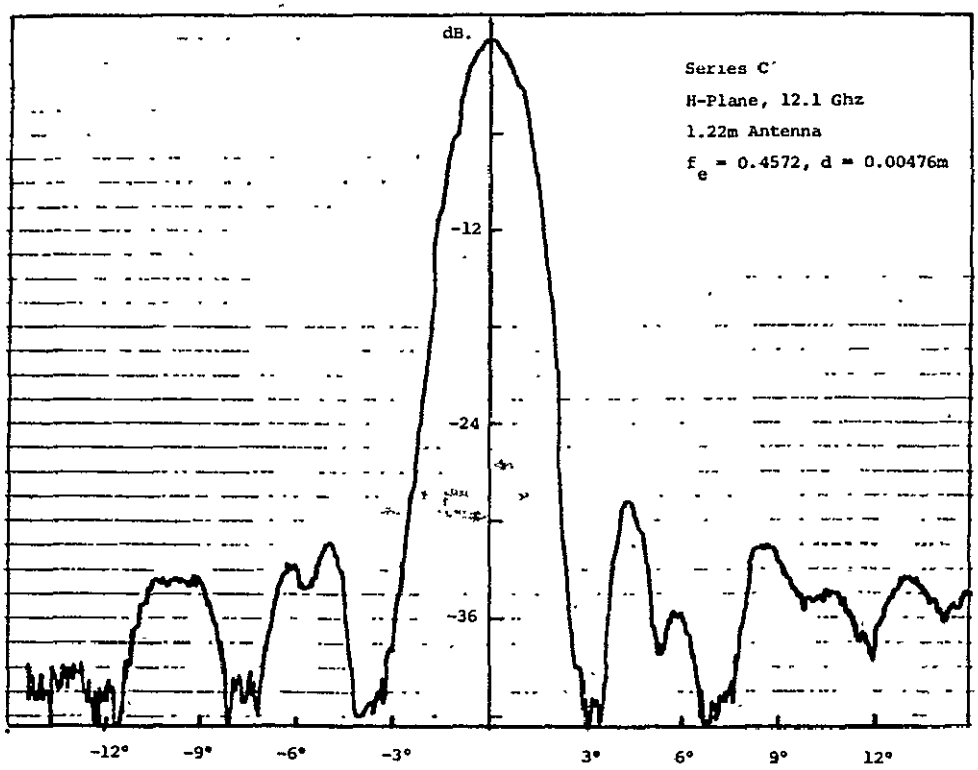

Figure 4.17 H-plane radiation pattern.

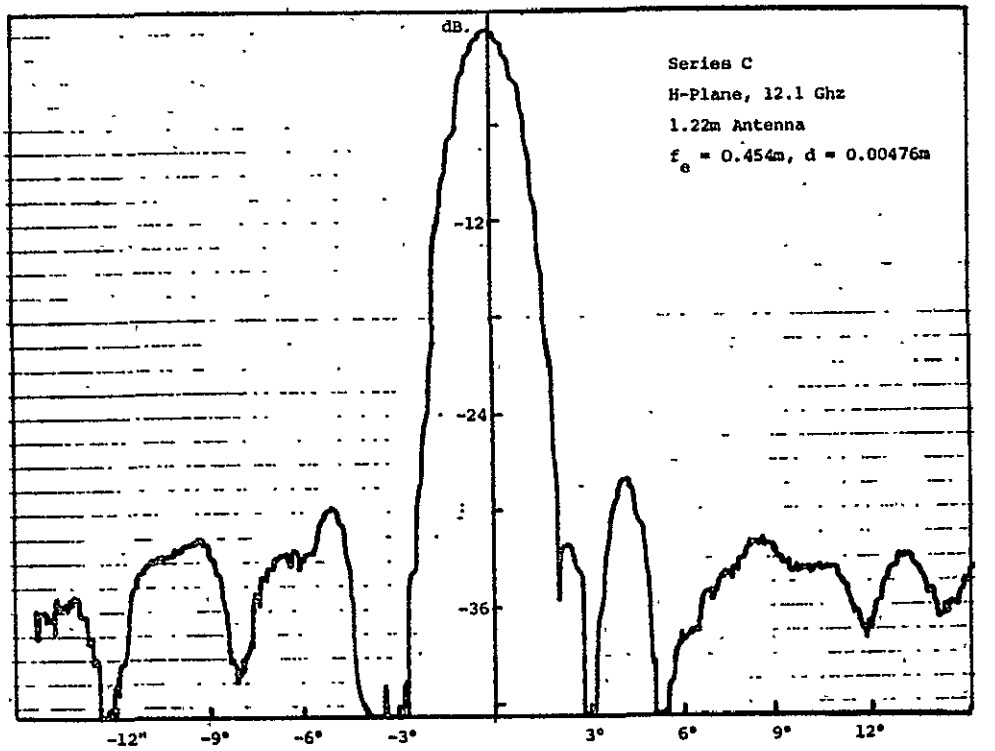

Figure 4.18 H-plane radiation pattern.

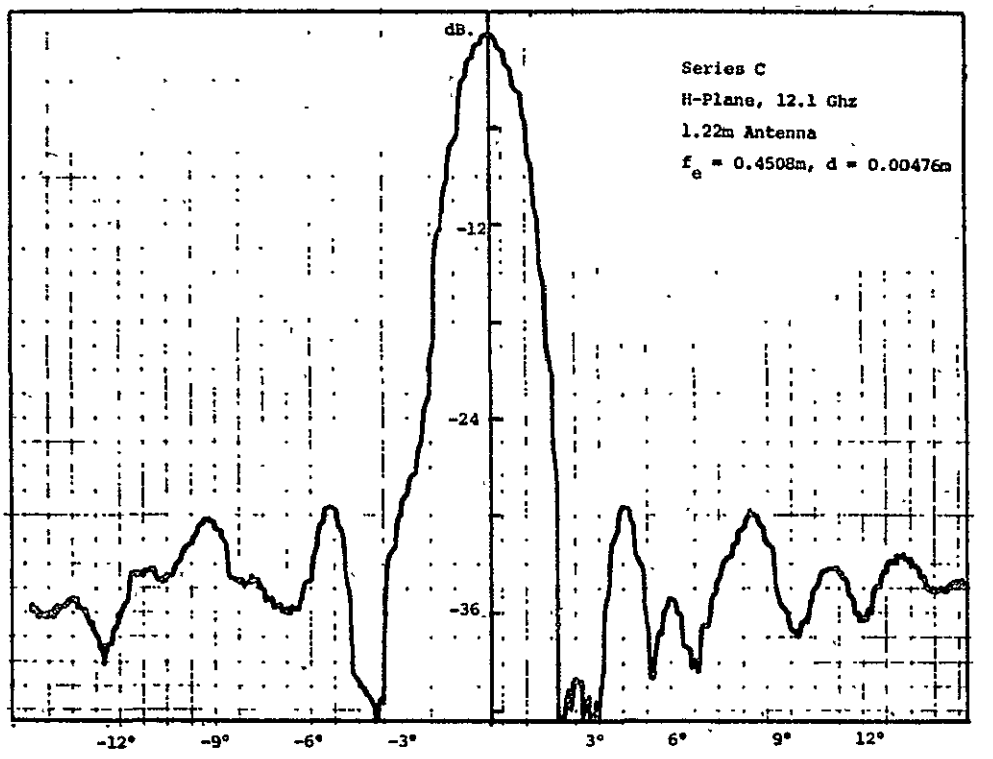

Figure 4.19 H-plane radiation pattern.

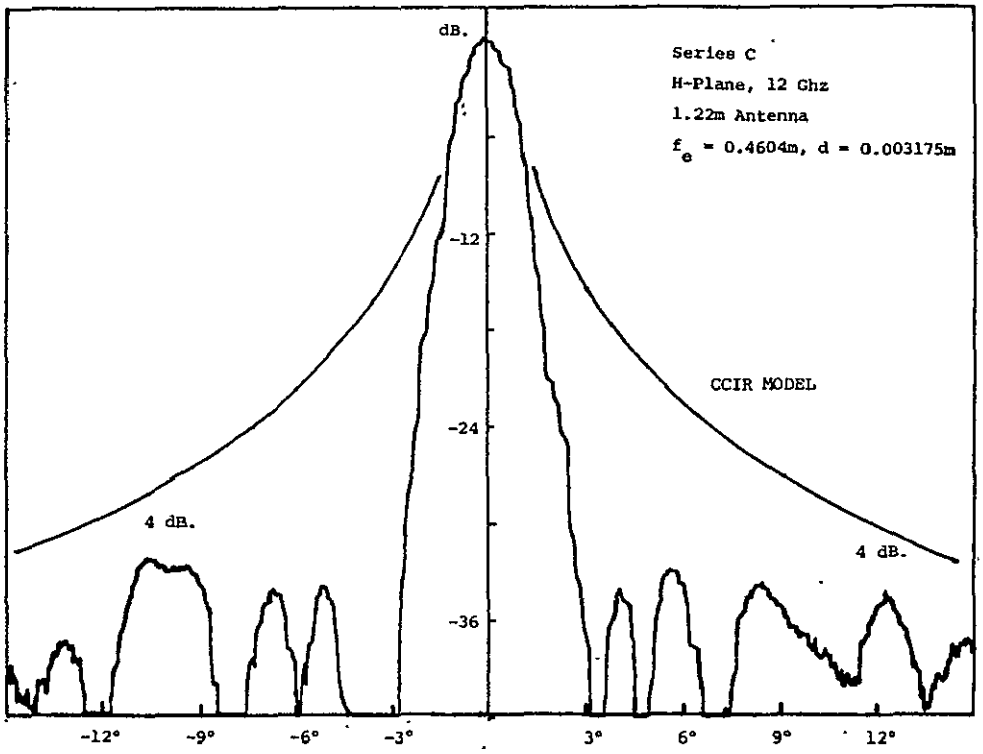

Figure 4.20 H-plane radiation pattern.

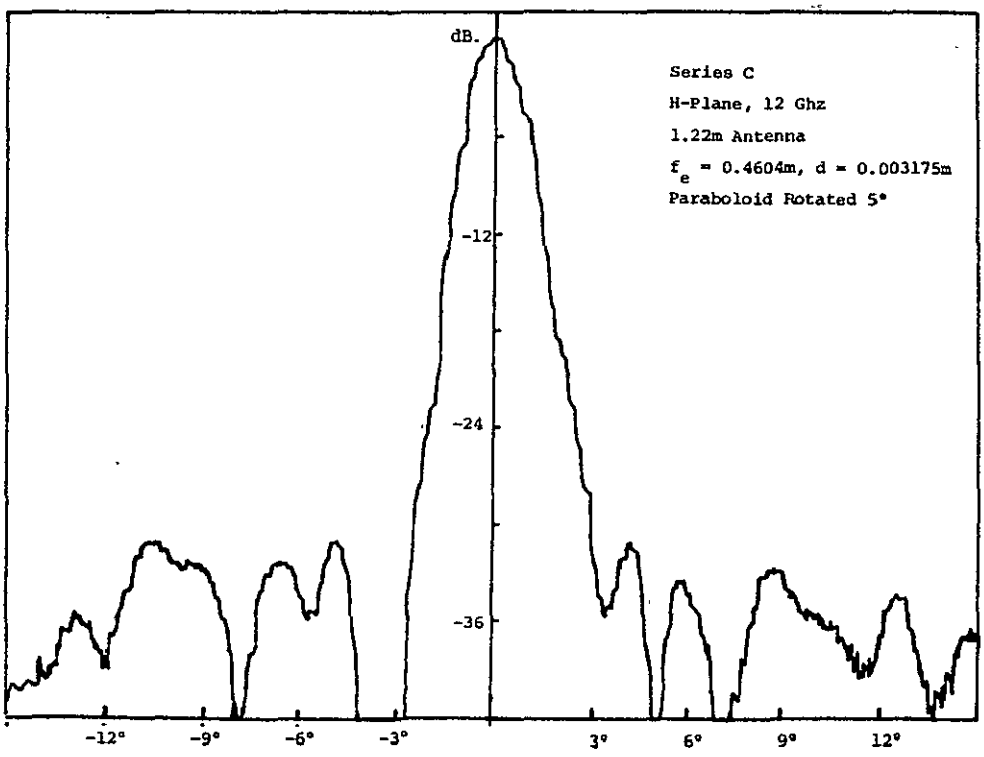

Figure 4.21 H-plane radiation pattern.

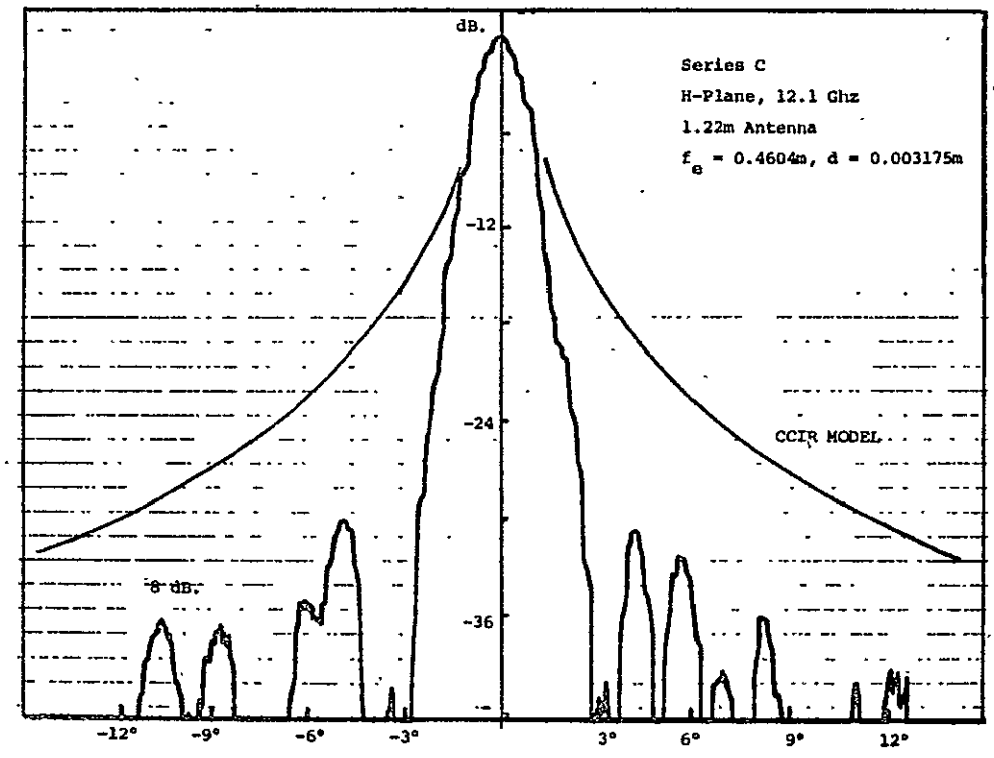

Figure 4.22 H-plane radiation pattern.

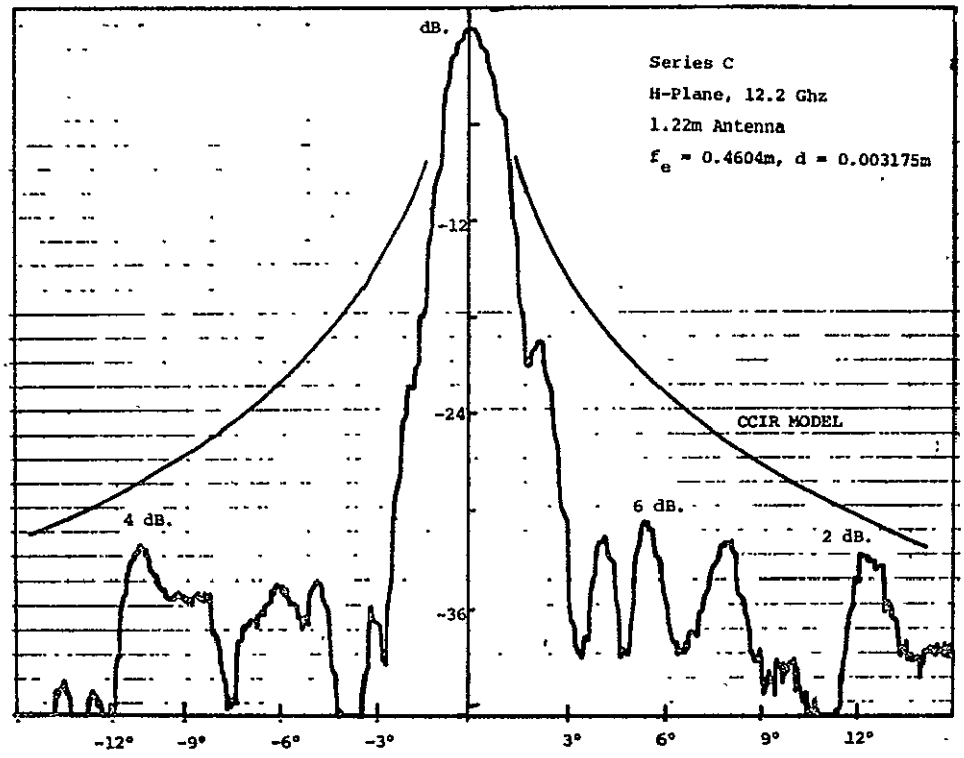

Figure 4.23 H-plane radiation pattern.

of the paraboloid. The sidelobes are below the CCIR model by 5 dB. or more with the exception of the sidelobes at $\pm$ 12° in Fig's. 4.21 and 4.23 (12.0 Ghz. and 12.2 Ghz) which are less than 5 dB. below the model pattern.

Figures 4.24 to 4.27 show E-plane patterns at various frequencies. Note that on one side the far out sidelobes are higher than on the other side. It was determined that this is due to the mixer which is connected directly to the feed and aligned in the E-plane along with the coaxial cable which makes a loop before being taped to a support rod. Figure 4.26 shows a pattern with the mixer rotated 180° and the large amplitude far out sidelobe now appears on the other side of the main lobe. It was found that this lobe can be eliminated by turning the mixer so that the stub which provides the DC current return for the mixer is pointed outwards from the paraboloid. The series of E-plane patterns labeled Series D and shown in Fig's. 4.36 to 4.39 are taken with the stub pointed outwards and show that the spurious sidelobe is eliminated. The series D E-plane patterns have near in sidelobes below -30 dB. and exceed the CCIR model pattern by 5 dB. or more. In general the E-plane patterns exhibit lower sidelobe levels than the H-plane patterns do.

It is believed that the sidelobe produced by the mixer is due to energy scattered back into the paraboloid by the mixer stub. If the scattering center is taken as 0.076m (3 in.) off axis then back scattered radiation would be collimated by the paraboloid and produce a sidelobe at an angle of $\tan^{-1} 3/f = \tan^{-1} 3/18 = 9.5°$ on the opposite side of the axis as shown in Fig. 4.35. The large sidelobe does occur in this general direction.

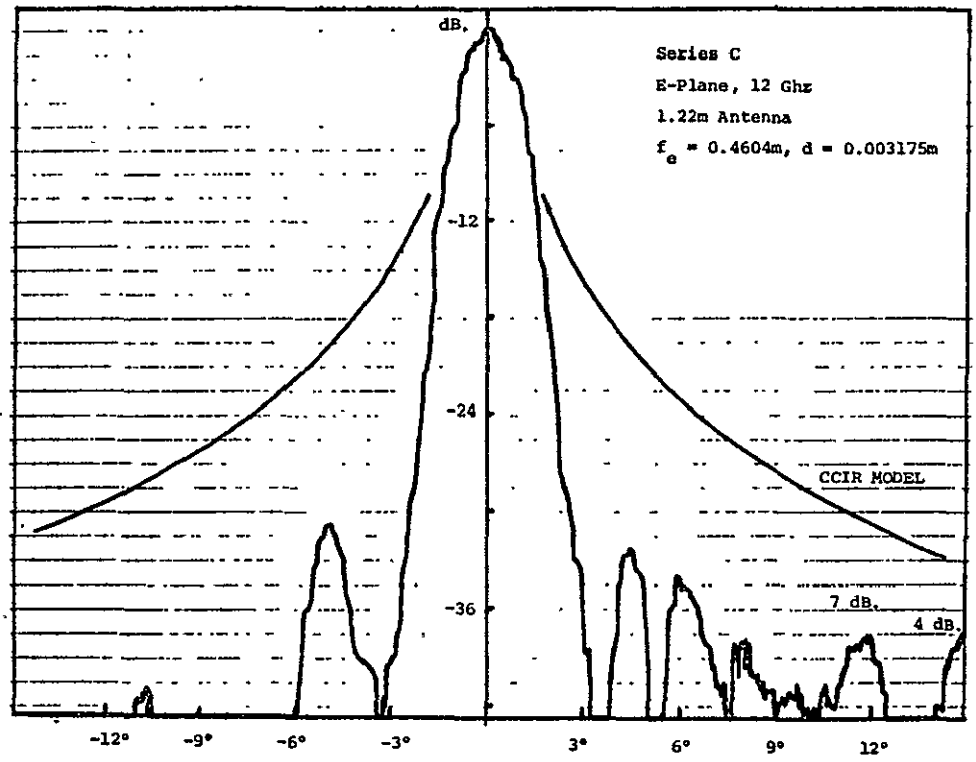

Figure 4.24 E-plane radiation pattern.

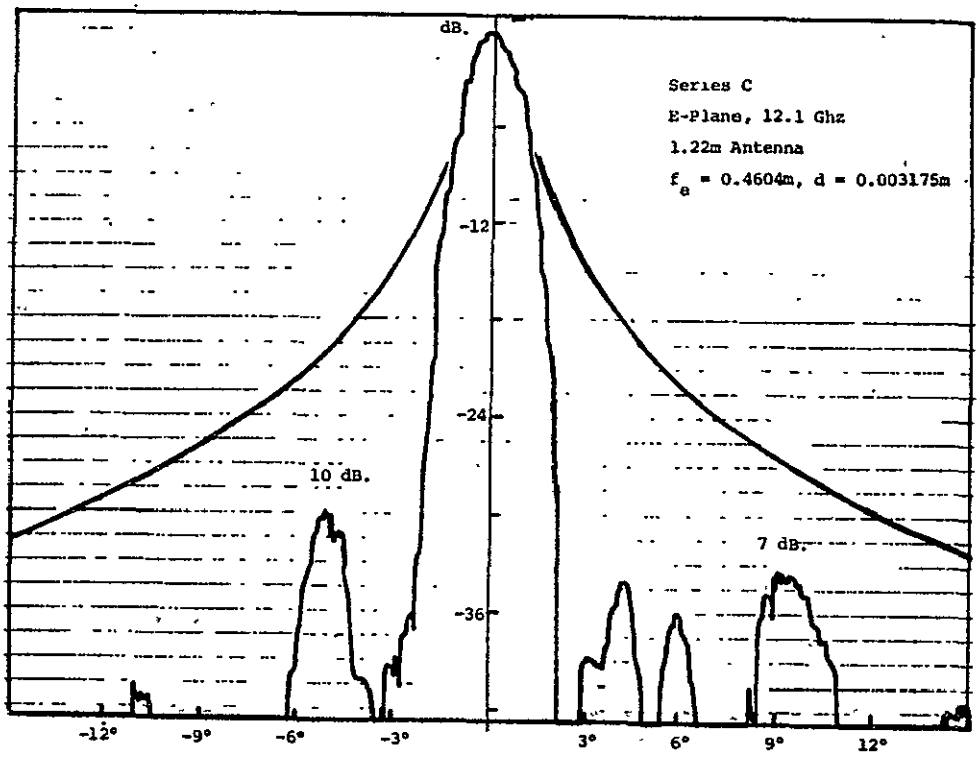

Figure 4.25 E-plane radiation pattern.

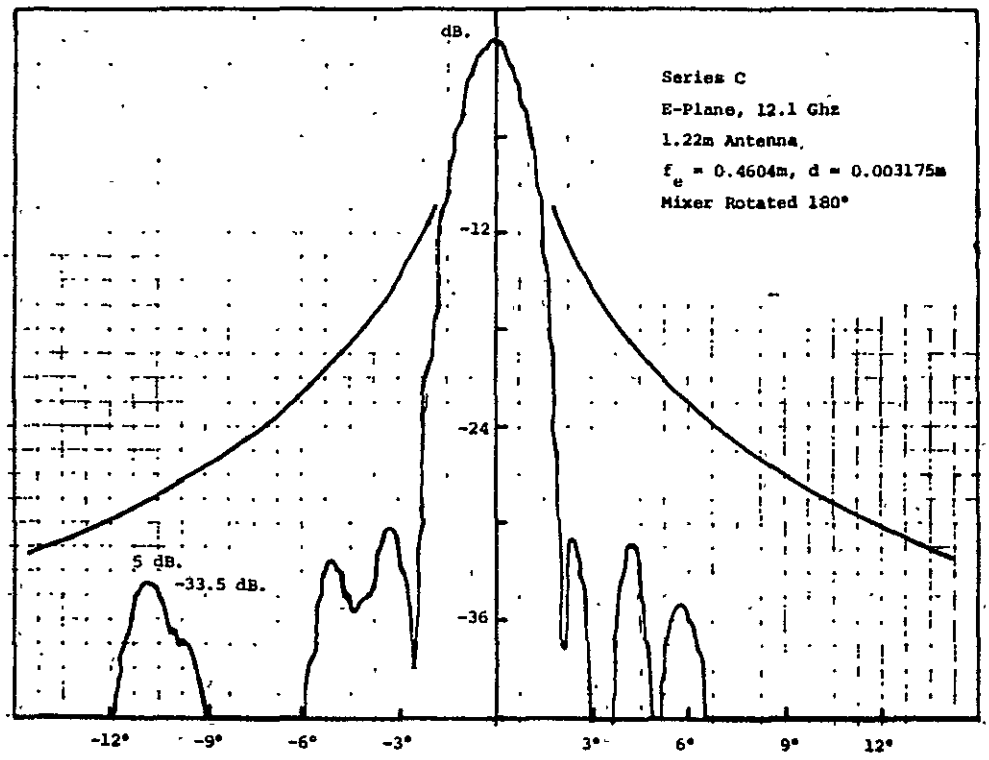

Figure 4.26 E-plane radiation pattern.

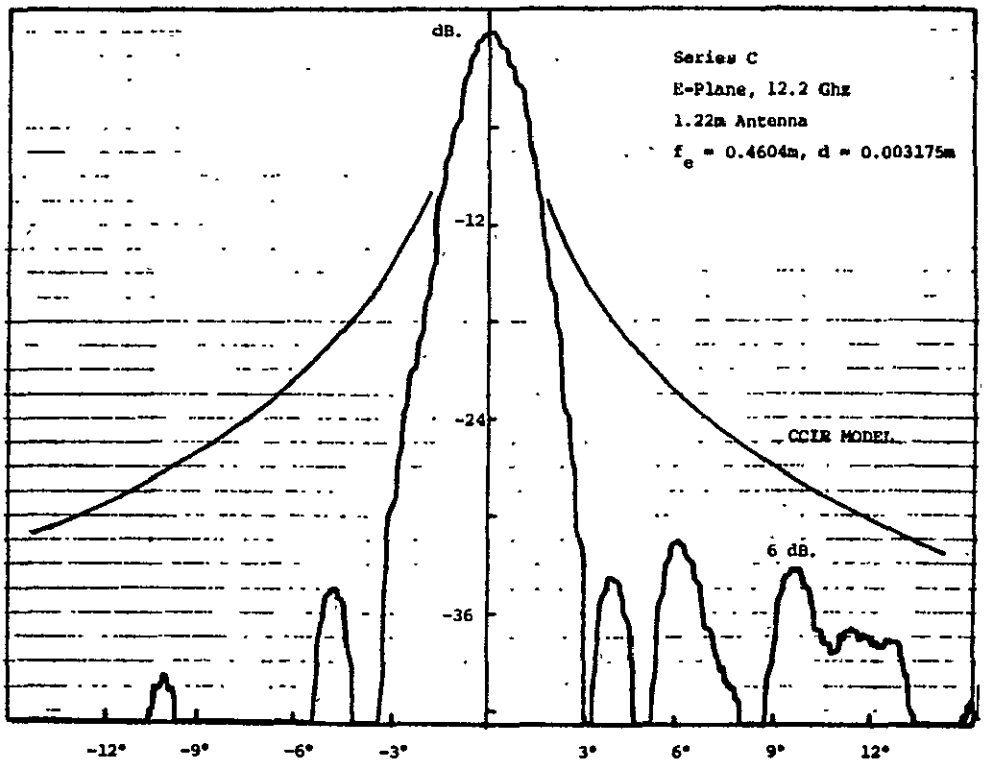

Figure 4.27 E-plane radiation pattern.

Although the recorded patterns cover the range from -15° to 15° only it was verified that the sidelobes beyond this range are below - 38 dB.

The gain of the 1.22m antenna with the Kumar feed was measured by comparison with that of an optimum gain horn. A gain of 41.4 dB. was measured. This compares very well with the calculated gain which is 41.6 dB. The gain measurement is subject to some error since the VSWR of the coaxial to waveguide transition of the horn was not known. The feed was matched with two tuning screws. The quality of the main lobe, its 3 dB. beamwidth, and width between nulls is such that the gain is expected to be very close to the calculated value. The gain of the horn was measured by connecting the microwave mixer directly to the coaxial waveguide transition of the horn and thus there was no need to account for any attenuation in the coaxial transmission line.

Several measurements were carried out to show the affect of using two absorber pads 0.0508m x 0.0635m (2 in. x 2.5 in.) in size and two phase reversal plates 0.0475 m x 0.04128m (1-7/8 in. x 1-5/8 in.) in size. It requires only very small pads or plates to modify sidelobes - 30 dB. or more down by several dB. A photograph of the 1.22m antenna with the absorber pads is shown in Fig. 4.40. The results of these measurements are shown in Fig's. 4.29 to 4.33. In Fig. 4.33 (see Fig. 4.28 for uncompensated pattern), it can be seen that the phase reversal plates reduced the first sidelobe at 4° by 3 dB., increased the sidelobe at 6° by 3 dB., reduced the one at 8° by 3 dB., reduced the sidelobes at 10.5° and 16° below - 42 Db., and increased the sidelobe at 13° by 3 dB. The sidelobe spacing in Fig. 4.28 is not regular enough to get a cancellation effect on all sidelobes. On the left side of the main lobe the sidelobe at -4°

was reduced by 4.5 dB., the one at -6° was increased by 1.5 dB., the one at -8° reduced below -42 dB., and the one at -10.5° was reduced by 3.5 dB. The results for this particular example are summarized in Fig. 4.34. The theoretical amplitude pattern as given by (2.10b) multiplied by 2 for the phase reversal plates is also shown in Fig. 4.34. The compensating field has a maximum normalized value of 0.0176 which is sufficient to reduce a -29 dB. sidelobe to -36 dB., reduce a sidelobe of -35 dB. to zero, and to increase a sidelobe of -33 dB. to -28 dB. If the phases of the sidelobes shown in Fig. 4.34 were 180°, 0°, 180°, 0°, 180° then the first sidelobe at 4° should have been reduced to -36 dB., the sidelobe at 6° should have been increased to -29 dB., the sidelobe at 8° should have been increased to -39 dB., the sidelobe at 10.5° should have been reduced to -38 dB., and the sidelobe at 13.5° should have been essentially cancelled. The correct trend was obtained for sidelobes one, two and four but the wrong effect was obtained for sidelobes three and five. There are several factors that would explain these differences. The expression (2.10b) is not expected to be very accurate for plates less than two wavelengths on a side. Since the sidelobes are caused by various factors such as surface errors, scattering from support rods, etc. there is no reason to expect that the phase will alternate exactly between 0° and 180°. If the phase is different from either 0° or 180° the amount of cancellation obtained would be less. For a phase of 90° an increase is always obtained in the sidelobe level. In view of these many unknown variables it can be concluded that the experimental results have demonstrated that small phase reversal plates can be used to achieve

sidelobe cancellation. This particular example has also shown that in practice it would be necessary to maintain very close tolerances on the antenna in order to obtain reproducible sidelobe patterns. In this regard the two small phase reversal plates that were used could be viewed as a small perturbation or error in the paraboloid surface. Two dents of this size and $\lambda_o/4$ deep would have produced the same effect.

A final series of patterns were taken with strips of absorber (1/2 in. by 1/2 in. by 6 in.) placed on the front and rear of each support rod in the vicinity of the feed, and on the mixer. This series is labelled series E and is shown in Fig's. 4.41 to 4.47. No general worthwhile improvement was obtained. In Fig. 4.46 the absorber was placed on the mixer alone and as can be seen by referring to Fig. 4.45 there is a noticeable change in the sidelobe detail when the absorbers are added to the support rods.

For the H-plane patterns the use of absorbers did reduce the far out sidelobes by a few dB. but tended to increase the level of the near-in sidelobes.

The addition of absorbers on the mixer and support rods would be expected to be useful only if there was significant backscatter from these structures into the paraboloid with a collimination or focusing of this radiation to produce high level sidelobes. Absorbing material would reduce such backscattered radiation. For example, the sidelobe produced by backscatter from the mixer stub and discussed earlier could be eliminated by placing absorber material around the stub (this was verified experimentally). In the forward direction the use of absorbing material will change the forward radiated field but there is no a priori reason to expect that this would necessarily reduce the sidelobe level.

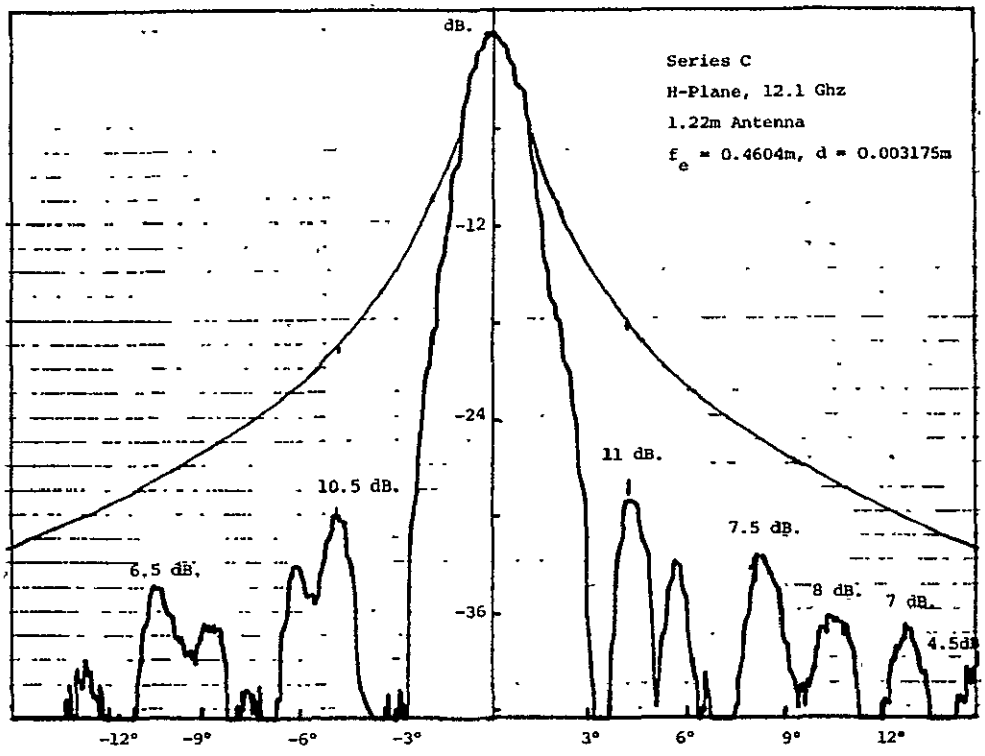

Figure 4.28 H-plane radiation pattern.

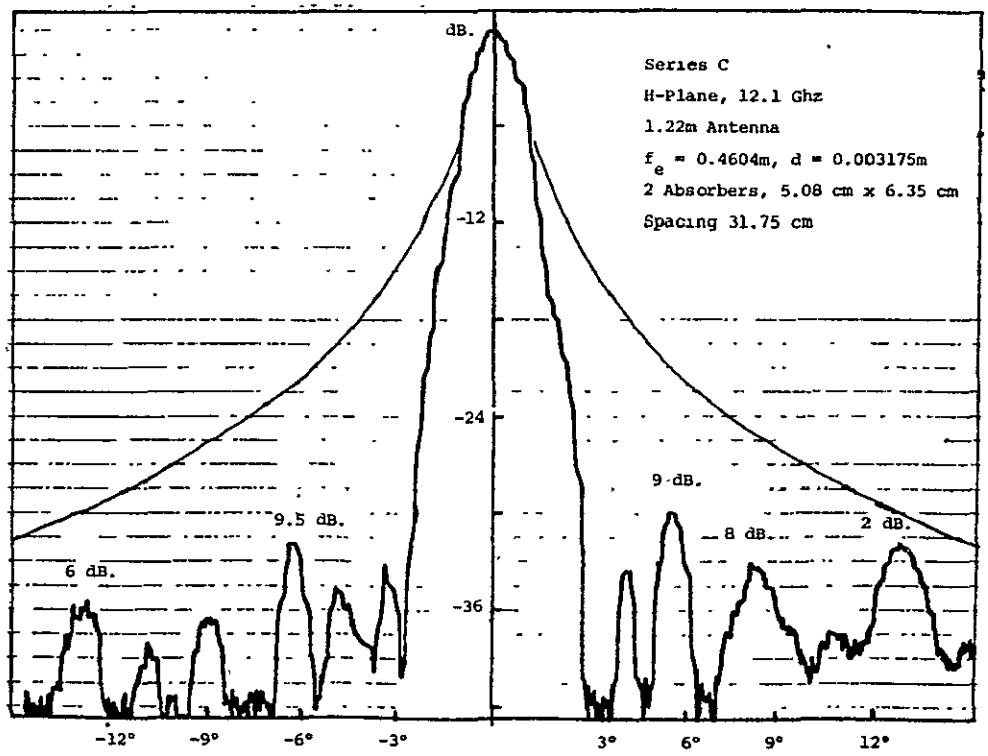

Figure 4.29 H-plane radiation pattern.

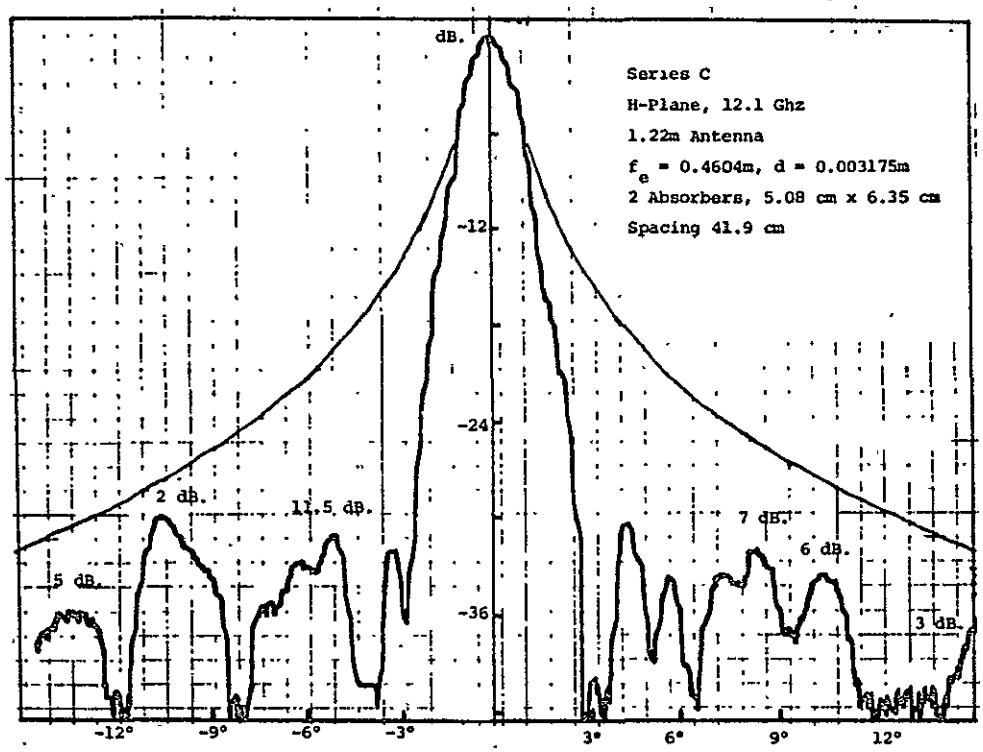

Figure 4.30 H-plane radiation pattern.

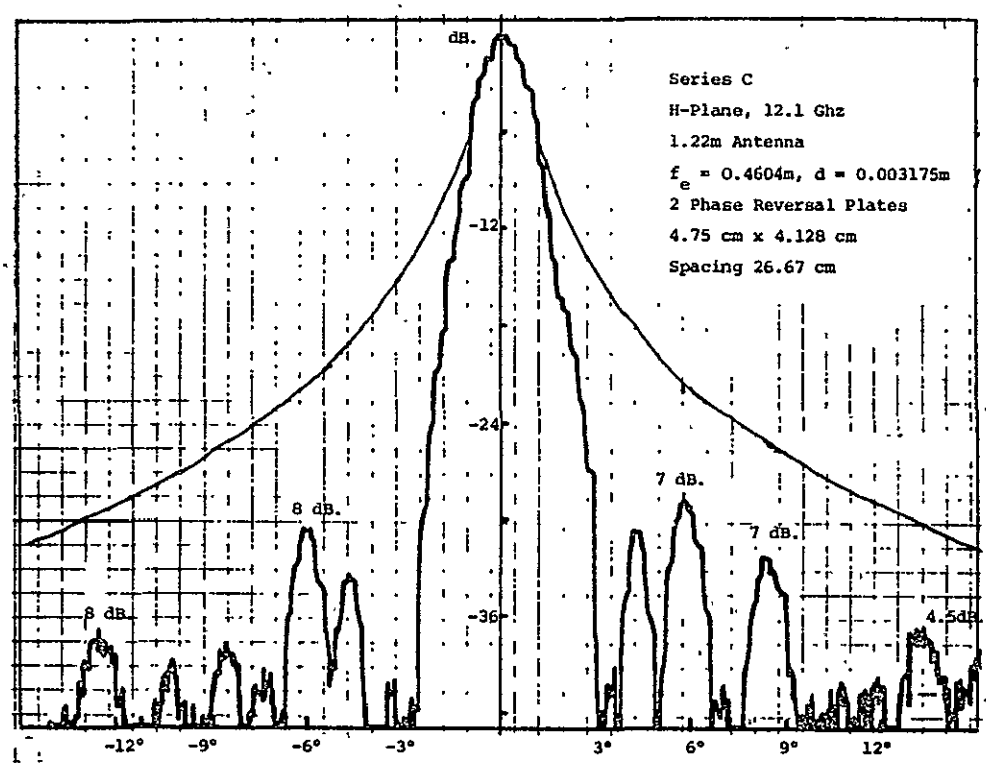

Figure 4.31 H-plane radiation pattern.

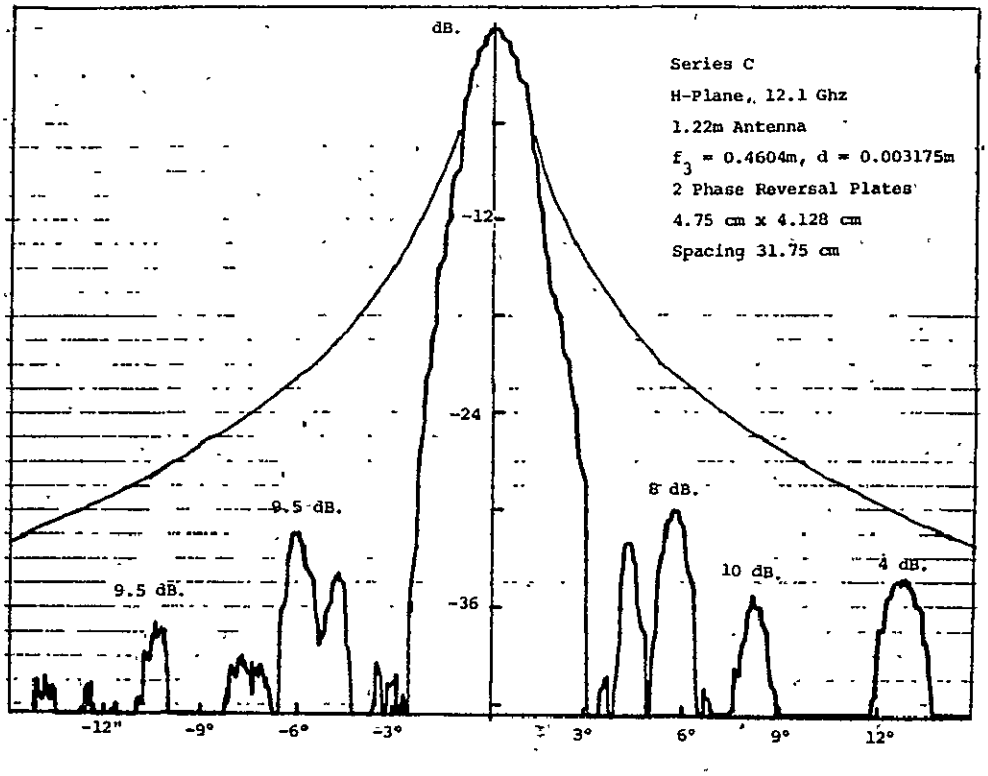

Figure 4.32 H-plane radiation pattern.

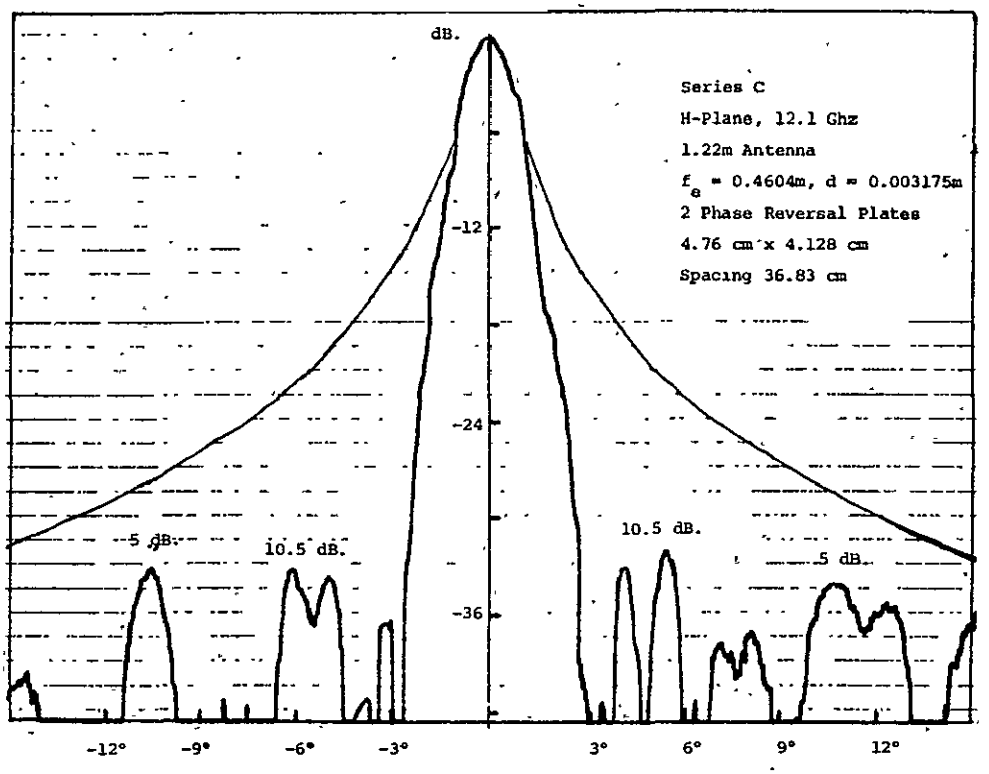

Figure 4.33 H-plane radiation pattern.

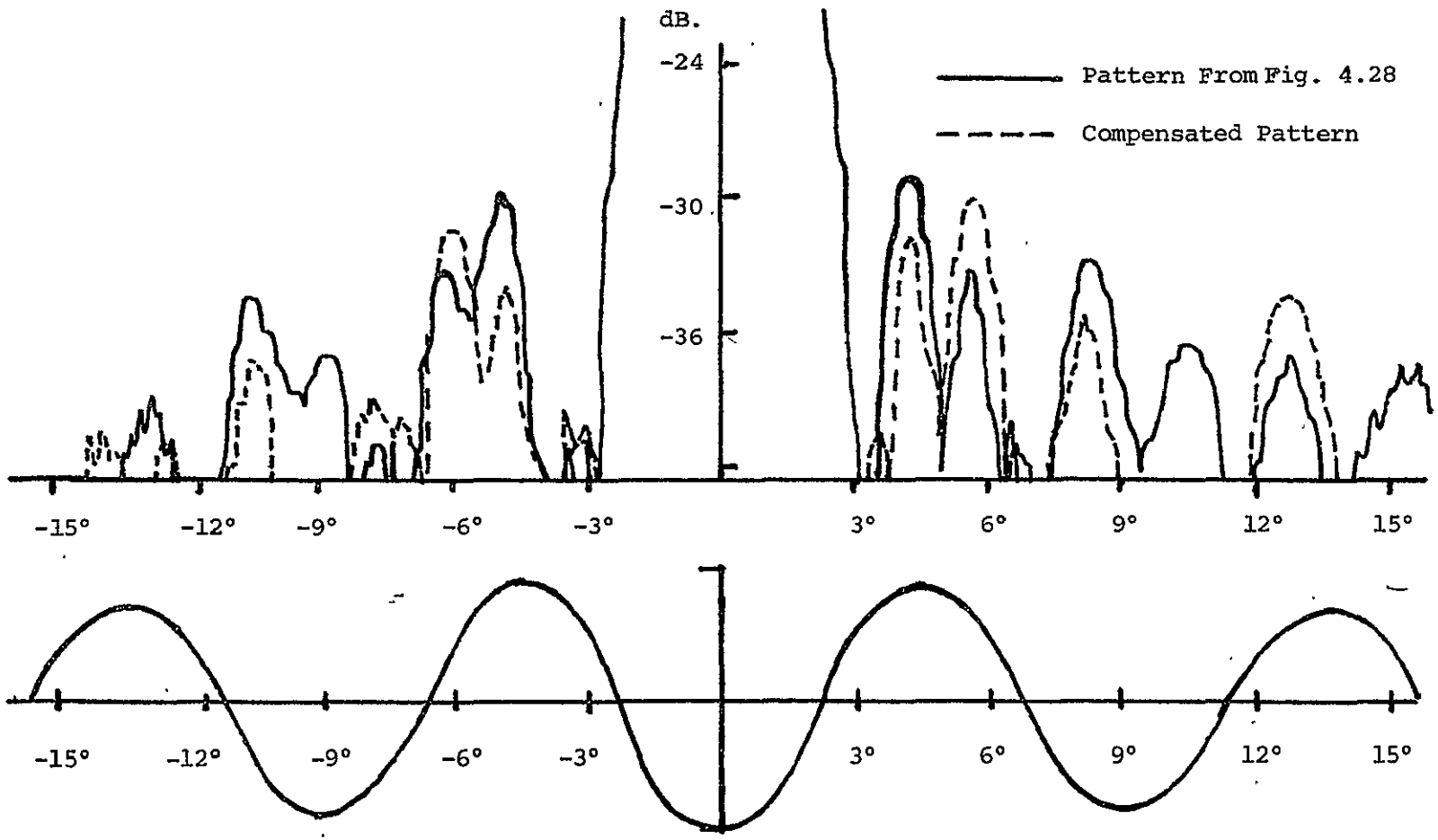

Figure 4.34 Illustration of sidelobe compensation using two phase reversal plates 4.75 cm. by 4.128 cm. and spaced 31.75 cm. apart in H-plane of 1.22m paraboloid with Kumar feed. H-plane pattern at 12.1 Ghz.

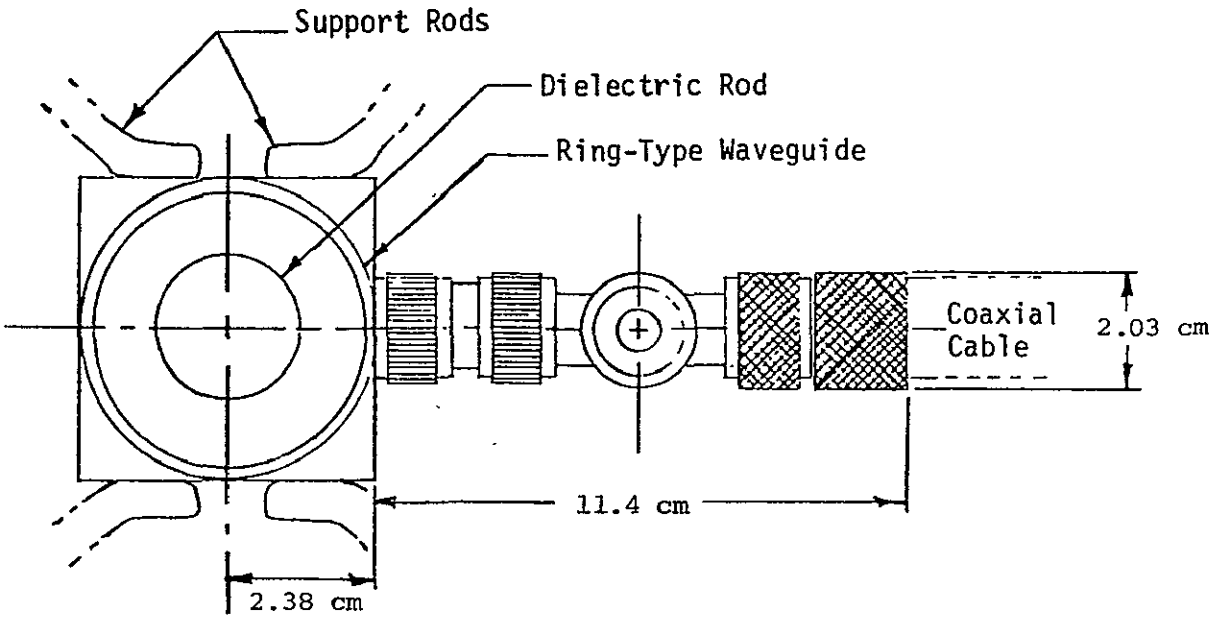

(a)

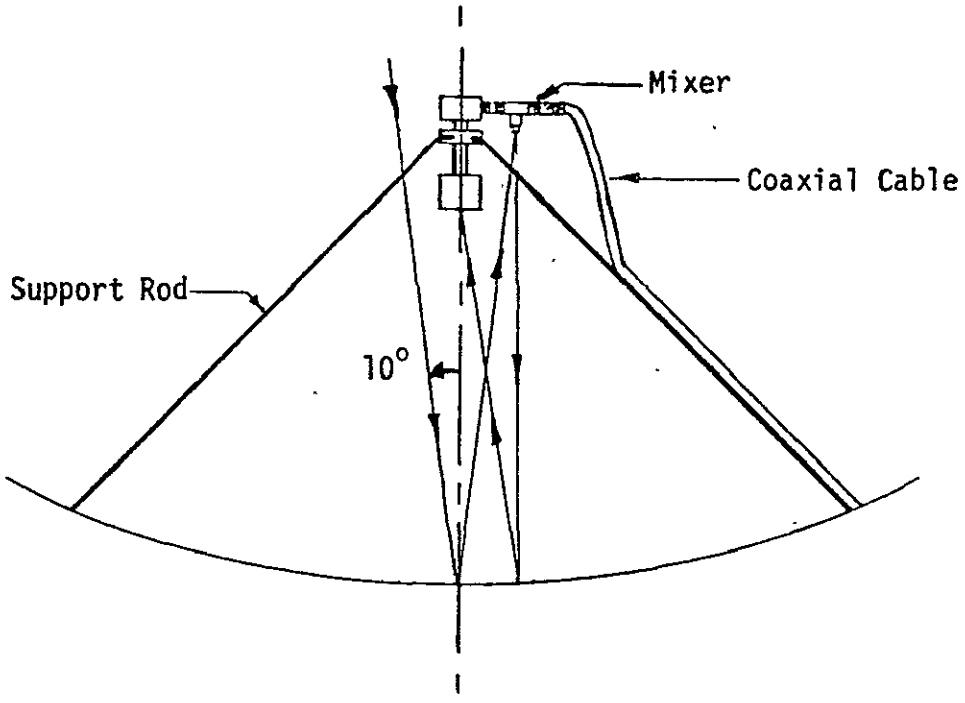

(b)

Figure 4.35 (a) View of feed and mixer as seen from paraboloid vertex. (b) Top view of antenna showing scattering from mixer stub.

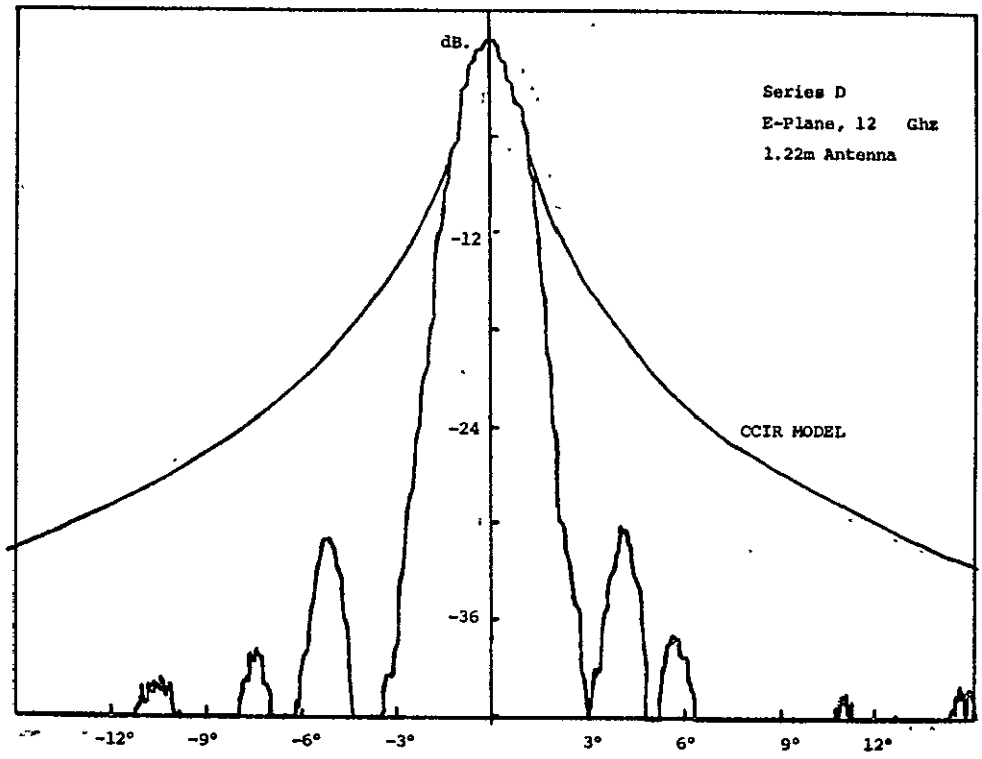

Figure 4.36 E-plane radiation pattern.

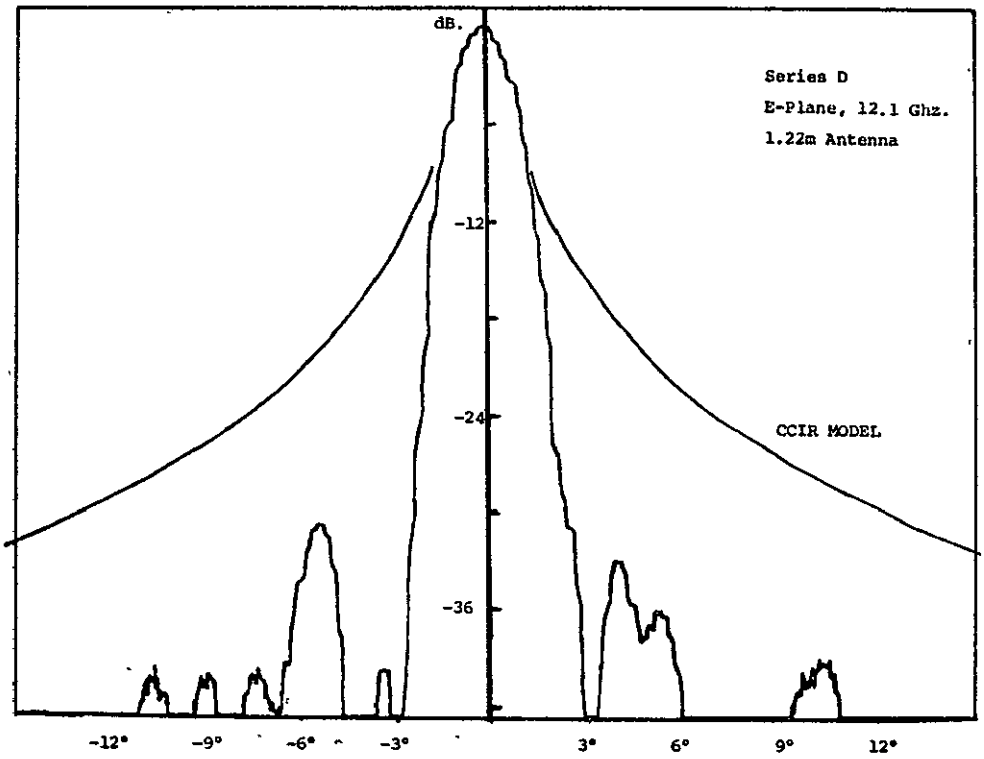

Figure 4.37 E-plane radiation pattern.

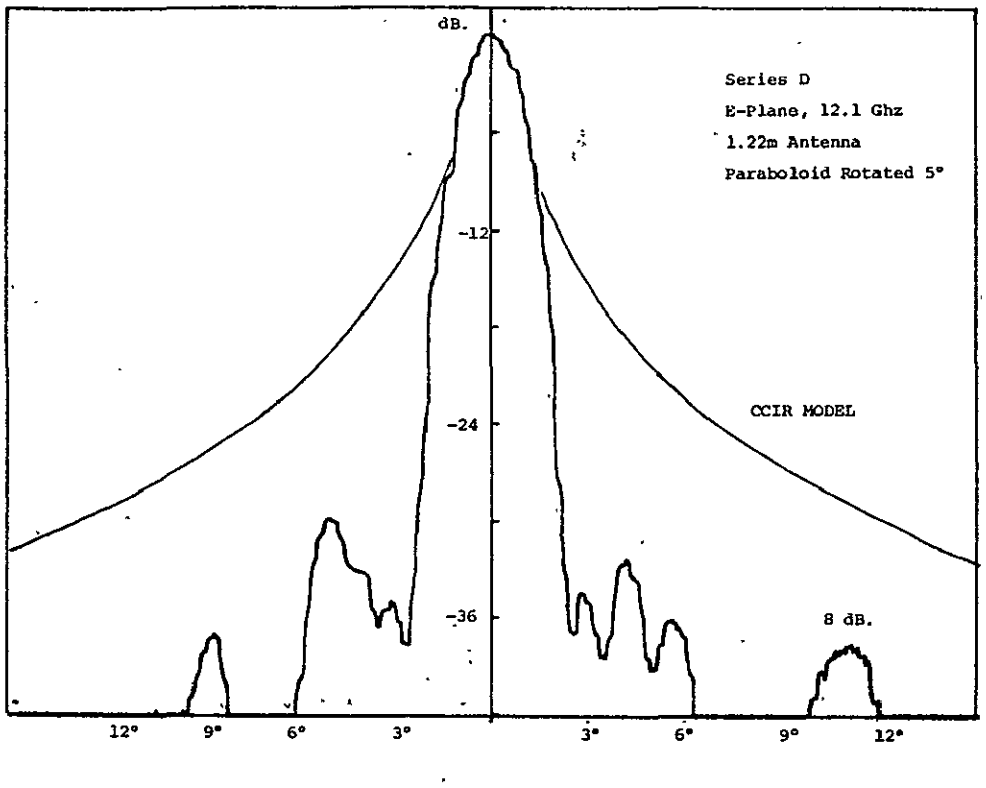

Figure 4.38 E-plane radiation pattern.

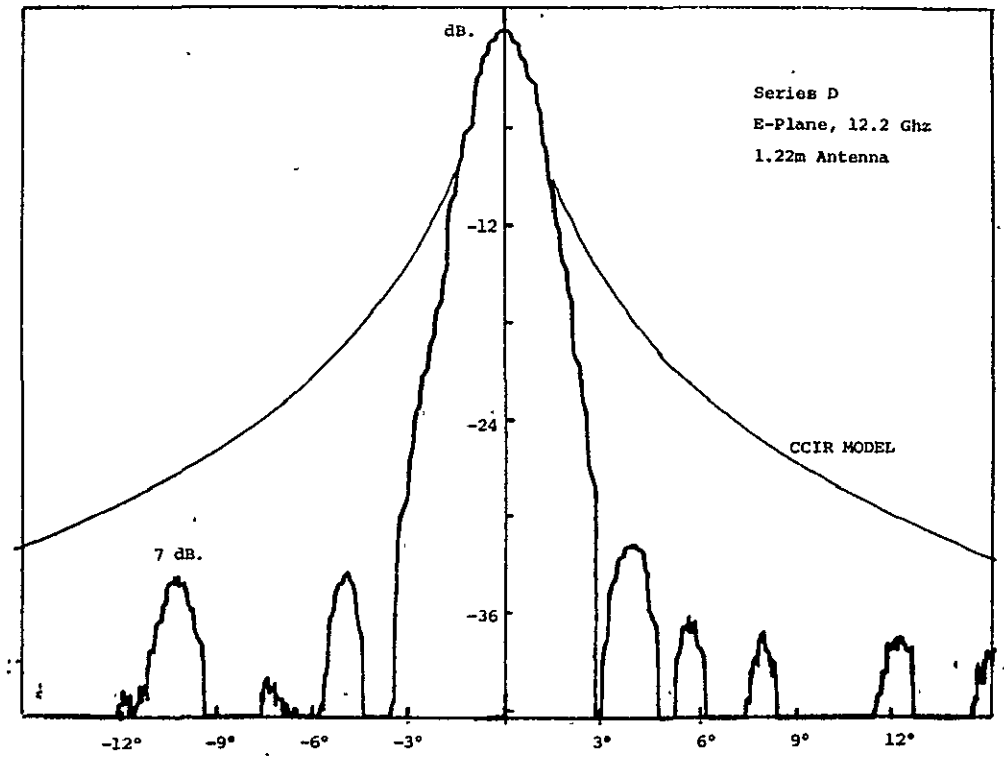

Figure 4.39 E-plane radiation pattern.

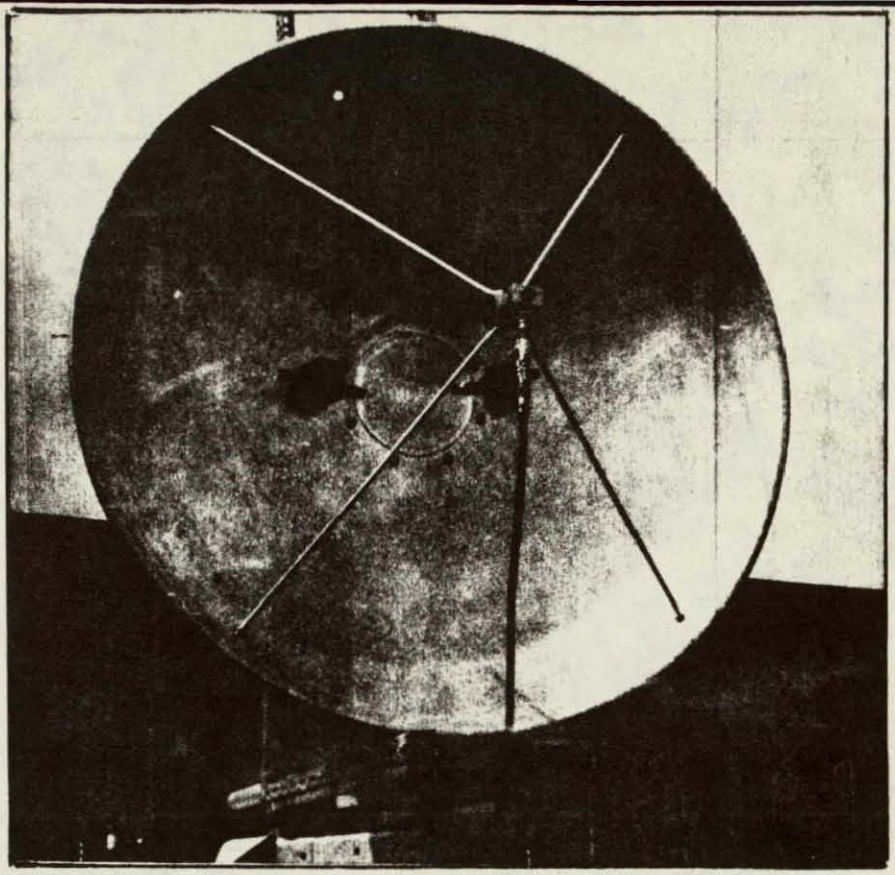

Figure 4.40 View of 1.22m antenna with absorber pads.

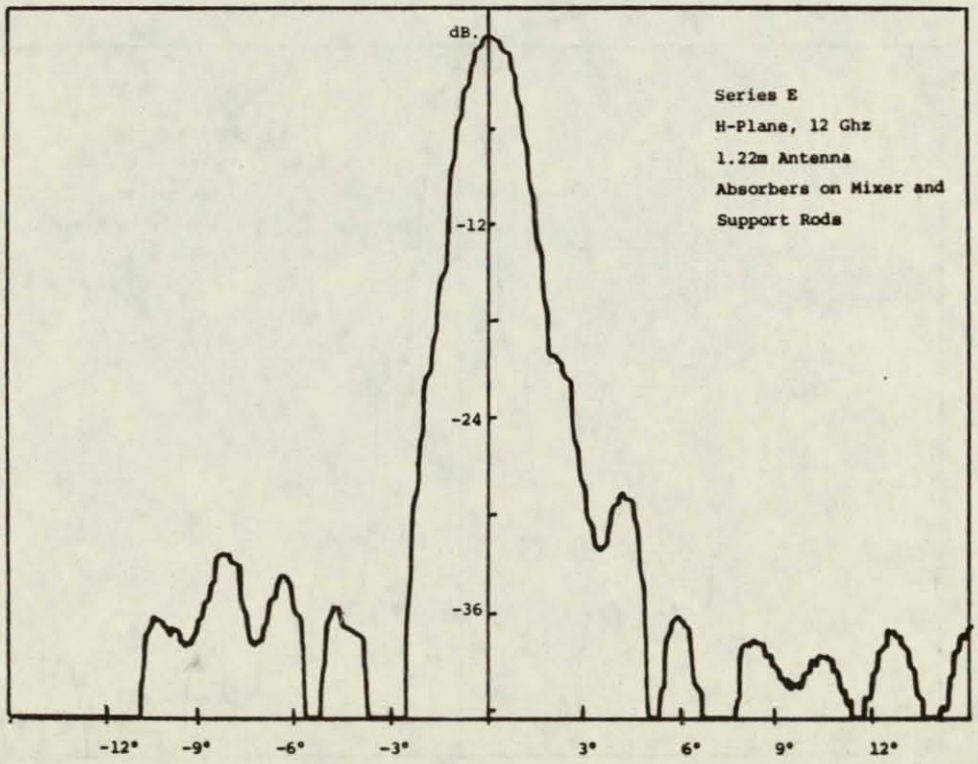

Figure 4.41 H-plane radiation pattern.

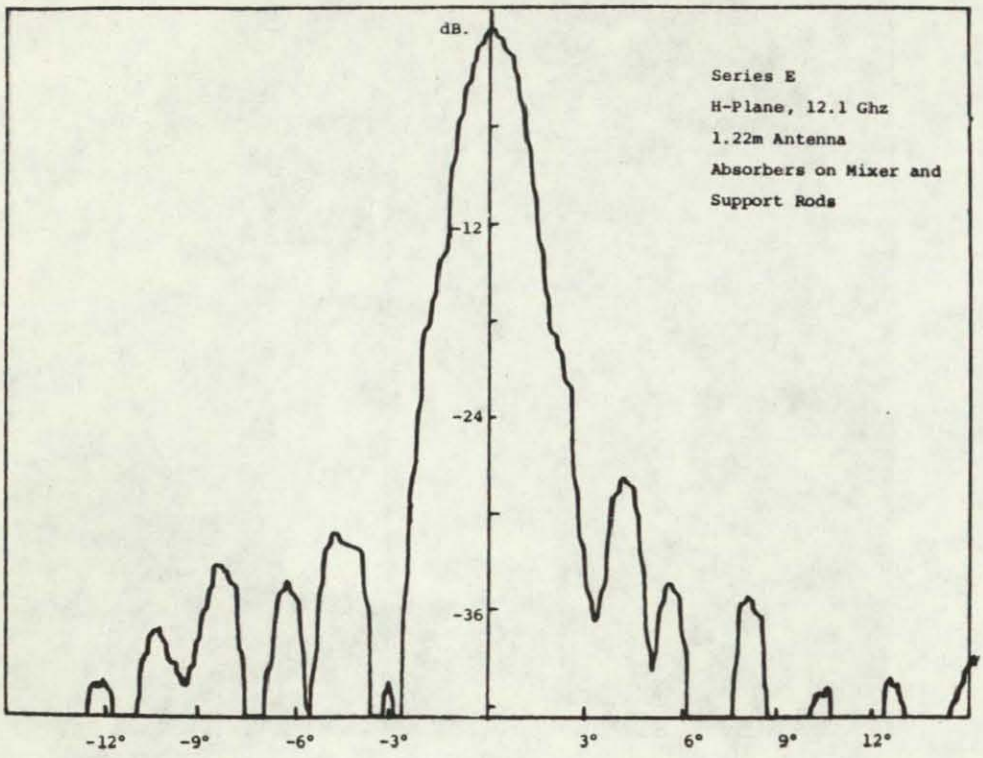

Figure 4.42 H-plane radiation pattern.

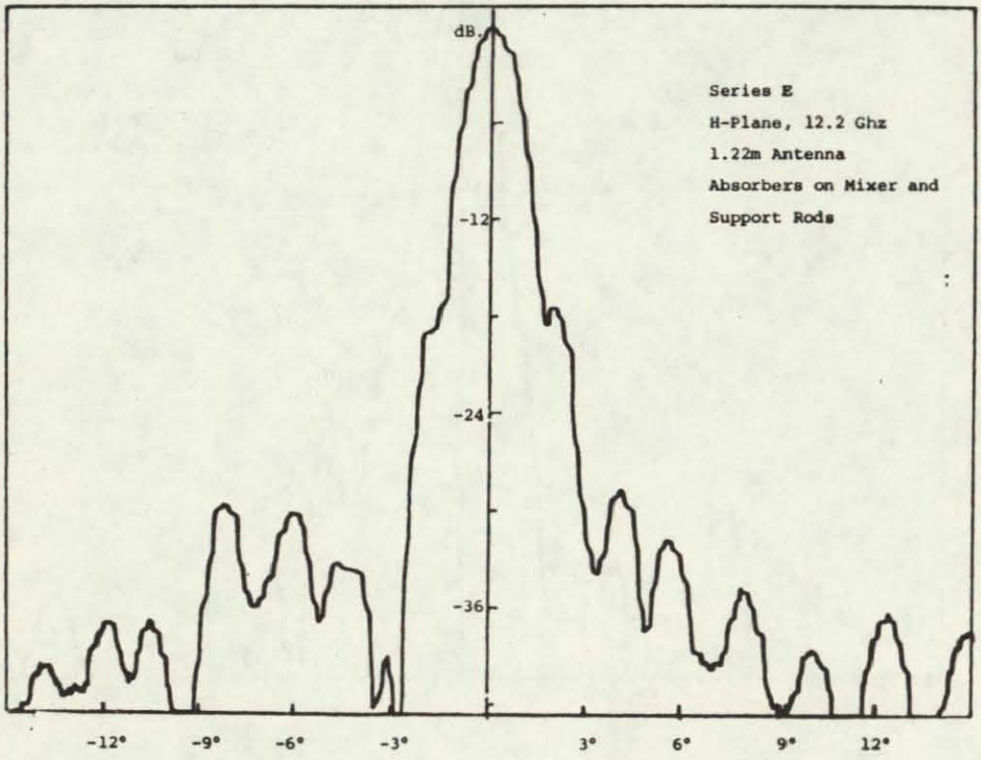

Figure 4.43 H-plane radiation pattern.

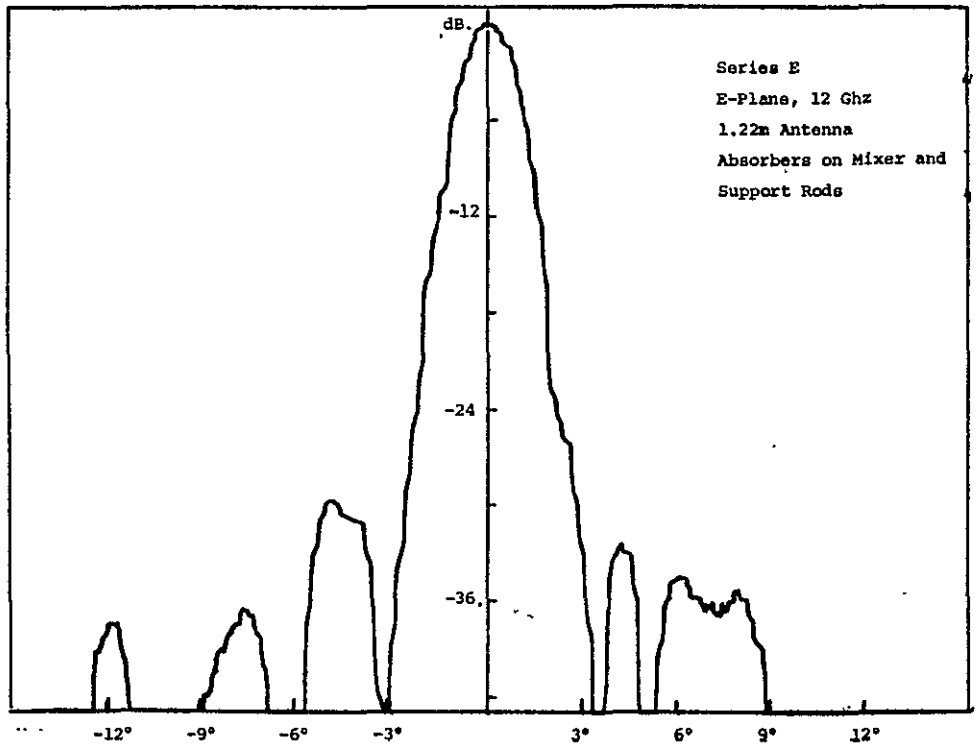

Figure 4.44 E-plane radiation pattern.

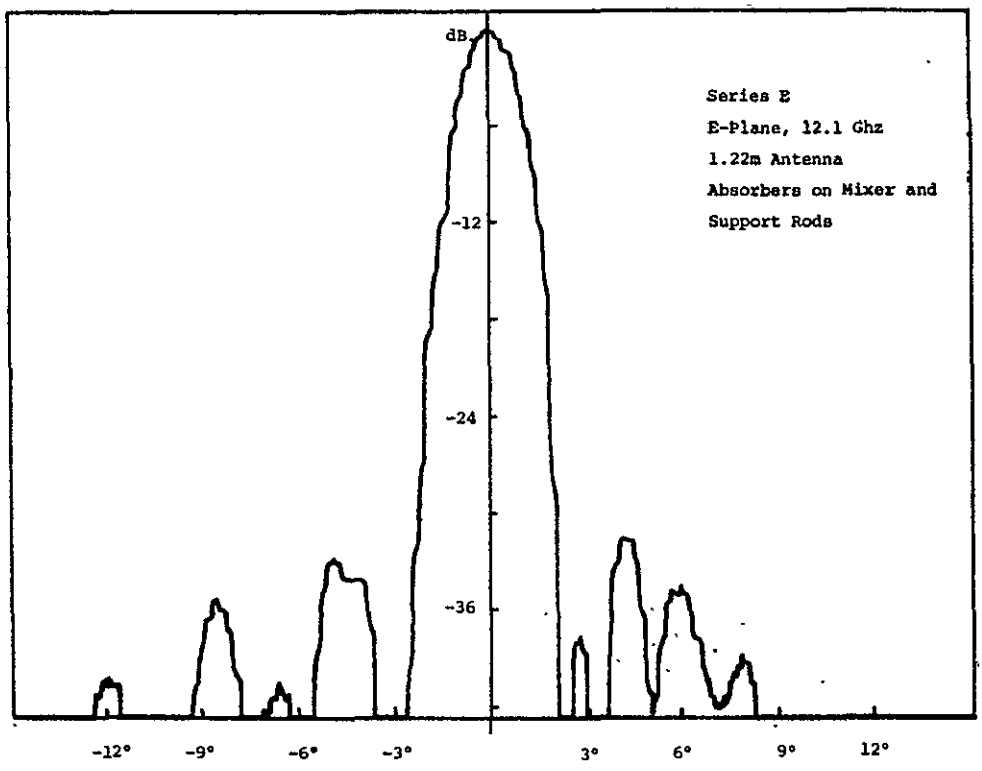

Figure 4.45 E-plane radiation pattern.

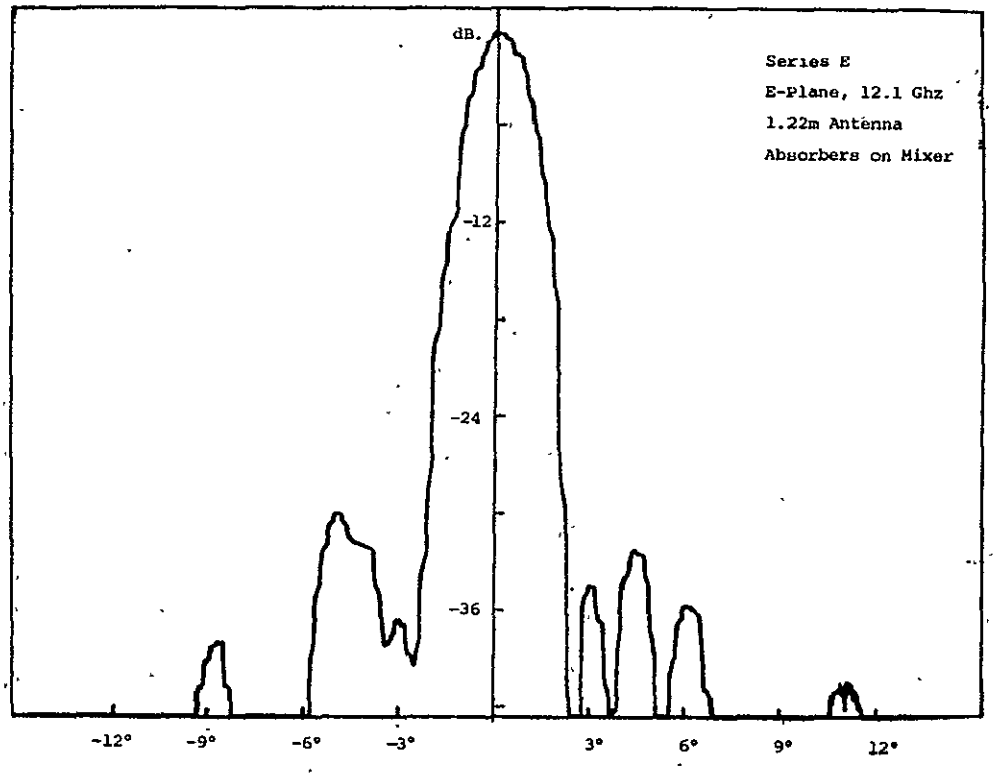

Figure 4.46 E-plane radiation pattern.

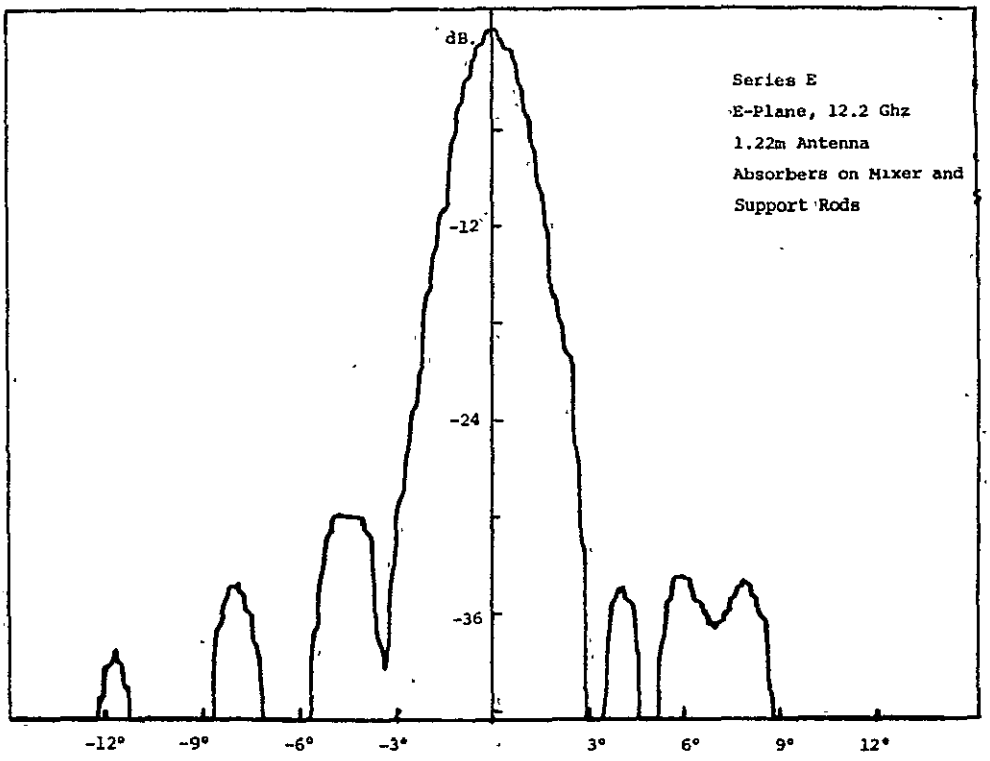

Figure 4.47 E-plane radiation pattern.

4.3 Experimental Results for the 1.83m Paraboloid

The same general surface distortion that was found in the 1.22m paraboloid also existed in the 1.83m paraboloid. In addition the latter also had a small periodic radial variation in the surface contour. In view of the theoretical predictions presented in Chap. 3 as to the effects of clam-shell and periodic radial distortion on sidelobe levels it is not surprising that the initial patterns taken were of poor quality. Less effort was spent in removing the surface contour errors than was spent on the 1.22m antenna and hence the final patterns obtained were not as good. An improvement of 4 dB. or more over that of the CCIR model pattern was nevertheless achieved.

The 1.83m (6 ft.) paraboloid as received had both clam-shell distortion as well as a periodic radial variation of approximately $\pm$ 0.8 mm ($\pm$ 1/32 in.) in the surface contour. The initial patterns measured for this antenna showed very poor focusing and high sidelobe levels. Figures 4.48 and 4.49 show two typical patterns for the 1.83m paraboloid as received and using the manufacturer's waveguide feed. Note the large filled in sidelobe region on each side of the main lobe, which is indicative of poor focusing, i.e., large phase errors.

Figure 4.50 shows a pattern taken using the Kumar feed. The best focusing was obtained with the feed 0.686m (27 in.) from the vertex but the sidelobe level was very high. Since the focal length was supposed to be 0.698m (27.5 in.) it was expected that large clam-shall distortion was present.

A second pattern was taken in a plane at 90° relative to the first pattern plane and as seen from Fig. 4.51 the focusing in this plane was very poor with the feed 0.686m from the vertex. By moving the feed to

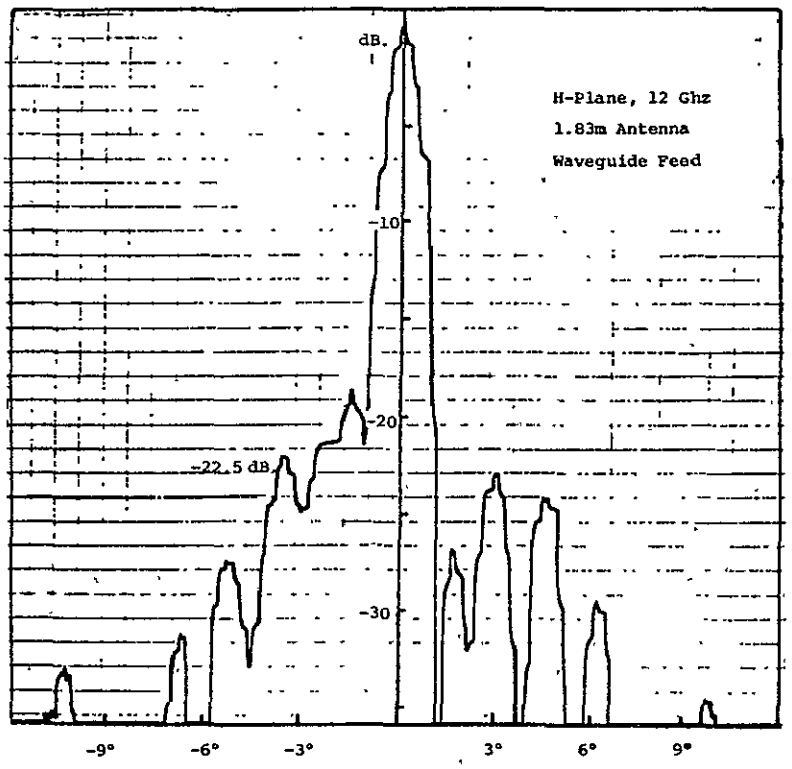

Figure 4.48 H-plane radiation pattern.

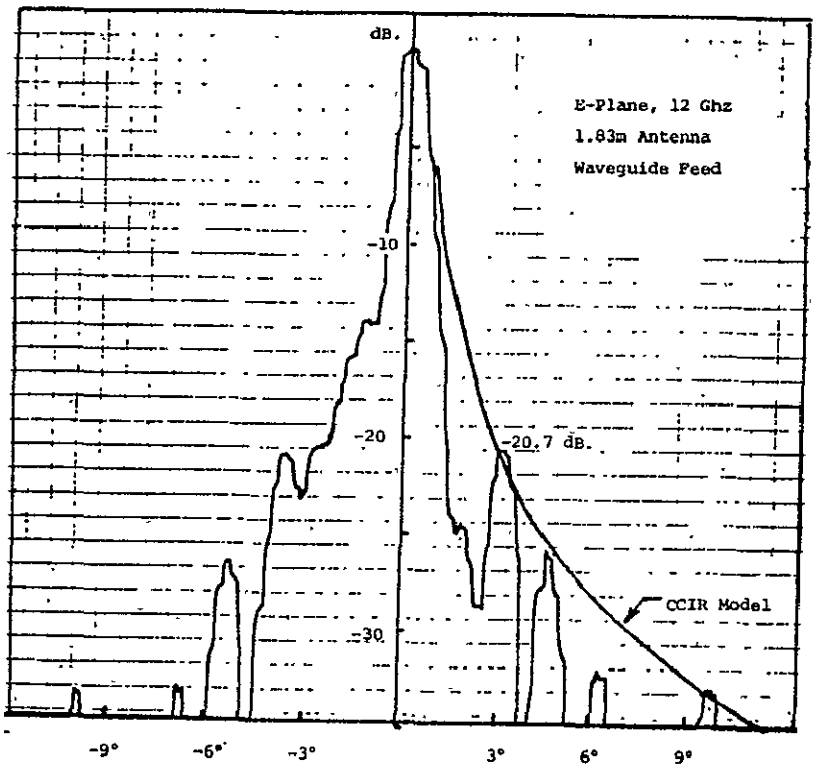

Figure 4.49 E-plane radiation pattern.

0.695m (27-3/8 in.) from the vertex, better focusing was obtained as shown in Fig. 4.52 but the sidelobe level was very high (around -24 dB.). The surface contour was then checked with a template and it was found that the relative deviation from a true paraboloid surface in two orthogonal planes was about 6.4 mm (1/4 in.) at the rim. It was found possible to remove most of this clam-shell distortion.

Figures 4.53 to 4.56 shows the patterns obtained after the above corrections were made. Note that in the E-plane it was possible to obtain sidelobes below the CCIR model pattern by more than 5 dB. with the exception of a sidelobe at -9° which was about 4.5 dB. below the CCIR model pattern for the two E-plane patterns shown. The H-plane patterns were of poorer quality but still at least 4 dB. below the CCIR model pattern.

A further attempt to improve on the surface contour led to the 12 Ghz. H-plane pattern shown in Fig. 4.57. This pattern has a main lobe only 3° wide at the base instead of the expected theoretical value of 4°. However the sidelobe level was lower and below -30 dB. with the exception of one sidelobe at -4° which was only - 27 dB. below the main lobe.

It was found experimentally that small variations in the surface contour made very large changes in the sidelobe detail. The theoretical analysis given earlier for the effect of phase errors showed that this should be expected and that very little error in the contour can be tolerated if sidelobes below - 30 dB. are to be obtained.

Two phase reversal plates 0.152 m x 0.038 m (6 in. x 1-1/2 in.) were tried for the purpose of reducing the near-in sidelobes. Theoretically two plates this size should reduce a -28 dB. sidelobe to -36 dB.

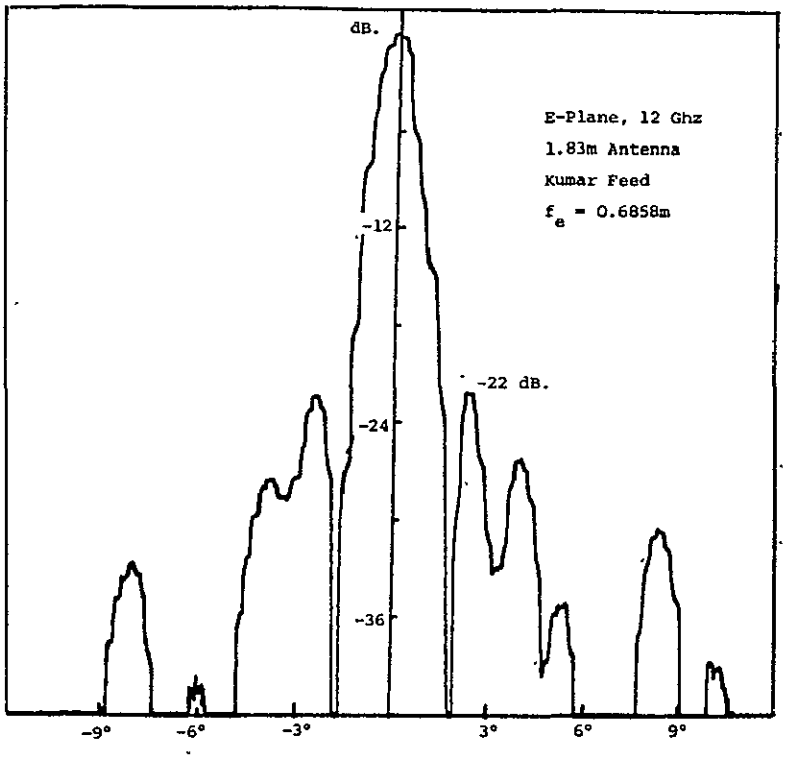

Figure 4.50 E-plane radiation pattern.

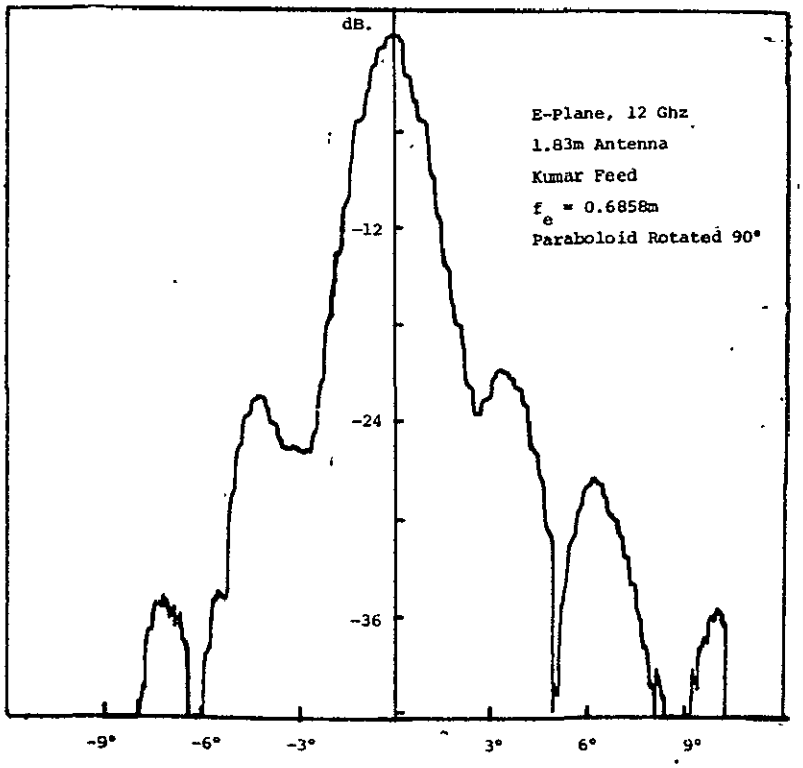

Figure 4.51 E-plane radiation pattern.

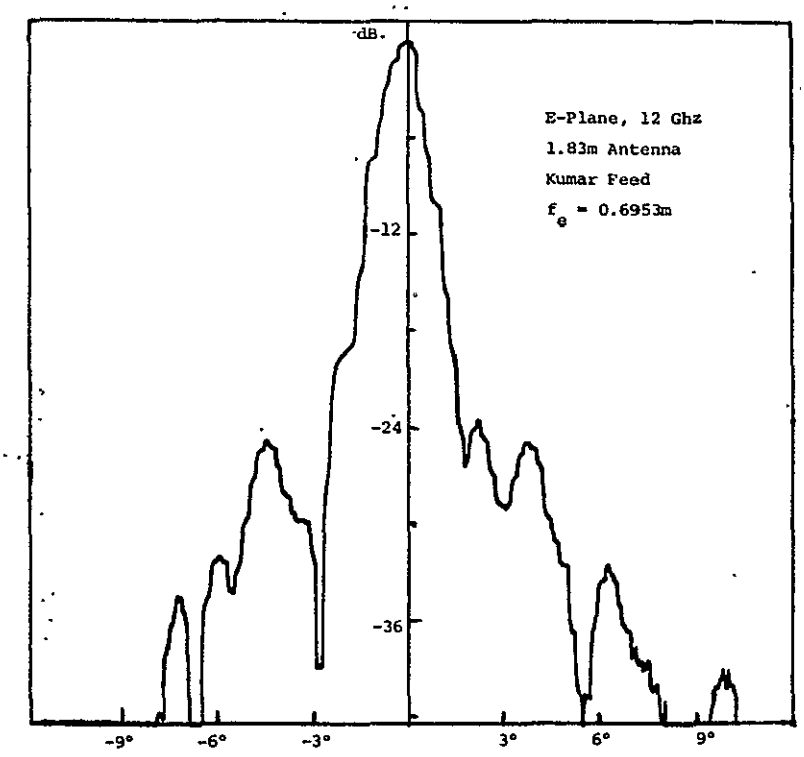

Figure 4.52 E-plane radiation pattern.

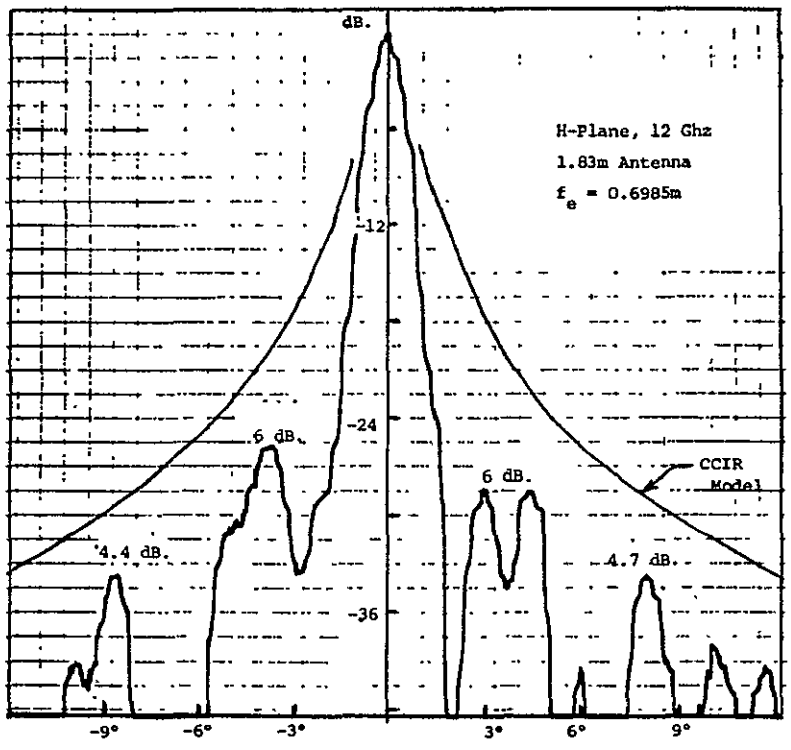

Figure 4.53 H-plane radiation pattern.

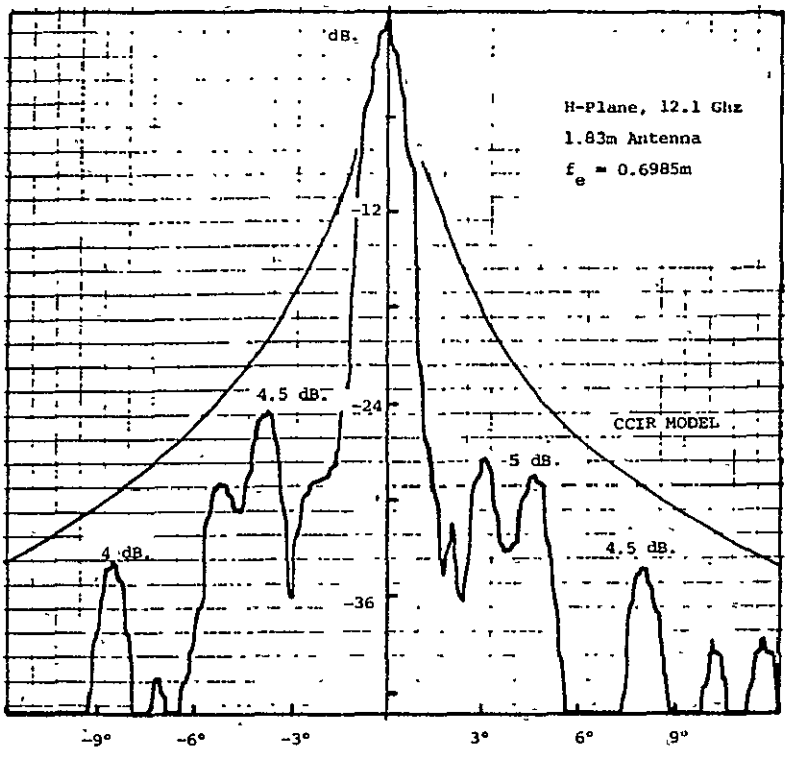

Figure 4.54 H-plane radiation pattern.

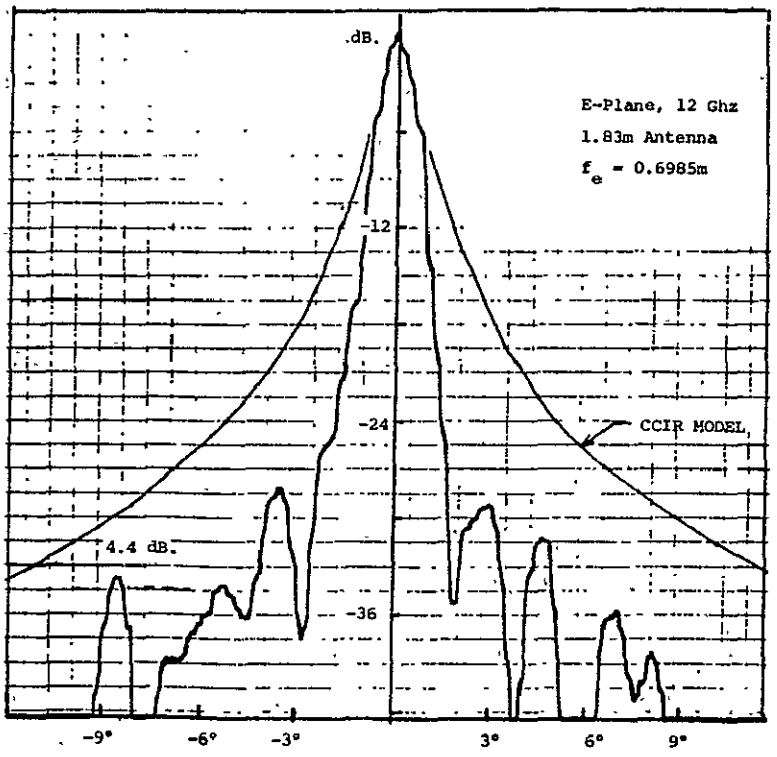

Figure 4.55 E-plane radiation pattern.

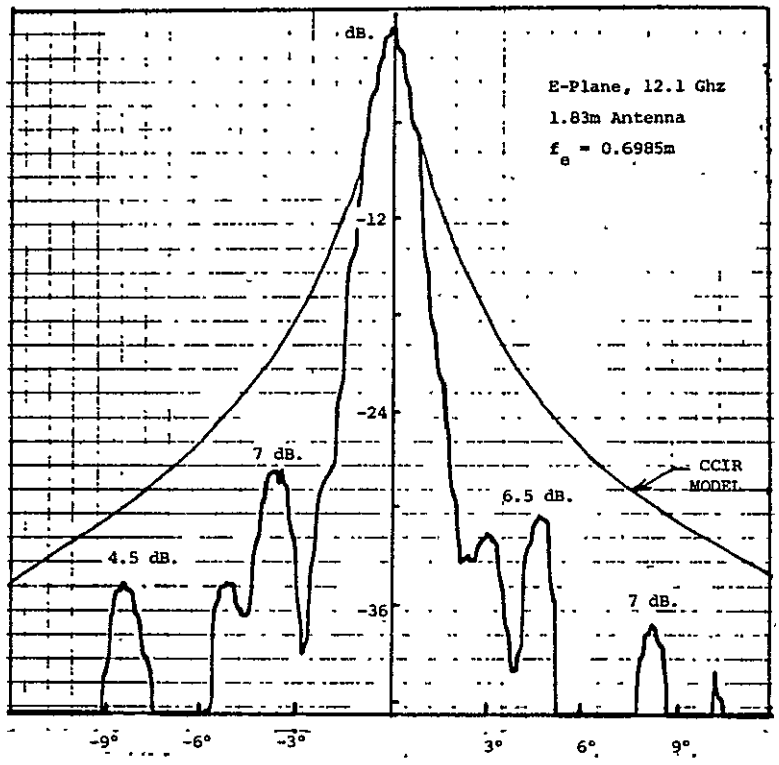

Figure 4.56 E-plane radiation pattern.

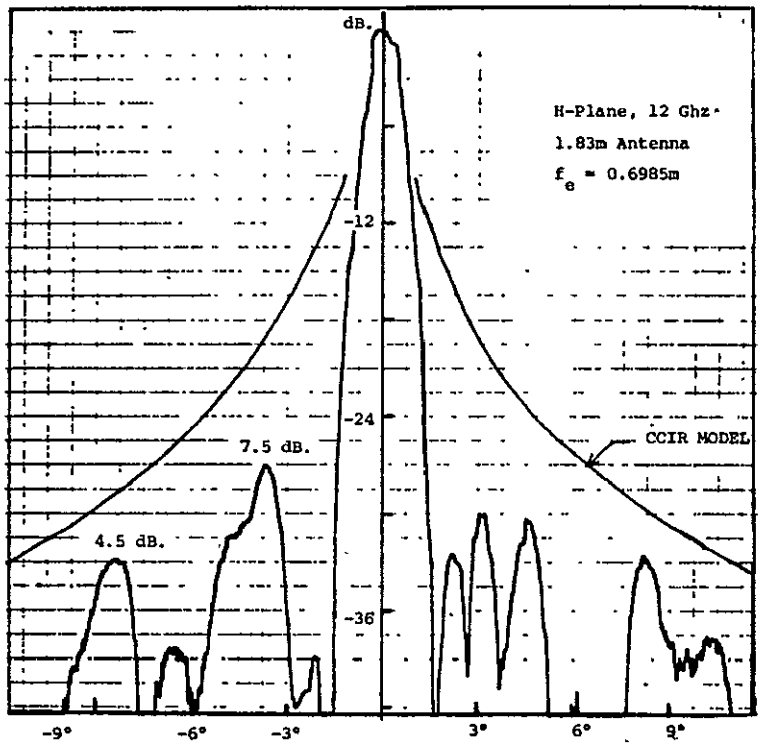

Figure 4.57 H-plane radiation pattern.

if the correct phase was achieved. Several patterns were taken with different separations and it was found that very little cancellation was obtained. It is believed that the reason for this is that the phase of the field in the sidelobes was quite different from 0° or 180°. The analysis of clam-shell distortion given earlier shows that this is to be expected. Figure 4.58 shows a compensated pattern when the plate spacing was 0.235m (9-1/4 in.). The broken curve is the pattern from Fig. 4.57. As is apparent the effect was primarily to increase the sidelobe level, which is the expected result if the phase is in error by close to 90°. If the phase error is 90° it would be expected that a -30 dB. sidelobe would be increased to -28 dB. which was the observed effect for the sidelobes between 2° and 6°. In addition the sidelobe region between -5° and -8° was filled in.

4.4 Experimental Results Using CTS Satellite Source

Several attempts were made to measure the H-plane pattern of the 1.22m paraboloid with the Kumar feed using the CTS satellite as a signal source.* Figure 4.59 shows a view of the mounting arrangement used for the 1.22m antenna in order to obtain an H-plane scan. The frequency stability was not adequate to operate with a bandwidth of less than 100 khz. so patterns below -25 dB. to -27 dB. could not be obtained. Figure 4.60 shows a measured pattern taken at 30° to the H-plane and using the microwave receiver along with a preamplifier having a gain of 27 dB. This pattern shows that the sidelobes are below -27 dB. in this particular plane.

Fig's. 4.61 and 4.62 show two additional measured patterns and clearly

---

* The personnel at NASA Lewis Research Center assisted in these measurements by providing CW transmission from the CTS satellite.

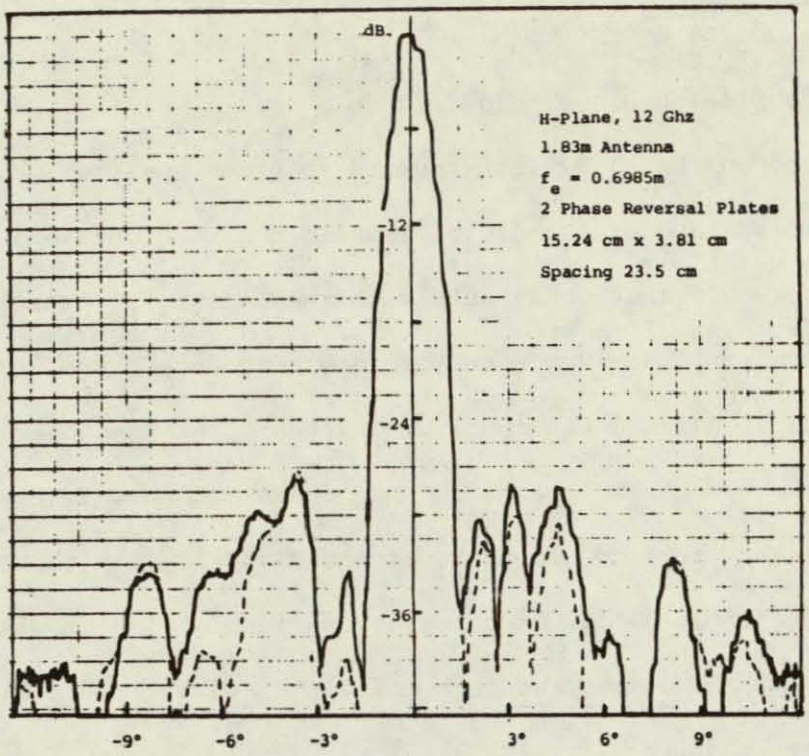

Figure 4.58 H-plane radiation pattern.

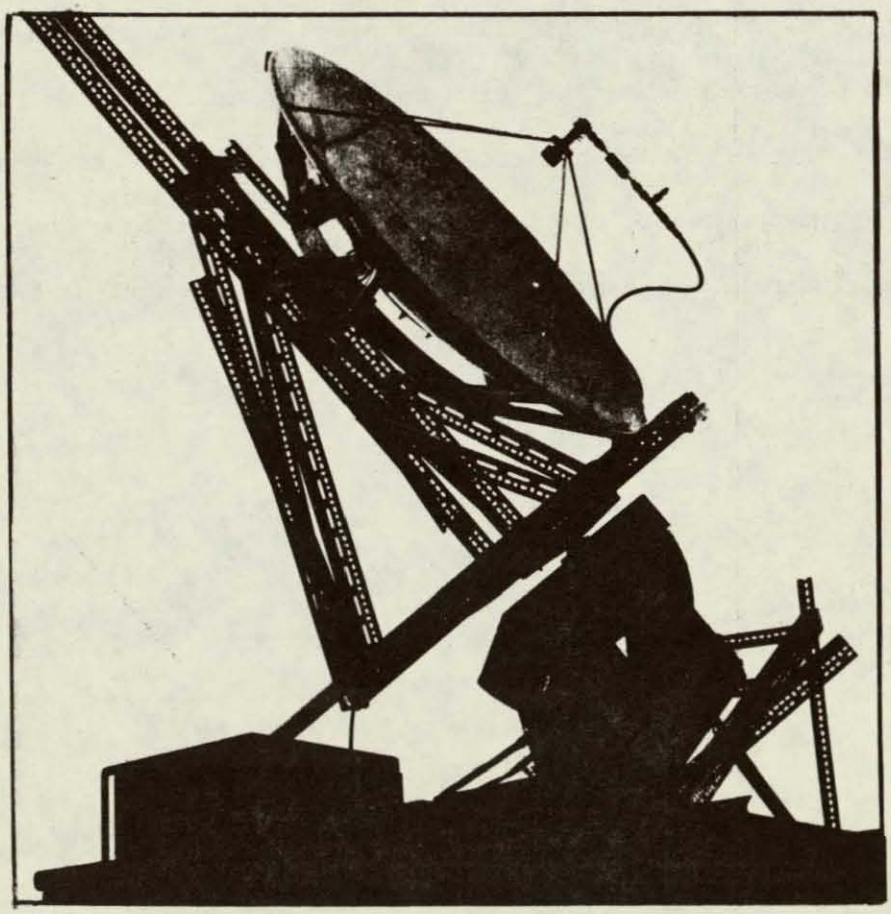

Figure 4.59 View of 1.22m antenna mounted to receive CTS satellite signal.

show that the sidelobes are below -24 dB.

It was hoped that a Hewlett-Packard spectrum analyzer could be used with a bandwidth of 10 khz. or less in order to obtain a sensitivity greater than that obtainable with the Scientific Atlanta microwave receiver. However, the combined frequency stability of the CTS satellite signal and the spectrum analyzer precluded operation with a bandwidth less than 100 khz. and thus gave about the same sensitivity as the microwave receiver did. It was verified visually that the sidelobe level was below 30 dB. by using a bandwidth of 100 hz. and slowly scanning the spectrum analyzer back and forth about the central frequency using the manual scan.

On the 100 khz. bandwidth range the spectrum analyzer has a sensitivity of -80 dBm. The CTS satellite CW signal at ground level is expected to be around -122 dBm. With an antenna gain of 41 dB. and a preamplifier gain of 27 dB. the received signal would be at a -54 dBm. level. The 2 meter length of coaxial cable introduced some loss also so the signal margin was less than 26 dB. which is in agreement with observation.

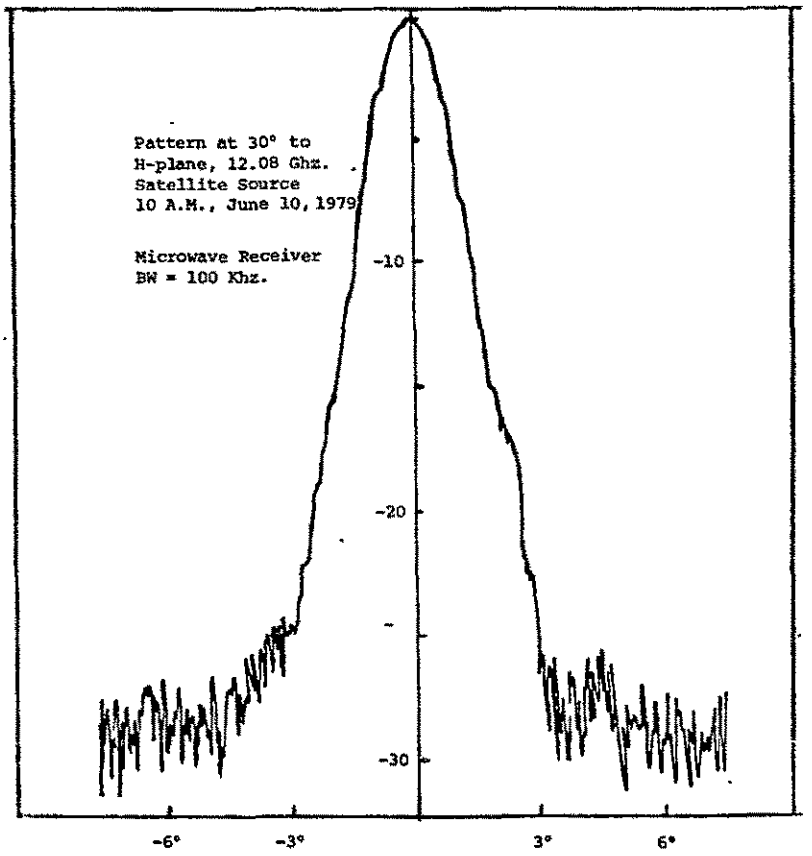

Figure 4.60 Radiation pattern at 30° to H-plane using satellite source.

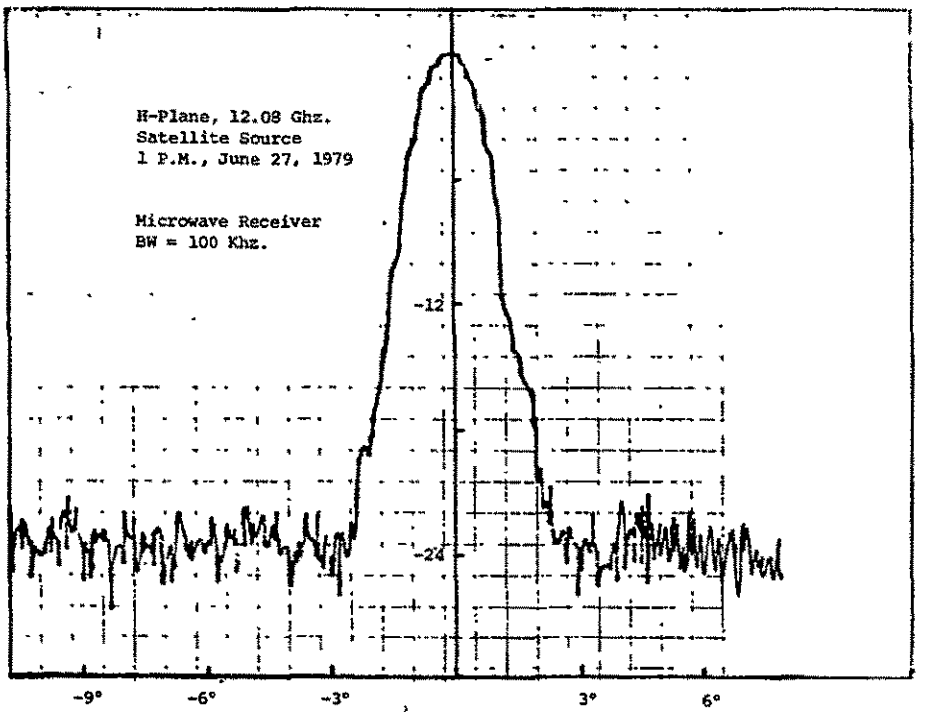

Figure 4.61 H-plane radiation pattern using satellite source.

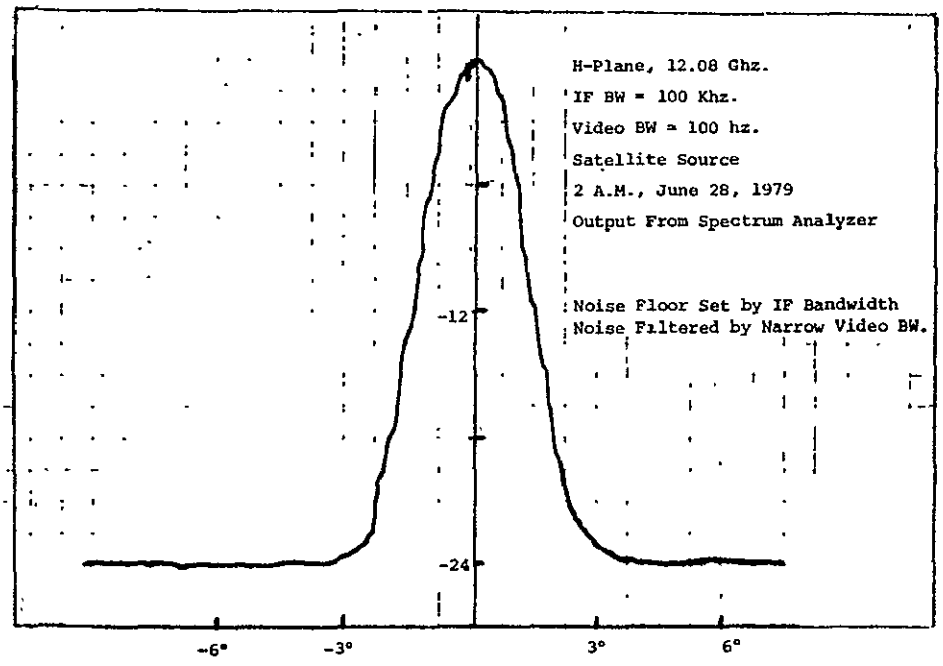

Figure 4.62 H-plane radiation pattern using satellite source.

C -2

CHAPTER 5

CONCLUSIONS AND RECOMMENDATIONS

The results of the work carried out on this project has led to a number of conclusions as regards the present state of the art in achieving low sidelobe levels for low cost earth station satellite receiving antennas for use in the 12 Ghz. band. Also identified are a number of areas where further research and development work needs to be carried out in order to provide the necessary information for the design of small low cost antennas with sidelobes below -35 dB. These conclusions and recommendations are summarized in point form below.

5.1 Conclusions

1. Sidelobes that are at least 5 dB. below those specified by the CCIR model pattern can be achieved by using a feed producing about 20 dB. edge taper in the aperture illumination provided the paraboloids are free of large scale surface contour errors exceeding about $\lambda_o/16$ in magnitude.

2. Good aperture efficiency with low sidelobes can be achieved by using a hybrid mode feed. One particular type of feed that is of simple construction and suitable for paraboloids with f/D = 0.38 is the Kumar feed.

3. In order to obtain sidelobes as low as -35 dB. the surface contour of the paraboloid will probably have to be accurate to within $\pm \lambda_o/25$ at least.

4. Small errors in the surface of a paraboloid produces large variations in the sidelobe pattern below -30 dB. and hence does not result in reproducible sidelobe patterns from one antenna to the next. Thus unless a high quality paraboloid is used the use of either absorber pads or reflector plates to reduce the sidelobe level is not practical because the design of such sidelobe cancelling arrays would be different for each antenna.

5. The use of small reflector plates is a simple way to reduce the sidelobe level provided the sidelobes are caused by the aperture illumination function and not random errors or phase errors due to large scale surface distortions of the paraboloid.

6. At the present time the demand for small (1m to 2m diameter) antennas for the 12 Ghz. band and with very low sidelobes is not sufficient to have induced manufacturers to mass produce them. Currently the accepted tolerance on surface deviations is $\lambda_o/16$ which is not sufficient to generally obtain sidelobes below -35 dB. The structural rigidity of many of the commercially available low cost paraboloids is not good enough to ensure that surface distortions considerably greater than $\lambda_o/16$ does not occur with normal handling and shipping procedures.

7. Antennas designed for transmitting use and incorporating a vertex plate in order to maintain a low VSWR for the feed are not suitable for low sidelobe level receiving purposes. The typical vertex plate usually raises the sidelobe level about -30 dB. even if a large amount of aperture field taper is used. (The use of a 0.216m diameter flat vertex plate on a 1.22m paraboloid produces a considerable amount of unfocused radiation. The author has calculated a theoretical radiation pattern for this case and the predicted sidelobe level was several dB. above the -30 dB. level).

8. A -35 dB. sidelobe objective for low cost small diameter 12 Ghz. antennas appears realistic and attainable, at least for sidelobes in a single plane.

5.2 Recommendations for Further Work

1. Further case studies of the effects of various types of paraboloidal surface distortions on sidelobe levels for different aperture illuminations, and of the effects of random errors with different correlation lengths and illumination functions on sidelobe levels, are needed in order to establish the required tolerances for paraboloids that will permit sidelobe levels of -35 dB. or less to be achieved.

2. Further work needs to be carried out on feeds in order to obtain design information for low cost feeds that have low cross polarization, yield high aperture illumination efficiency, low spillover loss, and produce the necessary aperture field taper to give low sidelobes. A considerable amount of work on various types of hybrid mode feeds has already been done. However, the objective behind a lot of this work has been motivated by radio astronomy requirements and not specifically by a low sidelobe requirement. Many of the feeds that have been developed have been optimized experimentally and design data that will permit a design of a feed for any particular application is not available.

3. Techniques to mass produce low cost but accurate paraboloids need to be developed in order to achieve the objective of optimum utilization of the geostationary orbit.

If large quantities of antennas in the 1m to 2m size were needed, they could be mass produced by stamping and it would be expected that the tolerances could then be controlled to the extent that with a suitable feed sidelobes below - 35 dB. could be readily maintained. More rigid low cost supporting structures for paraboloids need to be developed.

4. The ultimate potential of the Kumar feed and the use of small reflector plates to further reduce the sidelobe level was not established in the course of the work carried out because of the poor quality of the available paraboloids. Further investigation of the Kumar feed should be carried out. By designing a feed for operation at 6 Ghz. and using the 1.83m antenna, the effect of errors would be scaled down by a factor of 2. Thus a reasonably accurate paraboloid that simulated a 0.91m paraboloid at 12 Ghz. would be available. Similarly the 1.22m paraboloid could be used at a lower frequency to reduce the effects of contour errors.

5. A low attenuation feed line for the Kumar feed and other similar feeds needs to be designed. This could consist of a rigid coaxial line or a waveguide with a suitable coupler to couple it to the circular waveguide feed input.

6. For antennas designed for sidelobes below -35 dB. the scatter from the feed supporting structure will probably not be entirely negligible. Thus optimization of the feed supporting system is probably needed.

REFERENCES

1. CTS Reference Book, NASA TM X-71824, NASA Lewis Research Center, Cleveland, Ohio, Oct. 15, 1975.

2. Sciambi, A. F., The Effect of Aperture Illumination on the Circular Aperture Pattern Characteristics, Microwave Journ., Vol. 8, pp. 79-84, Aug. 1965.
See Also
Albernaz, J.C.F., Sidelobe Control in Antenna for an Efficient Use of the Geostationary Orbit. Ph.D. Dissertation, Stanford University, Nov. 1972.

3. Computer Sciences Corporation. Satellite communication systems, studies and investigations. Report No. 4031-05, Contract No. NAS 5-11672, 1971.

4. International Telecommunications Union: C.C.I.R. Study Group, Subjective Assessment of the quality of television pictures. Geneva: I.T.U., 5 (2), 1965-1970, 89.

5. C.C.I.R. Study Group (Internation Telecommunications Union sub-committee). Report of the European Broadcasting Union ad-hoc group on colour television. Document XI/33-E, February, 1965.

. . . Subjective assessment of the quality of television pictures. Document XI/140-E, January, 1966.

. . . Subjective assessment of the quality of television pictures. Document XI/8-E, December, 1967.

. . . Subjective tests carried out with PAL colour television signals affected by distortion. Document XI/45-E, April, 1968.

. . . Subjective assessment of the quality of television pictures. Document XI/155-E, June, 1969.

. . . Subjective asssessment of the quality of television pictures, comparison between the 5-grade and 6-grade assessment scales. Document XI/158-E, June, 1969.

. . . Method of fidelity for subjective tests on colour television. Document XI/181-E, July 1969.

. . . Subjective assessment of the quality of television pictures. Study Programme 3A/XI, Replacing Report 405-1, C.C.I.R. XII Plenary Assembly Document, Doc. XI/1037-E, November, 1969.

6. Miller, E. F. and Myhre, R. W. Power ratio of wanted to unwanted signals for frequency-sharing between FM and AM-VSB television transmission systems. Washington, D.C.: National Aeronautics and Space Administration Technical Memorandum Report TM X-2080, September, 1970.

7. Miller, R. H., Testing and Co-Channel Video Interference on Television, Institute for Communication Research, Stanford University, Report No. NASA CR-121184 issued on Contract NAS 3-14362, May, 1972.

8. CCIR Documents of the XIIth Plenary Assembly (New Dehli), Vol. IV, Parts 1 and 2, 1970.

9. CCIR, Protection Ratios for Television, Sec. 3.4.1.3, Report of the Special Joint Meeting, Geneva, 1971.

10. Kumar, A., Experimental Study of a Dielectric Rod Enclosed by a Waveguide for Use as a Feed, Elec. Letters, Vol. 12, pp. 666-668, December, 1976.

11. Silver S., Microwave Antenna Theory and Design, McGraw-Hill Book Co., Inc., New York, 1949.

12. Collin, R. E. and F. J. Zucker, Antenna Theory, Part I, McGraw-Hill Book Co., Inc., New York, 1969.

13. Ramsay, J. F. Fourier Transforms in Aerial Theory, Marconi Review, Parts I to VI, Issue No's. 83-89, 1946.

14. Goebels, F. J., et. al., Analytical and Experimental Investigation of Side-Lobe Suppression Techniques for Reflector Type Space Craft Antenna. NASA Report CR-72462, Sept. 1968.

15. Rudge, A. W., and M. J. Withers, Design of Flared-Horn Primary Feeds for Parabolic Reflector Antennas, Proc. IEE, Vol. 117, pp. 1741-1749, Sept., 1970.

16. Clarricoats, P.J. B., and G. R. Poulton, High Efficiency Microwave Reflector Antennas - A Review. Proc. IEEE, Vol. 65, pp. 1470-1504, October, 1977.

17. Rumsey, V. H., Horn Patterns with Uniform Power Patterns Around Their Axes, IEEE Trans., Vol. AP-14, pp. 656-658, Sept. 1966.

18. Minnett, H. C., and B. MacA. Thomas, A Method of Synthesizing Radiation Patterns with Axial Symmetry, IEEE Trans., Vol. AP-14, pp. 654-656, September, 1966.

19. ibid. Fields in the Image Space of Symmetrical Focusing Reflectors, Proc. IEE., Vol. 115, pp. 1419-1430, 1968.

20. Kay, A. F., The Scalar Feed, U. S. Air Force Cambridge Res. Labs., Rept. No. 62-347, March, 1964.

21. Potter, P. D., A New Horn Antenna With Suppressed Sidelobes and Equal Beamwidths, Microwave Journal, Vol. 6, pp. 71-78, 1963.

22. Ajioka, J. S., and H. E. Harry, Jr., Shaped Beam Antenna for Earth Coverage from a Stabilized Satellite, IEEE Trans., Vol. AP-18, pp. 323-327, May 1970.

23. Ludwig, A. C., Radiation Pattern Synthesis for Circular Aperture Horn Antennas, IEEE TRANS., Vol. AP-14, pp. 434-440, July, 1966.

24. Vu, T. B., Optimization of Performance of Corrugated Feed for Paraboloid Antenna, Int. Jour. Elec., Vol. 29, pp. 449-459, No. 5, 1970.

25. Narashiman, M. S., and B. V. Rao, Hybrid Modes in Conical Horns, Elec. Letters, Vol. 22, pp. 32-34, June, 1970.

26. Knop, C. M., and H. J. Wiesenforth, On the Radiation from an Open-Ended Corrugated Pipe Carrying the HE_{11} Mode, IEEE Trans., Vol. AP-20, pp. 644-648, September, 1972.

27. Vu, T. B., Low-Noise Dual Hybrid-Mode Horn - An Experimental Model, Int. Jour. Elec., Vol. 34, pp. 391-400, No. 3, 1973.

28. Clarricoats, P. J. B., and P. K. Saha, Propagation and Radiation Behavior of Corrugated Feeds, Pts. I and II, Proc. IEE., Vol. 118, pp. 1167-1186, Sept. 1971.

29. Narasimhan, M.S., and B. V. Rao, Diffraction by Wide Flare Angle Corrugated Conical Horns, Elec. Letters, Vol. 6, pp. 469-471, 1970.

30. Thomas, B. MacA., Theoreitcal Performance of Prime Focus Paraboloids Using Cylindrical Hybrid-Mode Feeds, Proc. IEE., Vol. 118, pp. 1539-1549, 1971.

31. ibid. - Bandwidth properties of Corrugated Conical Horns, Elec. Letters, Vol. 5, pp. 561-563, 1969.

32. Narasimhan, M. S., and Y. B. Malla, Paraboloidal-Reflector Illumination With Conical Scalar Horns, Elec. Letters, Vol. 8, pp. 111-112, March, 1972.

33. Vokurka, V. J., One-Hybrid-Mode Feed with High Aperture Efficiency and Low Spill-Over, 5th European Microwave Conference, Hamburg, Germany, Sept. 1975.

34. Koshy, V. K., and Calla, O.P.N., Development of a High Efficiency Scalar Feed for Communication Antenna, Jour. Inst. Elec. and Telecom. Engrs., Vol. 22, pp. 28-31, January, 1976.

35. Chan, K. B., A Design Handbook for Conical Corrugated Horns, Queen Mary College Report KBC/7216, 1972.

36. Koch, G. F., Coaxial Feeds for High Aperture Efficiency and Low Spillover of Paraboloidal Reflector Antennas, IEEE Trans., Vol. AP-21, pp. 164-169, March, 1973.

37. Scheffer, H., Improvements in the Development of Coaxial Feeds for Paraboloidal Reflector Antennas, 5th European Microwave Conference, Hamburg, Germany, September, 1975.

38. Kumar, A., Reduce Cross Polarization in Reflector Type Antennas, Microwaves, Vol. 17, pp. 48-51, March, 1978.

39. Kumar, A., Waveguide Feed Reduces Cross Polarization Levels, Microwave Journal, Vol. 21, pp. 8-688, March, 1978.

40. Wohlleben, R., H. Mattes, and O. Lochner, Simple Small Primary Feed for Large Opening Angles and High Aperture Efficiency,, Elec. Letters, Vol. 8, pp. 474-476, 1972.

41. LaGrone, A. H., and G. F. Roberts, Minor Lobe Suppression in a Rectangular Horn Antenna through Utilization of a High Impedance Choke Flange, IEEE Trans., Vol. AP-14, pp. 102-103, Jan. 1966.

42. James, G. L., and D.P.S. Malik, Towards the Theoretical Design of Splash-Plate Feeds, Elec. Letters, Vol. 11, p. 593, 1975.

43. Malik, D.P.S., and G. L. James, Splash Plate Feed Designs, 5th European Microwave Conference, Hamburg, Germany, September, 1975.

44. Ohkobo, K., C.C. Han, J. Albernaz, J.M. Janky, and B.B. Lusignan, Optimization in the Design of a 12 Gigahertz Low Cost Ground Receiving System for Broadcast Satellites. NASA Report CR-121184, October 15, 1972.

45. Williams, W. F., Reduction of Near-In Sidelobes Using Phase Reversal Aperture Rings, JPL Quart. Tech. Review, Vol. 1, No. 4, pp. 34-41, January 1972.

46. Ruze, J., Physical Limitations on Antennas, M.I.T. Research Laboratory of Electronics Tech. Rept. No. 248, October, 1952.

APPENDIX I

DERIVATION OF FORMULAS FOR SATELLITE ANGULAR COORDINATES AND POLARIZATION MISMATCH

Figure AI-1 shows a number of satellites in the equatorial orbit. The xyz position coordinates of the n'th satellite are $r(\cos \phi_n, \sin \phi_n, 0)$ where the distance r is measured in terms of the radius R_e of the earth. The coordinates of the ground station are given by $(\sin \theta_1, 0, \cos \theta_1)$. The unit vector from the ground station to the n'th satellite is

$$\vec{n}_n = \frac{[\vec{a}_x(r \cos \phi_n - \sin \theta_1) + \vec{a}_y(r \sin \phi_n) - \vec{a}_z \cos \theta_1]}{R_n} \qquad \text{(AI-1)}$$

where R_n is the distance from the ground station to the n'th satellite and is given by

$$R_n = (1 + r^2 - 2r \sin \theta_1 \cos \phi_n)^{1/2}$$

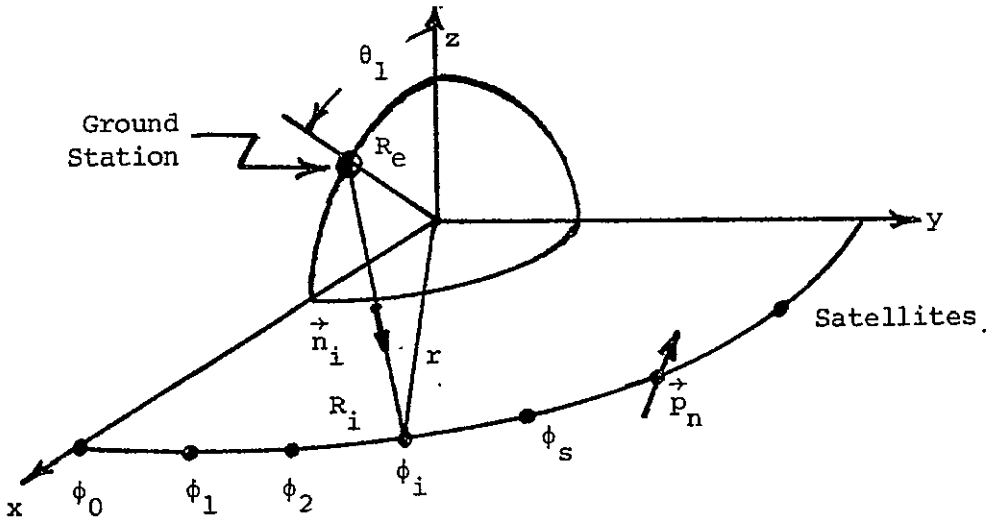

Fig. AI-1 Satellites in an equatorial orbit.

We will now assume that the antenna feed for each satellite is vertically oriented so the unit polarization vector $\vec{p}_n$ describing the feed orientation lies in the $\vec{n}_n$, $\vec{a}_z$ plane and is perpendicular to $\vec{n}_n$.

$$\vec{p}_n = a\,\vec{n}_n + b\,\vec{a}_z$$

$$\vec{p}_n \cdot \vec{n}_n = 0 \ , \quad p_n^2 = 1$$

These equations lead to the following solutions for the constants a and b,

$$b = \frac{R_n}{(R_n^2 - \cos^2 \theta_1)^{1/2}}$$

$$a = \frac{b \cos \theta_1}{R_n}$$

We next assume that the ground station antenna is pointed toward the i'th satellite with unit line-of-sight position vector $\vec{n}_i$ and has its feed oriented parallel to $\vec{p}_i$. We will choose $\vec{n}_i$ along a new polar axis z' and let x' be oriented along $\vec{p}_i$. Then y' is directed along $\vec{n}_i \times \vec{p}_i$. Relative to this coordinate system the n'th satellite has a position described by the polar angle θ_{in} and aximuth angle ϕ_{in} where

$$\cos \theta_{in} = \vec{n}_i \cdot \vec{n}_n \qquad \text{(AI-2a)}$$

$$\cos \phi_{in} = \frac{[\vec{n}_n - (\vec{n}_i \cdot \vec{n}_n)\vec{n}_i] \cdot \vec{p}_i}{|\vec{n}_n - (\vec{n}_i \cdot \vec{n}_n)\vec{n}_i|} \qquad \text{(AI-2b)}$$

Note that $\vec{n}_n - (\vec{n}_i \cdot \vec{n}_n)\vec{n}_i$ is the projection of a line-of-sight vector to satellite n unto the x'y' plane and the scalar product with $\vec{p}_i$ will determine ϕ_{in}.

The polarization mismatch factor between the field radiated by the n'th satellite and the ground station antenna is given by

$$\text{Polarization} = \vec{p}_i \cdot \vec{p}_n \qquad \text{(AI-3)}$$

To facilitate computation we note that

$$\vec{n}_i \cdot \vec{n}_n = \frac{1+r^2\cos(\phi_n-\phi_i)-r\sin\theta_1(\cos\phi_n+\cos\theta_i)}{R_i R_n}$$

The results shown in Fig's. 1.3 and 1.4 were computed using (AI-2) and (AI-3 for ϕ_i chosen equal to 0° and 30°.

The above equations may also be used to determine the ground station antenna orientation and feed rotation from the local vertical line in order to receive a signal from the i'th satellite. As an example consider a Cleveland, Ohio ground station with coordinates -81.6° longitude and 41.5° latitude. For the CTS satellite the coordinates are -116° longitude, 0° latitude, and height 35.8×10^3 km. Hence $\theta_1 = 48.5°$ and $\phi_i = -33.4°$. The earth's radius R_e equals 6378 km. so r = 6.613 earth radii and R_i = 6.036 earth radii. From (AI-1) the unit vector $\vec{n}_i$ is found to have the components (0.7906, -0.603, - 0.1098). The polarization vector $\vec{p}_i$ has components (0.0873, - 0.0666, 0.99387). At the ground station the local vertical unit vector $\vec{a}_r$ has the components (cos 41.5°, 0, sin 41.5°) or (0.74895, 0, 0.6626).

The required antenna elevation angle is given by $\sin^{-1}(\vec{a}_r \cdot \vec{n}_i) = \sin^{-1} 0.51963 = 31.3°$. The local north pointing unit vector is $-\vec{a}_\theta = (-\sin 41.5°, 0, \cos 41.5°) = (-0.6626, 0, 0.74895)$. The west pointing unit vector is $-\vec{a}_y$. The component of $\vec{n}_i$ along $\vec{a}_r$ is $(\vec{n}_i \cdot \vec{a}_r)\vec{a}_r = 0.519\ \vec{a}_r$. Then $\vec{n}_{it} = \vec{n}_i - 0.519\ \vec{a}_r = (0.4019, -0.603, -0.4537)$ and the normalized unit vector $\vec{n}_{it}$ is $(0.470, -0.7053, -0.5307)$. The ground station antenna must be rotated about the local vertical line toward the west through an angle $\cos^{-1}(\vec{n}_{it} \cdot \vec{a}_\theta) = \cos^{-1}(0.70889) = 44.85°$.

The receiving antenna feed should be positioned along $\vec{p}_i$. The unpositioned feed is directed along the local vertical $\vec{a}_r$ and we let $\vec{p} = \vec{a}_r$. When the elevation angle is changed by 31.3° $\vec{p}$ changes to $\vec{p}'$ where

$$\vec{p}' = \vec{a}_r \cos 31.3° - \vec{a}_\theta \sin 31.3°$$

When the antenna is rotated through 44.85° in azimuth $\vec{p}'$ changes to $\vec{p}''$ where

$$\vec{p}'' = \vec{a}_r \cos 31.3° - \sin 31.3° (\vec{a}_\theta \cos 44.85° - \vec{a}_y \sin 44.85°)$$

$$= (0.39586, 0.3664, 0.8419)$$

The required feed rotation is given by $\cos^{-1} \vec{p}_i \cdot \vec{p}'' = \cos^{-1} 0.84689 = 32.12°$ in order to align the feed with the incoming radiation polarized along $\vec{p}_i$.

APPENDIX II

TI-59 PROGRAMS

The numerical evaluation of the radiation pattern of a circular aperture for different illumination functions having rotational symmetry was carried out using a Texas Instruments TI-59 programmable calculator and associated printer. The effects of clam-shell distortion and periodic radial distortion discussed in Chapter 3 were also evaluated numerically using the TI-59 instrument. The programs used are summarized in this Appendix.

The program labelled Program A evaluates the following expression:

$$\int_0^1 f(x)\ J_o(ux)\ x\ dx$$

where f(x) must be entered as subroutine 150. Program B evaluates

$$\int_0^1 f(x)\ J_2(ux)\ x\ \beta(x)\ dx$$

where $\beta(x)$ f(x) is entered as subroutine 150. Program C evaluates

$$\int_0^1 f(x)\ J_4(ux)\ x\ \beta(x)\ dx$$

where again $\beta(x)$ f(x) is entered as subroutine 150.

The Bessel functions $J_n(ux)$ are evaluated by the subroutine B' using the series expansion (B' evaluates J_n-1)

$$J_n(v) = \left(\frac{v}{2}\right)^n \frac{1}{n!}\left[1 - \frac{(v/2)^2}{1!\,(n+1)} + \frac{(v/2)^4}{2!\,(n+1)\,(n+2)}\right.$$

$$\left. - \frac{(v/2)^6}{3!\,(n+1)\,(n+2)\,(n+3)} + - - - \right]$$

The number of terms used is increased with increasing values of u by multiplying u by 1.3, choosing the integer value, adding 6 to this number, and storing the result in R_{18}. Since the TI-59 has only 13 digit accuracy the Bessel function routine becomes increasingly inaccurate for ux > 25 and is not useful at all for ux > 30. If larger values of u were required it would be a simple manner to incorporate a branching to a new subroutine using the asymptotic formulas for the Bessel functions for u greater than some specified value.

User Instructions

1. Store $x_o = 0$ in R_1
2. Store $x_n = 1$ in R_2
3. Store n in R_{10}
4. Store $h = 1/n$ in R_3
5. Store $u = 0$ in R_{12}
6. Store 6 in R_{18}
7. Store 4 in R_9
8. Store Δu in R_{19}
9. Enter program for f(x) as subroutine 150. End with Inv. Sbr.

10. Reset counter and then set flag 0. The flag 0 is used to establish the normalization of the radiation pattern and is used in Program A only.

The radiation pattern for the Scheffer feed was evaluated using numerical values of f(x). The values of $f(x_i)$ were stored in registers R_{21}, R_{22}, etc. with f(0) in R_{21}. The required address was generated by multiplying x_i by n and adding 21.1 to this number and storing this address in R_{20} (the calculator uses the integer value as an address). Indirect addressing was then used to recall the values of $f(x_i)$ as needed. Subroutine 150 is entered as follows:

SUBR 150 ((RCL LL x n) + 21.1) STO 20 RCL IND 20

INV SBR.

The number added to nx_i is chosen as 21.1 to make sure that the integer value is 21 and not 20 because of the 13 digit accuracy of any number stored.

```
000  43 RCL
001  10  10
002  42 STO
003  05  05
004  61 GTO
005  36 PGM
006  76 LBL
007  16 A'
008  53  (
009  42 STO
010  11  11
011  65  ×
012  43 RCL
013  12  12
014  54  )
015  42 STO
016  13  13
017  17 B'
018  53  (
019  53  (
020  43 RCL
021  15  15
022  85  +
023  01  1
024  54  )
025  65  ×
026  53  (
027  43 RCL
028  11  11
029  65  ×
030  71 SBR
031  01  01
032  50  50
033  54  )
034  54  )
035  92 RTN
036  76 LBL
037  17 B'
038  53  (
039  43 RCL
040  13  13
041  55  ÷
042  02  2
043  54  )
044  33 X²
045  42 STO
046  14  14
047  94 +/-
048  42 STO
049  15  15
050  76 LBL
051  18 C'
052  53  (
053  24 CE
054  65  ×
055  43 RCL
056  14  14
057  55  ÷
058  53  (
059  43 RCL
060  18  18
061  75  -
062  43 RCL
063  09  09
064  54  )
065  33 X²
066  54  )
067  94 +/-
068  44 SUM
069  15  15
070  22 INV
071  97 DSZ
072  09  09
073  19 D'
074  61 GTO
075  18 C'
076  76 LBL
077  19 D'
078  53  (
079  43 RCL
080  18  18
081  75  -
082  02  2
083  54  )
084  42 STO
085  09  09
086  92 RTN
087  76 LBL
088  36 PGM
089  36 PGM
090  09  09
091  14  D
092  42 STO
093  16  16
094  43 RCL
095  19  19
096  44 SUM
097  12  12
098  22 INV
099  87 IFF
100  00  00
101  01  01
102  06  06
103  43 RCL
104  16  16
105  42 STO
106  17  17
107  53  (
108  43 RCL
109  16  16
110  58 FIX
111  04  04
112  99 PRT
113  55  ÷
114  43 RCL
115  17  17
116  54  )
117  99 PRT
118  33 X²
119  99 PRT
120  53  (
121  28 LOG
122  65  ×
123  01  1
124  00  0
125  54  )
126  58 FIX
127  02  02
128  99 PRT
129  98 ADV
130  53  (
131  43 RCL
132  12  12
133  65  ×
134  01  1
135  93  .
136  03  3
137  54  )
138  59 INT
139  42 STO
140  18  18
141  42 STO
142  09  09
143  06  6
144  44 SUM
145  18  18
146  04  4
147  44 SUM
148  09  09
149  81 RST
```

```
000  43 RCL
001  10  10
002  42 STO
003  05  05
004  61 GTO
005  36 PGM
006  76 LBL
007  16 A'
008  53  (
009  42 STO
010  11  11
011  65  ×
012  43 RCL
013  12  12
014  54  )
015  42 STO
016  13  13
017  17 B'
018  53  (
019  01  1
020  44 SUM
021  15  15
022  43 RCL
023  15  15
024  65  ×
025  53  (
026  43 RCL
027  13  13
028  33 X²
029  33 X²
030  55  ÷
031  03  3
032  08  8
033  04  4
034  54  )
035  54  )
036  53  (
037  24 CE
038  65  ×
039  43 RCL
040  11  11
041  65  ×
042  71 SBR
043  01  01
044  50  50
045  54  )
046  92 RTN
047  76 LBL
048  17 B'
049  53  (
050  43 RCL
051  13  13
052  55  ÷
053  02  2
054  54  )
055  33 X²
056  42 STO
057  14  14
058  94 +/-
059  53  (
060  24 CE
061  55  ÷
062  05  5
063  54  )
064  42 STO
065  15  15
066  76 LBL
067  18 C'
068  53  (
069  24 CE
070  65  ×
071  43 RCL
072  14  14
073  55  ÷
074  53  (
075  43 RCL
076  18  18
077  75  -
078  43 RCL
079  09  09
080  54  )
081  55  ÷
082  53  (
083  43 RCL
084  18  18
085  75  -
086  43 RCL
087  09  09
088  85  +
089  04  4
090  54  )
091  54  )
092  94 +/-
093  44 SUM
094  15  15
095  22 INV
096  97 DSZ
097  09  09
098  19 D'
099  61 GTO
100  18 C'
101  76 LBL
102  19 D'
103  53  (
104  43 RCL
105  18  18
106  75  -
107  02  2
108  54  )
109  42 STO
110  09  09
111  92 RTN
112  76 LBL
113  36 PGM
114  36 PGM
115  09  09
116  14  D
117  42 STO
118  16  16
119  43 RCL
120  19  19
121  44 SUM
122  12  12
123  43 RCL
124  16  16
125  58 FIX
126  04  04
127  99 PRT
128  98 ADV
129  53  (
130  43 RCL
131  12  12
132  65  ×
133  01  1
134  93  .
135  03  3
136  54  )
137  59 INT
138  42 STO
139  18  18
140  42 STO
141  09  09
142  06  6
143  44 SUM
144  18  18
145  04  4
146  44 SUM
147  09  09
148  81 RST
```

PROGRAM B

```
000  43 RCL
001  10  10
002  42 STO
003  05  05
004  61 GTO
005  36 PGM
006  76 LBL
007  16 A'
008  53  (
009  42 STO
010  11  11
011  65  ×
012  43 RCL
013  12  12
014  54  )
015  42 STO
016  13  13
017  17 B'
018  53  (
019  01  1
020  44 SUM
021  15  15
022  43 RCL
023  15  15
024  65  ×
025  53  (
026  43 RCL
027  13  13
028  33 X²
029  55  ÷
030  08  8
031  54  )
032  54  )
033  53  (
034  24 CE
035  65  ×
036  43 RCL
037  11  11
038  65  ×
039  71 SBR
040  01  01
041  50  50
042  54  )
043  92 RTN
044  76 LBL
045  17 B'
046  53  (
047  43 RCL
048  13  13
049  55  ÷
050  02  2
051  54  )
052  33 X²
053  42 STO
054  14  14
055  94 +/-
056  53  (
057  24 CE
058  55  ÷
059  03  3
060  54  )
061  42 STO
062  15  15
063  76 LBL
064  18 C'
065  53  (
066  24 CE
067  65  ×
068  43 RCL
069  14  14
070  55  ÷
071  53  (
072  43 RCL
073  18  18
074  75  -
075  43 RCL
076  09  09
077  54  )
078  55  ÷
079  53  (
080  43 RCL
081  18  18
082  75  -
083  43 RCL
084  09  09
085  85  +
086  02  2
087  54  )
088  54  )
089  94 +/-
090  44 SUM
091  15  15
092  22 INV
093  97 DSZ
094  09  09
095  19 D'
096  61 GTO
097  18 C'
098  76 LBL
099  19 D'
100  53  (
101  43 RCL
102  18  18
103  75  -
104  02  2
105  54  )
106  42 STO
107  09  09
108  92 RTN
109  76 LBL
110  36 PGM
111  36 PGM
112  09  09
113  14  D
114  42 STO
115  16  16
116  43 RCL
117  19  19
118  44 SUM
119  12  12
120  43 RCL
121  16  16
122  58 FIX
123  04  04
124  99 PRT
125  98 ADV
126  53  (
127  43 RCL
128  12  12
129  65  ×
130  01  1
131  93  .
132  03  3
133  54  )
134  59 INT
135  42 STO
136  18  18
137  42 STO
138  09  09
139  06  6
140  44 SUM
141  18  18
142  04  4
143  44 SUM
144  09  09
145  81 RST
```